Supporting Information

Stereocontrol as a tool for shaping abiotic, sequence-defined oligourethanes

Sara Njoku[1, ‡], Ariel F. Perez Mellor[2, ‡], Johanna Brazard[2], Simone G. Giuffrida[1], Wojciech Dudziak,[3] Céline Besnard,[4] Thomas Bürgi[2], Takuji B. M. Adachi[2*], and Róża Szweda[1,3*]

[1] *Łukasiewicz Research Network – PORT Polish Center for Technology Development, Stabłowicka 147, 54-066 Wrocław, Poland*

[2] *Department of Physical Chemistry, Sciences II, University of Geneva, 1211 Geneva, Switzerland, *Email: Takuji.Adachi@unige.ch*

[3] *Center for Advanced Technologies, Adam Mickiewicz University, Uniwersytetu Poznańskiego 10, 61-614 Poznań, Poland, *E-mail: roza.szweda@amu.edu.pl*

[4] *Laboratory of crystallography, University of Geneva, 1211 Geneva, Switzerland*

‡Authors contributed equally

TABLE OF CONTENTS

1. EXPERIMENTAL PROCEDURES

1.1. Materials

(R)-2-Aminopropan-1-ol, (R, 98%, Fluorochem, ee: 97%, [α]19/D −18°), (S)-2-Aminopropan-1-ol, (S, 98%, Apollo Scientific, ee: 97%, optical rotation: [α]20/D +18°), N,N'-Disuccinimidyl carbonate (dSu, >98%, TCI), Di-tert-butyl dicarbonate, ($(Boc)_2O$, 95%, Angene), Pyridine (99.8%, anhydrous, Sigma-Aldrich), Acetonitrile (99.8%, anhydrous, Sigma-Aldrich), Dichloromethane (DCM, >99.8%, Honeywell), Ethyl acetate (EtOAc, 99.5%, Chemsolute), Sodium chloride (≥ 99,5%, Sigma-Aldrich), Sodium sulfate (99.9%, Chempur) were used as received from the suppliers.

1.2. Synthesis of Boc-oligomers

In general, sequence-defined oligourethanes with Boc protection were synthesized in the liquid phase, as reported previously.[1] In the first step, the amino group of the amino alcohol monomer was blocked by the reaction with di-tert-butyl dicarbonate (Scheme S1a).[2] Afterward, the free hydroxyl group of the molecule was activated by N, N'-disuccinimidyl carbonate (dSu) (Scheme S1b) and coupled to the amino alcohol monomer (Scheme S1c). After each monomer coupling, the mid-product was isolated by extraction. Steps (b) and (c) were repeated until the tetramer was formed.

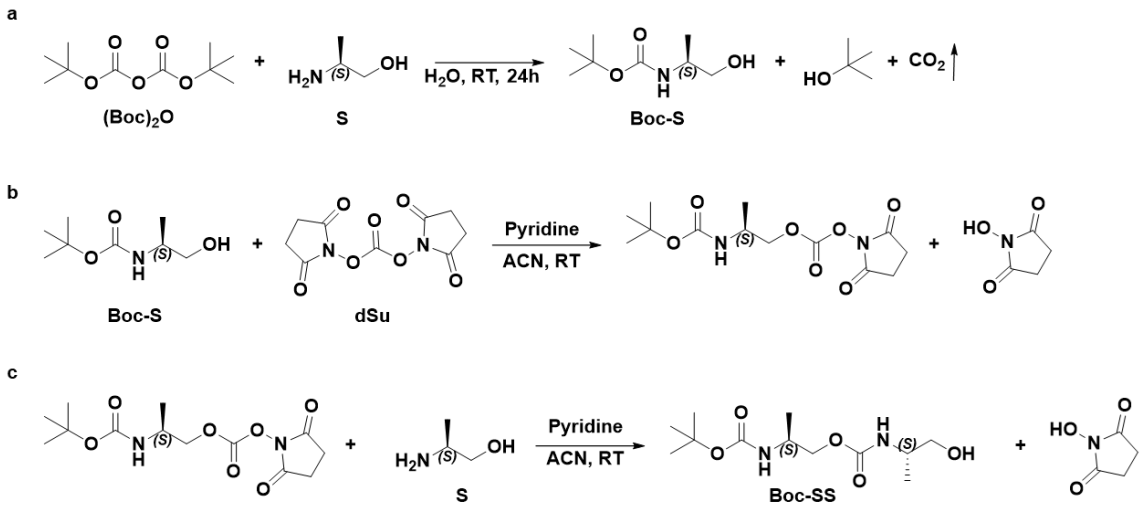

Scheme S1. Synthesis of sequence-defined oligourethanes: **(a)** protection of monomer amino group by di-tert-butyl dicarbonate, **(b)** activation of the hydroxyl group by N, N'-disuccinimidyl carbonate, **(c)** chemoselective coupling of amino alcohol monomer.

1.2.1. Synthesis of O1 SSSS

Protection of (S)-2-amino-1-propanol with Boc group

Protection of (S)-2-amino-1-propanol with Boc group was prepared following a previously described procedure.[3–5] In a round-bottomed flask, 3.20 g (14.6 mmol, 1.1 eq.) of $(Boc)_2O$ was solubilized in 10 mL of H_2O (HPLC grade). (S)-2-aminopropan-1-ol (S) (1.04 mL, 13.3 mmol, 1 eq.) was added to the stirring solution and left to react overnight at room temperature. Once the reaction was completed, the resulting mixture was extracted 3 times with EtOAc (3 times for 20 mL). The organic layer was collected, dried over Na_2SO_4, and the solvent was removed under reduced pressure. The compound was obtained as a white powder with 90% yield.

Chain elongation

(S)-2-Boc-aminopropan-1-ol (Boc-S, 2.28 g, 13.0 mmol, 1 eq.) and of N, N'-disuccinimidyl carbonate (dSu, 3.98 g 15.5 mmol, 1.2 eq.) were subjected to three cycles of nitrogen purging and vacuum to carry out the reaction under an inert atmosphere. Next, 15 mL of anhydrous ACN was added, and a white suspension was formed. Afterward, 6.5 mL (80.8 mmol, 6 eq.) of anhydrous pyridine was added to the reaction mixture. Due to the lack of chromophores, the reaction was not monitored on HPLC, relying on a UV-vis detector. Based on our previous experience,[3–5] both the activation and coupling steps were assumed to take 3 hours. After 3h of activation with dSu, monomer S (1.17 g, 15.6 mmol, 1.2 eq.) was added to the solution. After coupling, the solvent was removed under reduced pressure, and the product was isolated by extraction 3 times with EtOAc (20 mL) and H_2O (60 mL, HPLC grade). The organic layer was collected, dried over Na_2SO_4, and the solvent was removed under reduced pressure. The activation and coupling reactions were repeated three times to obtain tetramer O1 SSSS. The final product was dissolved in a water/acetonitrile mixture and lyophilized, yielding white powder.

1.2.2. Synthesis of oligourethanes O1-O4 and their enantiomers O1`-O4`

The synthetic procedure described for O1 SSSS was applied to fabricate all oligomers O1-O4 and their enantiomers O1`-O4` (Table S1, S2). During the preparation of sequences O4 SRSR and O4' RSRS after coupling of the fourth monomer, the final product was extracted with DCM due to

decreased solubility of tetramers in EtOAc. After final lyophilization, all products were received as white powders.

Table S1. Equivalents of reagents used for the synthesis of O1-O4 and O1`-O4`

Oligourethanes	Monomer S/R[1] (eq)	$(Boc)_2O$[1] (eq)	dSu[2] (eq)	Pyr[2] (eq)	ACN[2] (mL)	Monomer S/R[3] (eq)	I,II,III[4]	IV[4]
O1 SSSS	1	1.1	1.2	6	6	1.2	EtOAc	EtOAc
O1' RRRR	1	1.1	1.2	6	6	1.2	EtOAc	EtOAc
O2 SSSR	1	1.1	1.2	6	6	1.2	EtOAc	EtOAc
O2' RRRS	1	1.1	1.2	6	6	1.2	EtOAc	EtOAc
O3 SRSS	1	1.1	1.2	6	6	1.2	EtOAc	EtOAc
O3' RSRR	1	1.1	1.2	6	6	1.2	EtOAc	EtOAc
O4 SRSR	1	1.1	1.2	6	6	1.2	EtOAc	DCM
O4' RSRS	1	1.1	1.2	6	6	1.2	EtOAc	DCM

[1]Boc protection step was performed using 1-5 g of monomer S or R counted as 1 eq., the amount of other reagents was calculated accordingly; [2]Activation step was performed using 0.5-1 g of monomer Boc-S or Boc-R counted as 1 eq., the amount of other reagents was calculated accordingly, [3] Coupling step;[4] Extraction, organic solvent: ~10 mL/g of starting material, water: ~30 mL/g of starting material; Abbreviations: S - (S)-2-Aminopropan-1-ol, R - (R)-2-Aminopropan-1-ol, Boc - tert-butyloxycarbonyl protecting group, dSu - N, N'-disuccinimidyl carbonate, Pyr – pyridine, ACN – acetonitrile, EtOAc – ethyl acetate, DCM - dichloromethane.

Table S2. Stepwise and overall yields of oligourethane syntheses

O1 SSSS	
Reaction step	**Stepwise yield [%]**
I coupling	91
II coupling	87
III coupling	83
Overall yield 66%	
O1' RRRR	
Reaction step	**Stepwise yield [%]**
I coupling	88
II coupling	88
III coupling	75
Overall yield 58%	
O2 SSSR	
Reaction step	**Stepwise yield [%]**
I coupling	86
II coupling	84
III coupling	77
Overall yield 56%	
O2' RRRS	
Reaction step	**Stepwise yield [%]**
I coupling	95
II coupling	94
III coupling	83
Overall yield 74%	
O3 SRSS	
Reaction step	**Stepwise yield [%]**
I coupling	94
II coupling	97
III coupling	85
Overall yield 77%	

O3' RSRR	
Reaction step	**Stepwise yield [%]**
I coupling	99.5
II coupling	82.3
III coupling	92.4
Overall yield 75%	
O4 SRSR	
Reaction step	**Stepwise yield [%]**
I coupling	99.5
II coupling	76.3
III coupling	85.5
Overall yield 64%	
O4' RSRS	
Reaction step	**Stepwise yield [%]**
I coupling	98.7
II coupling	77.3
III coupling	63.2
Overall yield 48%	

Abbreviations: S - (S)-2-Aminopropan-1-ol, R - (R)-2-Aminopropan-1-ol, stepwise yield determined by gravimetric analysis.

2. METHODS

2.1. Nuclear Magnetic Resonance (NMR)

^{1}H NMR spectra of oligomers were recorded in deuterated chloroform (99.8 atom % D, Sigma Aldrich) using the Avance III HD 600 MHZ NMR Spectrometer (BRUKER) equipped with probes: BBI and BBO. Before analyses, crude oligomers were recrystallized from a water/ACN mixture and dried using a high-vacuum pump. The recorded spectra were calibrated according to the chloroform signal (7.28 ppm) and evaluated in MNova software.

2.2. Liquid Chromatography-Mass Spectrometry (LC-MS)

The measurements of crude oligomers were performed on a high-resolution Q-ToF spectrometer, maXis impact (Bruker Daltonics, Germany), equipped with an electrospray ionization (ESI) source and connected to a Dionex UltiMate 3000 RSLC (Thermo Scientific, USA) ultrahigh-performance liquid chromatography system. The chromatographic separations were carried out on Syncronis C18 100 x 2.1 mm × 1.7 μm column (Thermo Scientific) in a gradient mode with a column oven set to 40°C. Mobile phase A was 0.1% formic acid (FA, 99-100%, VWR) in water (LC-MS grade, Merck), and mobile phase B was 0.1% FA in ACN (LC-MS grade, Merck). The gradient started with 5% of mobile phase B and was held on 5% B for 1 min, reached 80% B in 21 min, and 95% B in 21.5 min, was held on 95% B for another 5 min, and in the end, the column was stabilized on 5% B for another 3 min.

The spectrometer operated in automatic MS/MS (DDA) mode with the maximum number of precursors set to 3, the intensity cutoff threshold of 50 000 units, and active precursor exclusion after 5 MS/MS spectra. The ESI source parameters were set as follows: end plate offset 0.5 kV, capillary voltage 4 kV, nebulizing gas 2 bar, drying gas 8.0 L/min, and dry gas temperature 220°C. Measurements in MS mode were performed with an ion energy of 5.0 eV, collision energy of 7.5 eV, collision RF of 500 Vpp, transfer time of 80 μs, pre-pulse storage of 8 μs, and low mass cutoff of 50 m/z. In MS/MS mode, ions from 50 m/z up to 1500 m/z were selected, and collision energy varied depending on precursor ion m/z and charge (for mainly observed 1^{+} charge values were set to 25 eV for 500 m/z, 35 eV for 1000 m/z, 45 eV for 1500 m/z). An internal calibration segment

was added at the beginning of each chromatographic run. Spectra were calibrated using sodium formate clusters in HPC mode with SD < 1 ppm.

For LC-MS/MS analyses, the oligourethane samples were dissolved in water: acetonitrile (H_2O: ACN) mixture. The resulting stock solutions had a concentration of 2 mg/mL. The stock solutions were then diluted to a final concentration of 50 µg/ml with a 1:1 H_2O: ACN solution containing 0.1% formic acid. 2 µl of each diluted sample was used for injection into the LC-MS system. The data were analyzed with Data Analysis 4.1 software. Molecular formulas corresponding to parent and fragment ions were generated using the SmartFormula algorithm with the maximum admissible error of 5 ppm.

2.3. Size Exclusion Chromatography (SEC)

The uniform structure of crude oligourethanes was confirmed by SEC analyses. The SEC setup consists of an Agilent system equipped with UV (260-700 nm), and RI detectors, and mixed PLGel E 3 µm, 300 x 7.5 mm column. For analysis, THF (HPLC grade, BHT stabilized, Chemsolute) was used as the mobile phase (0.5 mL/min flow rate).

2.4. Infrared and vibrational circular dichroism (IR/VCD)

Infrared and VCD spectra for O1, O2, O3, and O4 systems, along with their respective enantiomers in solution, were recorded in the 1000−1800 cm^{-1} range using a Fourier Transform Infrared (FTIR) spectrometer (Tensor 27 Bruker) coupled with a Vibrational Circular Dichroism (VCD) module (PMA 50 Bruker). Prior to analyses, oligomers were reprecipitated in water and dried. The spectra's clarity was enhanced by modulating the chirality of the circularly polarized light with a Hinds PEM 90 photoelastic modulator (PEM), set to a λ/4 retardation at a central frequency of 1400 cm^{-1} and utilizing a lock-in amplifier (SR830 DSP) for demodulation. An optical low-pass filter (800−2000 cm^{-1}) was installed before the PEM to improve the signal-to-noise ratio. Each solution was prepared in deuterated chloroform (99.80% D, Eurisotop) at a concentration of 15 mM. Spectra were gathered over 8 hours (34,080 scans) with a spectral resolution of 4 cm^{-1}. For baseline comparison, the average VCD spectra of the two enantiomers per system were used (as shown in Fig. 3c). The experiment was conducted at 300 K. In addition to the VCD measurements, IR spectra in the broader range of 1000−3600 cm^{-1} were recorded under similar conditions but with a replaced optical filter (800−4000 cm^{-1}). This time a finer spectral resolution of 2 cm^{-1} over 100 scans was

used. All the spectra were acquired in a sealed 200 μm path-length cell with calcium fluoride (CaF_2) windows.

2.5. Theoretical Methods

The approach utilized in this study is an extension of the methodology previously established and validated through research on carbamate (urethane) monomers, specifically Boc-2-aminopropan-1-ol.[6] Hence, an overview will be presented herein. The structural diversity of the O1, O2, O3, and O4 systems was obtained via a conformational analysis conducted with the conformational search functionality within the Maestro software suite.[7] This analysis employed a hybrid strategy combining torsional and low-mode sampling techniques within a chloroform solvent environment. The Generalized-Born/Surface-Area (GB/SA) model was employed to account for solvent effects. Molecular interactions were quantitatively assessed using the Optimized Potentials for Liquid Simulations (OPLS)-2005 force field.[8] After this, energy minimization was achieved through the Polak-Ribière Conjugate Gradient (PRCG) algorithm.[9] Initial molecular geometry per system was derived following an optimization process that leveraged chemical intuition to refine a molecular sketch. An energy threshold of 10.02 kcal/mol was established to guide the selection of conformers for further analysis. This approach gives around 300 distinct, enantiomerically non-superimposable conformations per system, highlighting the conformational diversity. All the geometries underwent further optimization utilizing Density Functional Theory (DFT) incorporated within the Gaussian 16 program. Subsequently, vibrational analyses were executed at an identical theoretical level. Initially, the B3LYP hybrid functional paired with Pople's basis set, particularly the 6-31g(d,p), was selected. Empirical D3 dispersion corrections were included. The simulation of solvation effects, with chloroform as the solvent, was facilitated by employing the Polarizable Continuum Model (PCM). This computational strategy denoted as B3LYP-D3/6-31g(d,p)/PCM, is herein referred to as LLT (Low-Level Theory). Subsequently, the structures were evaluated based on their Gibbs free energy under Standard Ambient Temperature and Pressure (SATP) conditions, selecting the 20 most stable for further analysis employing an expanded basis set, B3LYP-D3/6-311g++(d,p)/PCM, henceforth termed as HLT (High-Level Theory). These theoretical approaches have undergone prior validation against experimental data on carbamate monomers. For both LLT and HLT, the IR and VCD spectra at absolute zero were obtained through the convolution of the calculated transition dipole moments and rotatory strengths across frequencies. This convolution

employed a Lorentzian distribution characterized by a 10 cm^{-1} full-width at half-maximum (FWHM). Mode-specific scaling factors were applied to the theoretical calculations at each level of theory to address the limitations posed by basis set incompleteness, anharmonic effects, and solvent interactions. These scaling factors were adopted from prior research, wherein they were precisely calibrated against the experimental IR absorption spectra of the carbamate monomer. For the HLT, scaling factors of 0.988, 0.960, and 0.962 were utilized for the fingerprint and amide I and II regions, the CH stretching regions, and the NH and OH stretching regions, respectively. Conversely, within the LLT, the corresponding regions were adjusted with scaling factors of 0.990, 0.952, and 0.952.

We modeled the experimental VCD spectrum $y(\tilde{\nu})$ as a non-negative linear combination of conformer-resolved theoretical spectra with shared line-shape and frequency-scaling factors. For each conformer c, sticks at unscaled DFT wavenumbers $\tilde{\nu}_{ck}^{0}$ with rotatory strengths R_{ck} were broadened with a unit-area Voigt profile $V(\tilde{\nu}; \mu, \sigma, \gamma)$, using Gaussian and Lorentzian FWHM parameters ω_G and ω_L $\left(\sigma = \omega_G/[2\sqrt{2\ln 2}],\ \gamma = \omega_L/2\right)$. Line centers were piecewise frequency-scaled before convolution: $\mu_{ck} = sf_r\, \tilde{\nu}_{ck}^{0}$ with $sf_r = s_1$ for 1800–1600 cm^{-1} and $sf_r = s_2$ for 1600–1200 cm^{-1}. The conformer spectrum is $S_c(\tilde{\nu}) = \sum_k R_{ck}\, V(\tilde{\nu}; \mu_{ck}, \sigma, \gamma)$, and the model is $M(\tilde{\nu}) = \sum_{c=1}^{C} a_c\, S_c(\tilde{\nu}) + b(\tilde{\nu})$, where $a_c \geq 0$ are conformer amplitudes and $b(\tilde{\nu})$ is an optional low-order polynomial baseline. Parameters $\{a_c\}_{c=1}^{C}$, s_1, s_2, w_G, and $w_L$were obtained by weighted least squares, minimizing $\sum_i w_i\, [y(\tilde{\nu}_i) - M(\tilde{\nu}_i)]^2$ (non-negativity on a_c; simplex normalization is enforced by $\sum_c a_c = 1$). This formulation jointly optimizes amplitudes, the two frequency-scaling factors, and Gaussian/Lorentzian widths while keeping the Voigt kernel normalized, ensuring comparability of amplitudes across fits.

Intramolecular interactions within the studied molecules were elucidated and investigated employing the Non-Covalent Interaction (NCI) technique. This method is explained in various literature sources and is recognized for its effectiveness in analyzing molecular interactions. Essentially, the NCI technique is a topological approach that assesses the electron density (ρ) and its reduced gradient (s(ρ)) within areas characterized by weak electron densities and minimal reduced gradients. The electron density data, crucial for this analysis, was derived from the self-consistent field (SCF) wavefunction and obtained post geometry optimization utilizing the HLT

approach. To visualize these interactions, isosurfaces of s(ρ) were generated. These visual representations were color-coded using an RGB color map, which reflects the sign of the second eigenvalue (λ2) of the Hessian matrix, adjusted by the electron density value (ρ). Specifically, isosurfaces appearing in reddish tones denote regions of repulsive interactions (where $\lambda 2 > 0$), those in bluish tones indicate zones of attractive (favorable) interactions (where $\lambda 2 < 0$), and greenish tones highlight areas of weak, delocalized interactions (where $\lambda 2 \approx 0$). The visualization of these isosurfaces was facilitated through VMD (Visual Molecular Dynamics) software.

2.6. Differential scanning calorimetry (DSC)

DSC measurements were conducted using a Mettler Toledo Differential Scanning Calorimeter under a nitrogen atmosphere (50 mL/min) within a temperature range of -50 °C to 200 °C. Before the DSC analyses, samples were recrystallized from a water/ACN mixture and dried using a high-vacuum pump. To unify sample histories, all oligomers were heated in an oil bath at 100 °C under vacuum for 10 minutes and then cooled to RT. Approximately 3 mg of each sample was loaded into an aluminum pan. Indium was used as the reference material. Three heating-cooling-heating cycles were performed at a rate of 10 K/min for both heating and cooling.

2.7. Crystallography analyses

X-ray measurement of O3 SRSS oligourethane was done using a Rigaku XtaLAB Synergy DW single-crystal diffractometer with a HyPix-Arc 150° detector and an Oxford Cryosystems temperature control system. CuKα radiation was used (wavelength 1.5418 Å), and the measurement was carried out at 250 K. The reason for not measuring at 100 K was that the crystals underwent a phase transition below 250 K, resulting in a loss of diffraction. The measured crystal of O3 SRSS oligourethane was obtained by slow evaporation of a 1:1 MeOH/EtOH mixture at room temperature.

Data reduction was performed using CrysAlisPRO, whereas structure solution and refinement were done using SHELXT and SHELXL, respectively.[10] Hydrogen bond determination was additionally aided by the use of PLATON.[11] The CIF file of the new structure was verified with CheckCIF. Micro electron diffraction (MicroED) of O4 SRSR oligourethane was done by collecting data on a Tecnai G2 sphera equipped with a cheetah D detector. The crystal was cooled at liquid nitrogen temperature during the measurement, to decrease radiation damage.

RESULTS AND DISCUSSION

3.1. Synthesized oligourethanes and their characterization

Table S3. Summary of obtained oligomers

Sequence[a]	Molar mass[b]	m/z[c]	Overall yield [%][d]	Scale [g][e]
O1 SSSS	478.26	479.2713	66	0.58
O1' RRRR	478.26	479.2712	58	0.52
O2 SSSR	478.26	479.2713	56	0.53
O2' RRRS	478.26	479.2717	74	0.20
O3 SRSS	478.26	479.2717	77	0.43
O3' RSRR	478.26	479.2712	75	0.40
O4 SRSR	478.26	479.2715	64	0.45
O4' RSRS	478.26	479.2712	48	0.17

[a]Abbreviations: S: (S)-2-Aminopropan-1-ol, R: (R)-2-Aminopropan-1-ol; [b]calculated molar mass, [c]mass determined from HR-MS for $[M+H]^+$ with calculated m/z=479.2717; [d] overall yield; [e]mass of the obtained product.

3.2. Liquid chromatography-mass spectrometry (LC-MS)

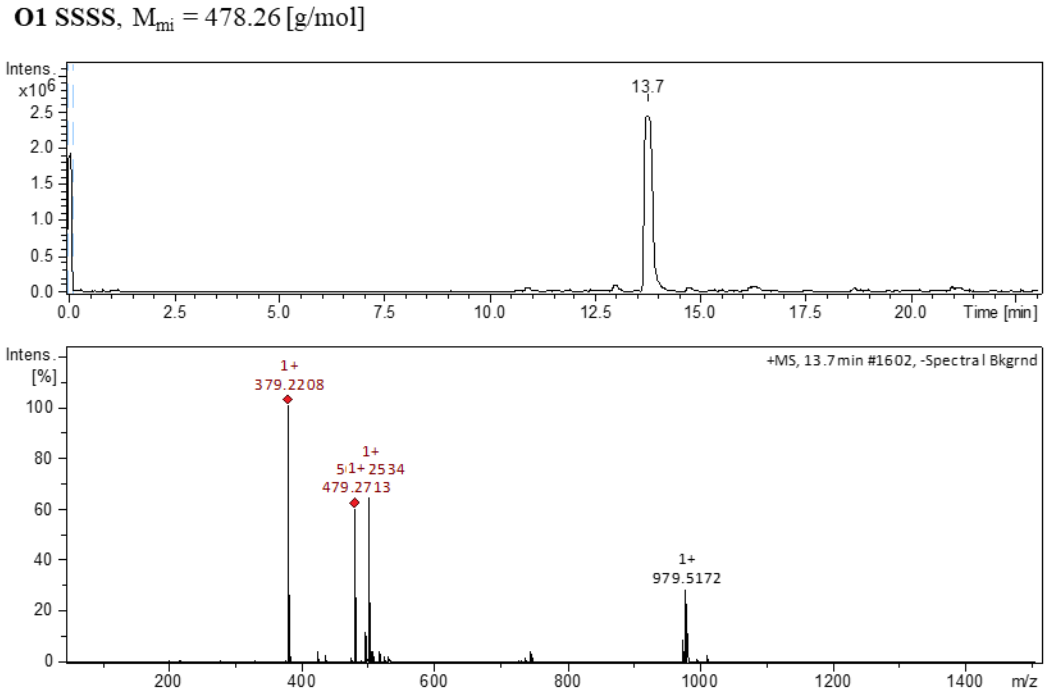

Figure S1. LC-MS characterization of crude **O1 SSSS.** The main signal at LC-MS base peak chromatogram (BPC) corresponds to the product **O1**. It appears in the spectrum as adducts: $[M\text{-Boc+H}]^+$ (m/z=379.22), $[M+H]^+$ (m/z=479.27), $[M+Na]^+$ (m/z=501.25) and [2M+Na] (m/z=979.52).

O1` RRRR, M_{mi} = 478.26 [g/mol]

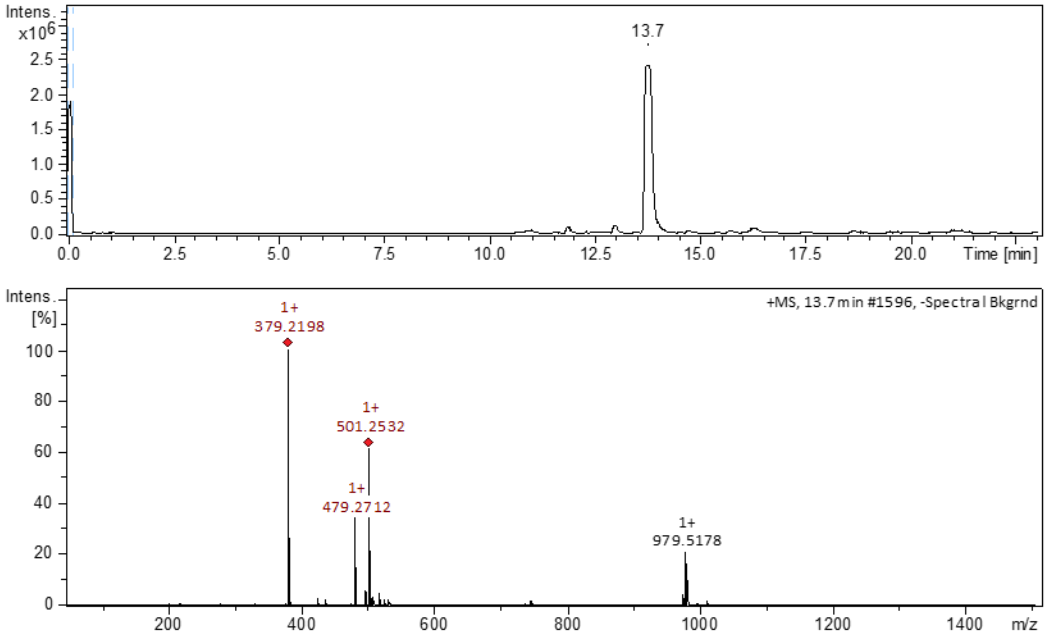

Figure S2. LC-MS characterization of crude **O1` RRRR.** The main signal at LC-MS base peak chromatogram (BPC) corresponds to the product **O1`**. It appears in the spectrum as adducts: $[M\text{-}Boc+H]^+$ (m/z=379.22), $[M+H]^+$ (m/z=479.27), $[M+Na]^+$ (m/z=501.25) and [2M+Na] (m/z=979.52).

O2 SSSR, M_{mi} = 478.26 [g/mol]

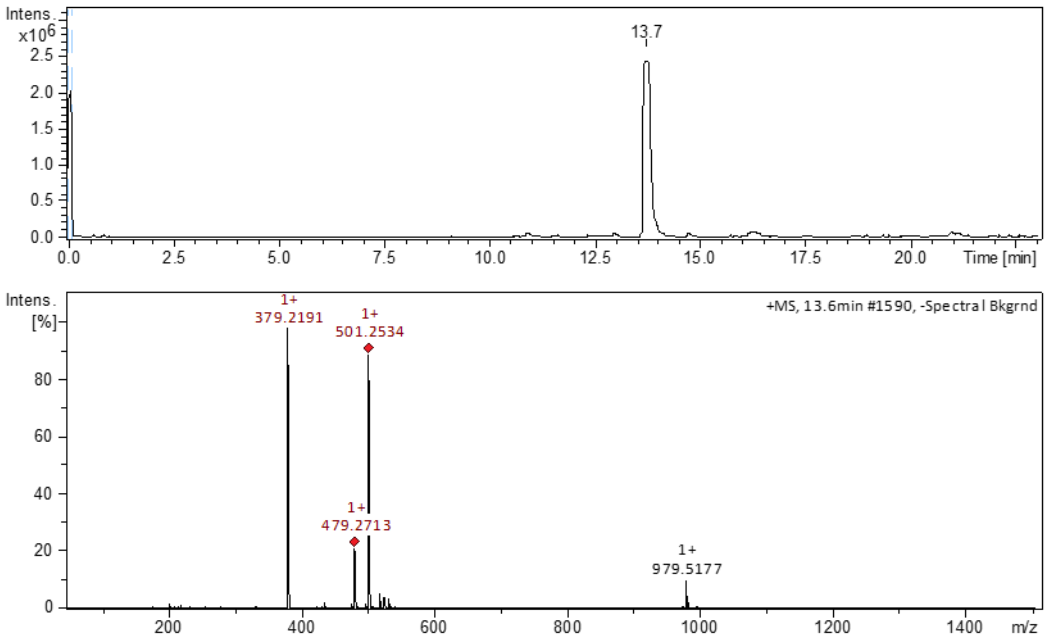

Figure S3. LC-MS characterization of crude **O2 SSSR.** The main signal at LC-MS base peak chromatogram (BPC) corresponds to the product **O2**. It appears in the spectrum as adducts: $[M\text{-}Boc+H]^+$ (m/z=379.22), $[M+H]^+$ (m/z=479.27), $[M+Na]^+$ (m/z=501.25) and [2M+Na] (m/z=979.52).

O2` RRRS, M_{mi} = 478.26 [g/mol]

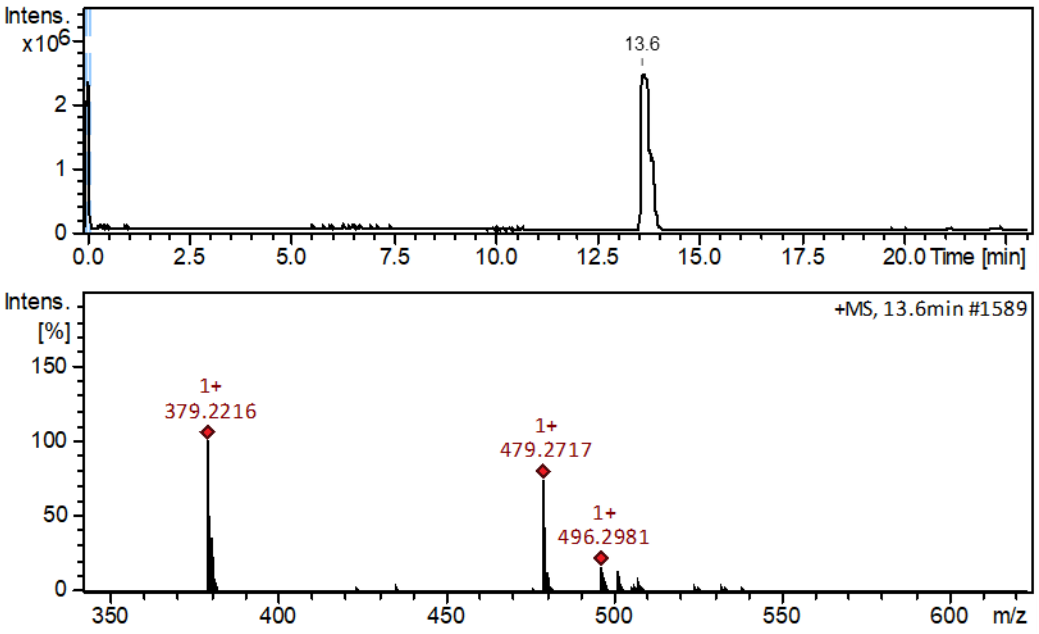

Figure S4. LC-MS characterization of crude **O2' RRRS.** The main signal at LC-MS base peak chromatogram (BPC) corresponds to the product **O2`**. It appears in the spectrum as adducts: $[M\text{-Boc+H}]^+$ (m/z=379.22), $[M+H]^+$ (m/z=479.27), $[M+NH_4]^+$ (m/z=496.30).

O3 SRSS, M_{mi} = 478.26 [g/mol]

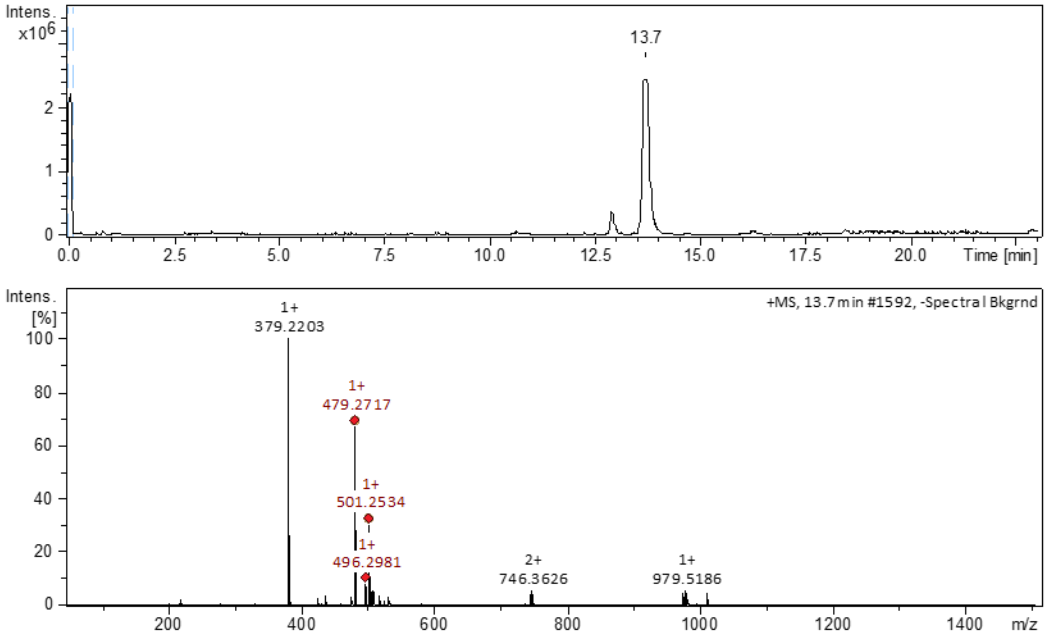

Figure S5. LC-MS characterization of crude **O3 SRSS.** The main signal at LC-MS base peak chromatogram (BPC) corresponds to the product **O3**. It appears in the spectrum as adducts: $[M\text{-}Boc+H]^+$ (m/z=379.22), $[M+H]^+$ (m/z=479.27), $[M+Na]^+$ (m/z=501.25) and [2M+Na] (m/z=979.52).

O3` RSRR, M_{mi} = 478.26 [g/mol]

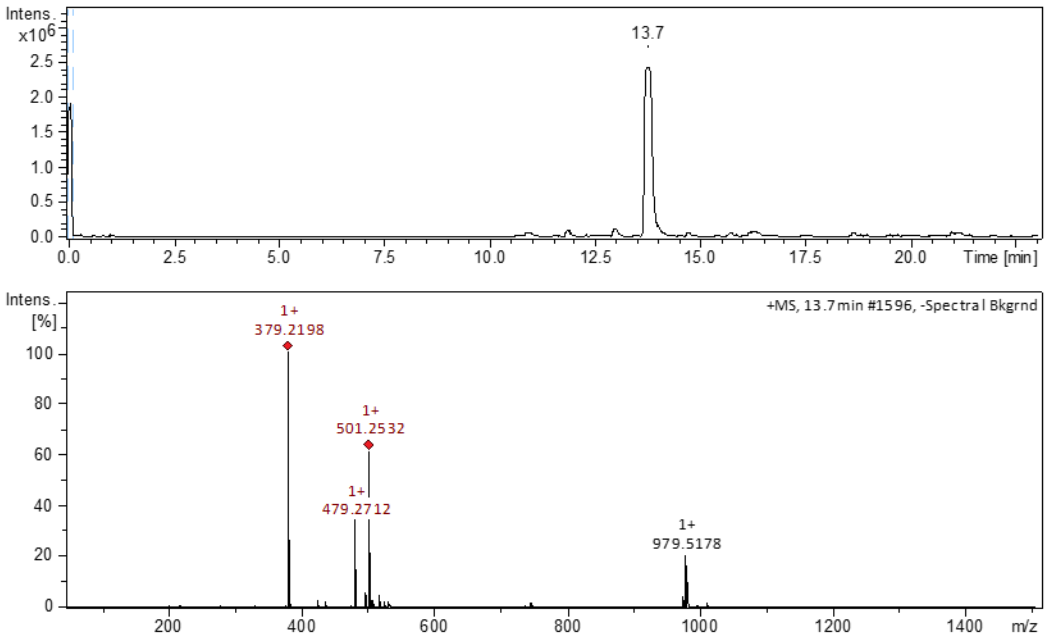

Figure S6. LC-MS characterization of crude **O3' RSRR.** The main signal at LC-MS base peak chromatogram (BPC) corresponds to the product **O3`**. It appears in the spectrum as adducts: $[M\text{-}Boc+H]^+$ (m/z=379.22), $[M+H]^+$ (m/z=479.27), $[M+Na]^+$ (m/z=501.25) and [2M+Na] (m/z=979.52).

O4 SRSR, M_{mi} = 478.26 [g/mol]

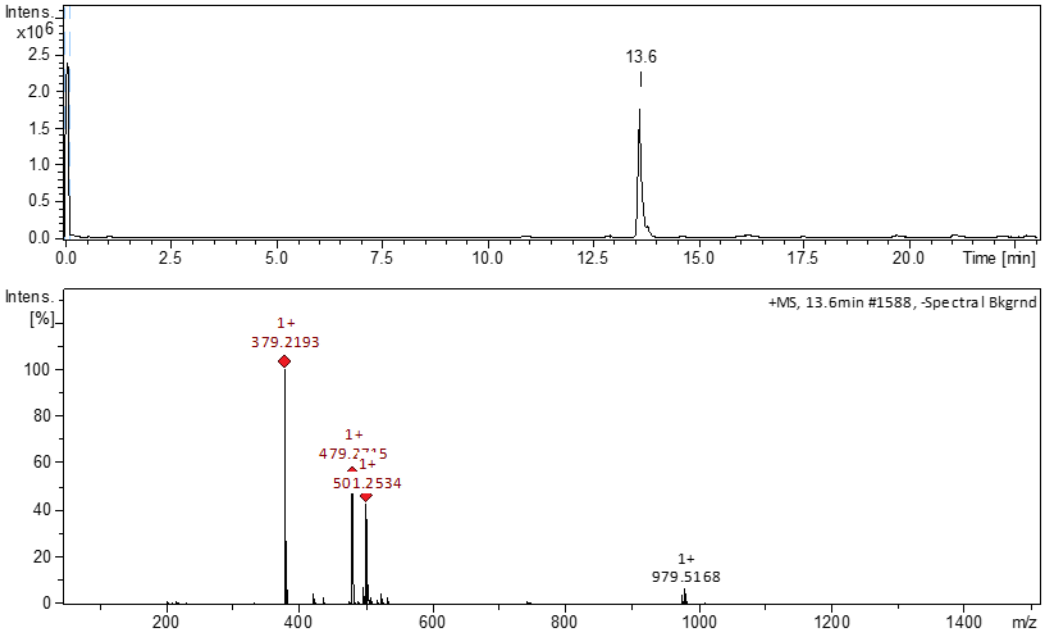

Figure S7. LC-MS characterization of crude **O4 SRSR.** The main signal at LC-MS base peak chromatogram (BPC) corresponds to the product **O4**. It appears in the spectrum as adducts: $[M\text{-}Boc+H]^+$ (m/z=379.22), $[M+H]^+$ (m/z=479.27), $[M+Na]^+$ (m/z=501.25) and [2M+Na] (m/z=979.52).

O4` RSRS, M_{mi} = 478.26 [g/mol]

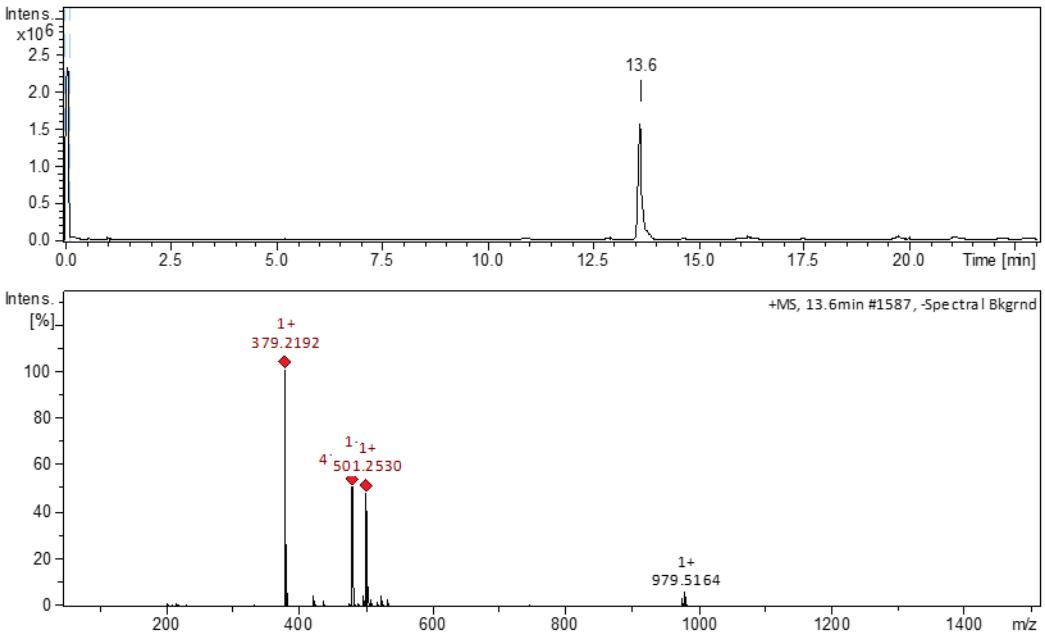

Figure S8. LC-MS characterization of crude **O4' RSRS.** The main signal at LC-MS base peak chromatogram (BPC) corresponds to the product **O4`**. It appears in the spectrum as adducts: $[M\text{-Boc+H}]^+$ (m/z=379.22), $[M+H]^+$ (m/z=479.27), $[M+Na]^+$ (m/z=501.25) and [2M+Na] (m/z=979.52).

3.3. Size exclusion chromatography (SEC)

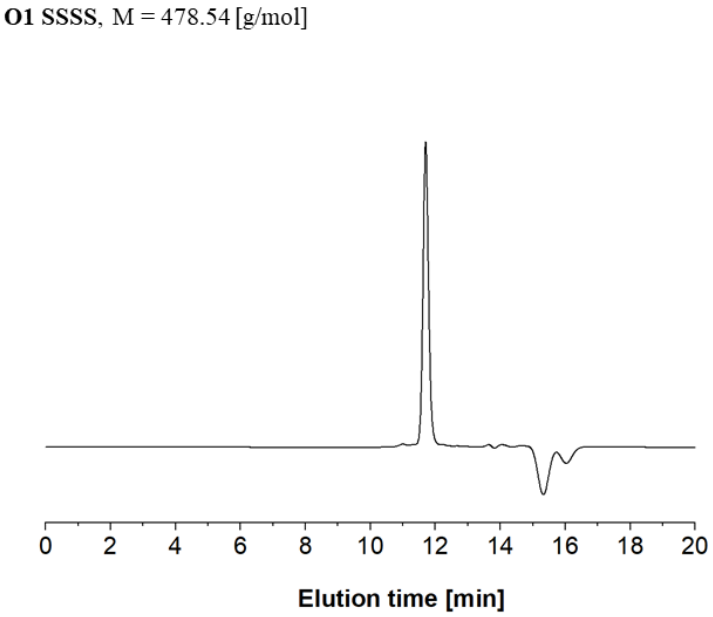

Figure S9. SEC chromatogram of **O1 SSSS** in THF**,** refractive index trace (RI).

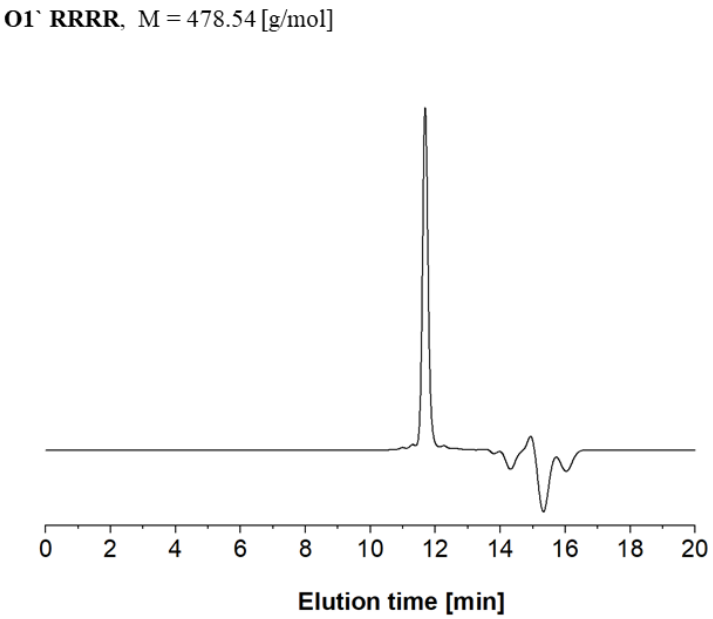

Figure S10. SEC chromatogram of **O1` RRRR** in THF**,** refractive index trace (RI).

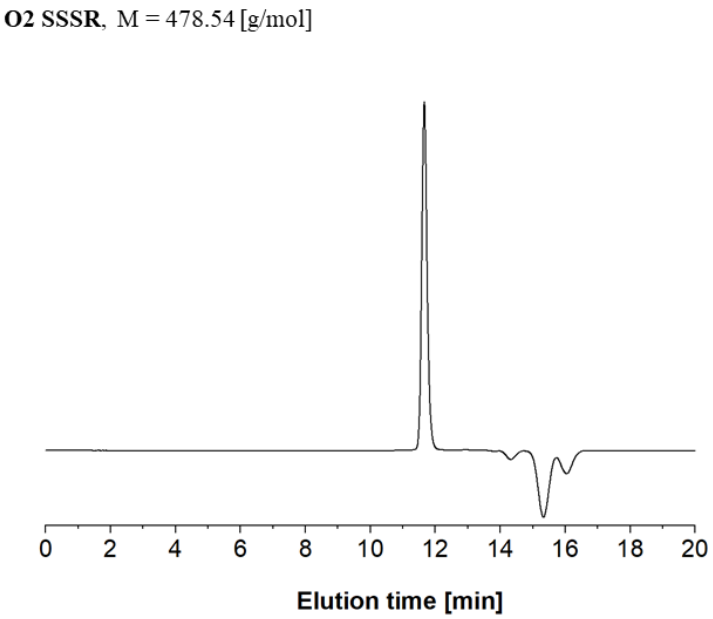

Figure S11. SEC chromatogram of **O2 SSSR** in THF**,** refractive index trace (RI).

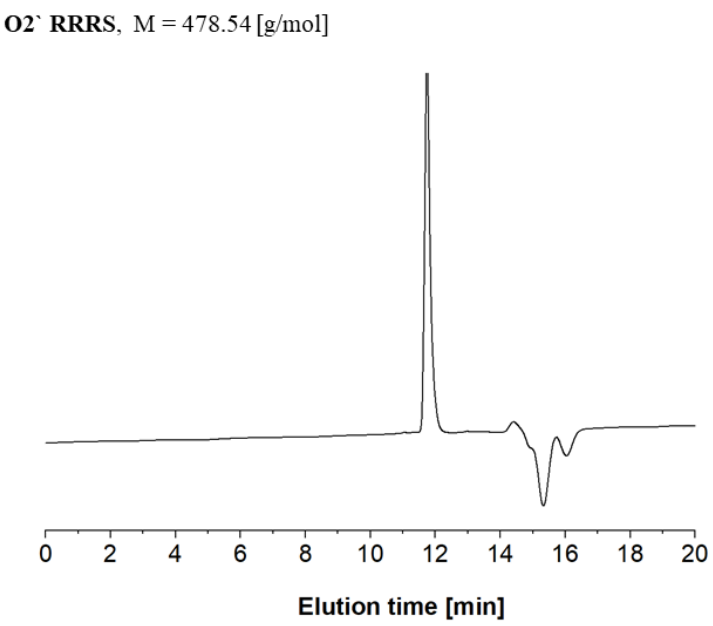

Figure S12. SEC chromatogram of **O2` RRRS** in THF**,** refractive index trace (RI).

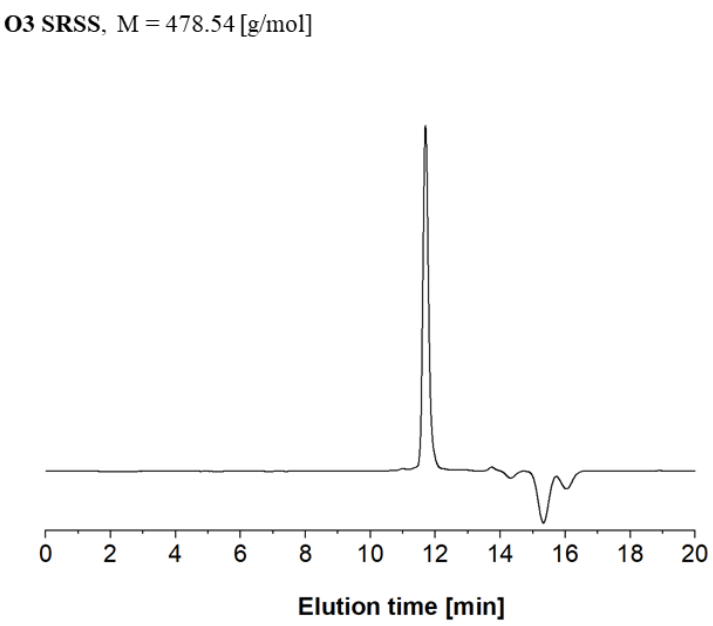

Figure S13. SEC chromatogram of **O3 SRSS** in THF**,** refractive index trace (RI).

O3` RSRR, M = 478.54 [g/mol]

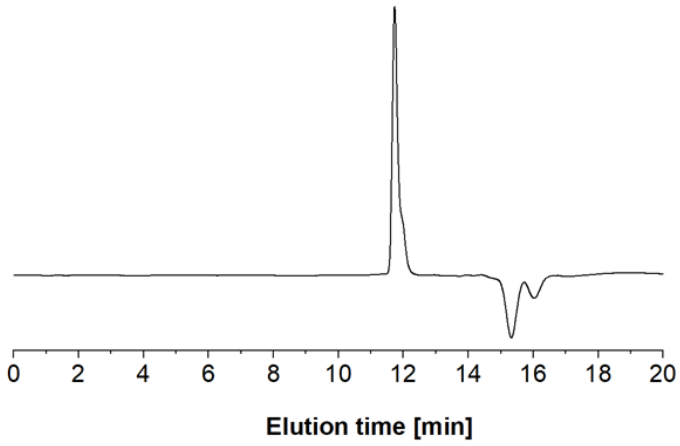

Figure S14. SEC chromatogram of **O3` RSRR** in THF**,** refractive index trace (RI).

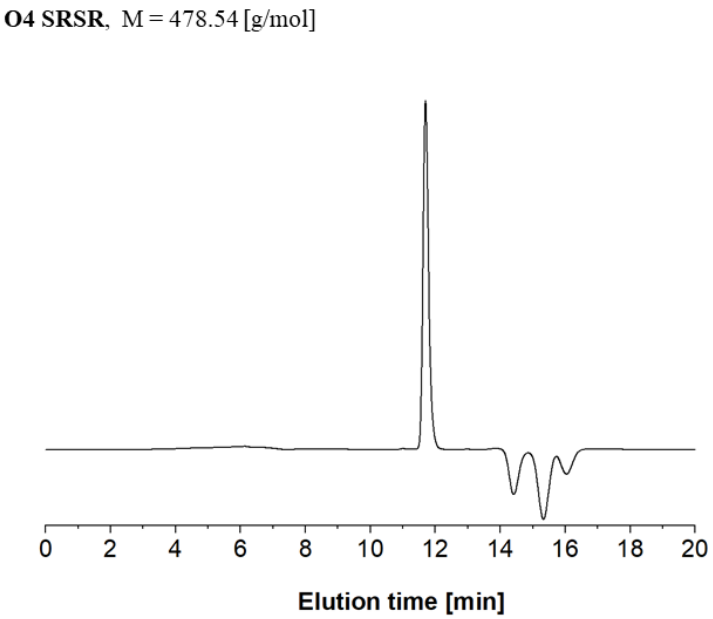

Figure S15. SEC chromatogram of **O4 SRSR** in THF**,** refractive index trace (RI).

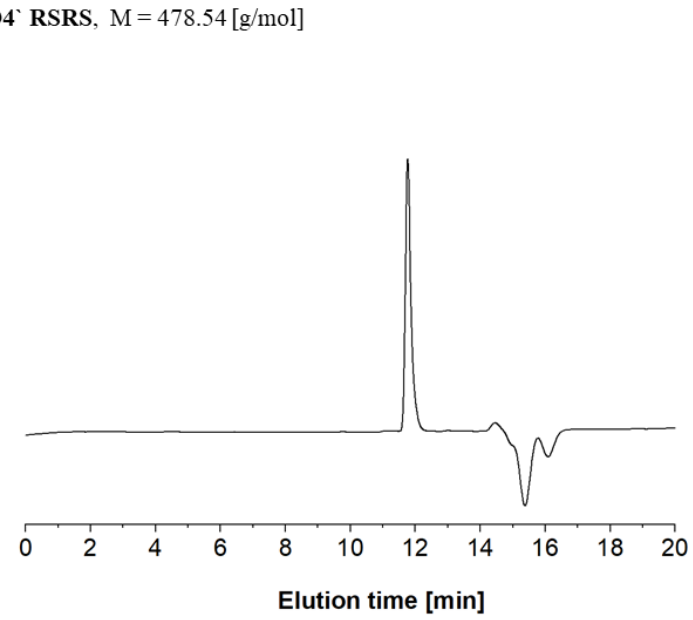

Figure S16. SEC chromatogram of **O4` RSRS** in THF**,** refractive index trace (RI).

3.4. ^{1}H Nuclear magnetic resonance spectroscopy (NMR)

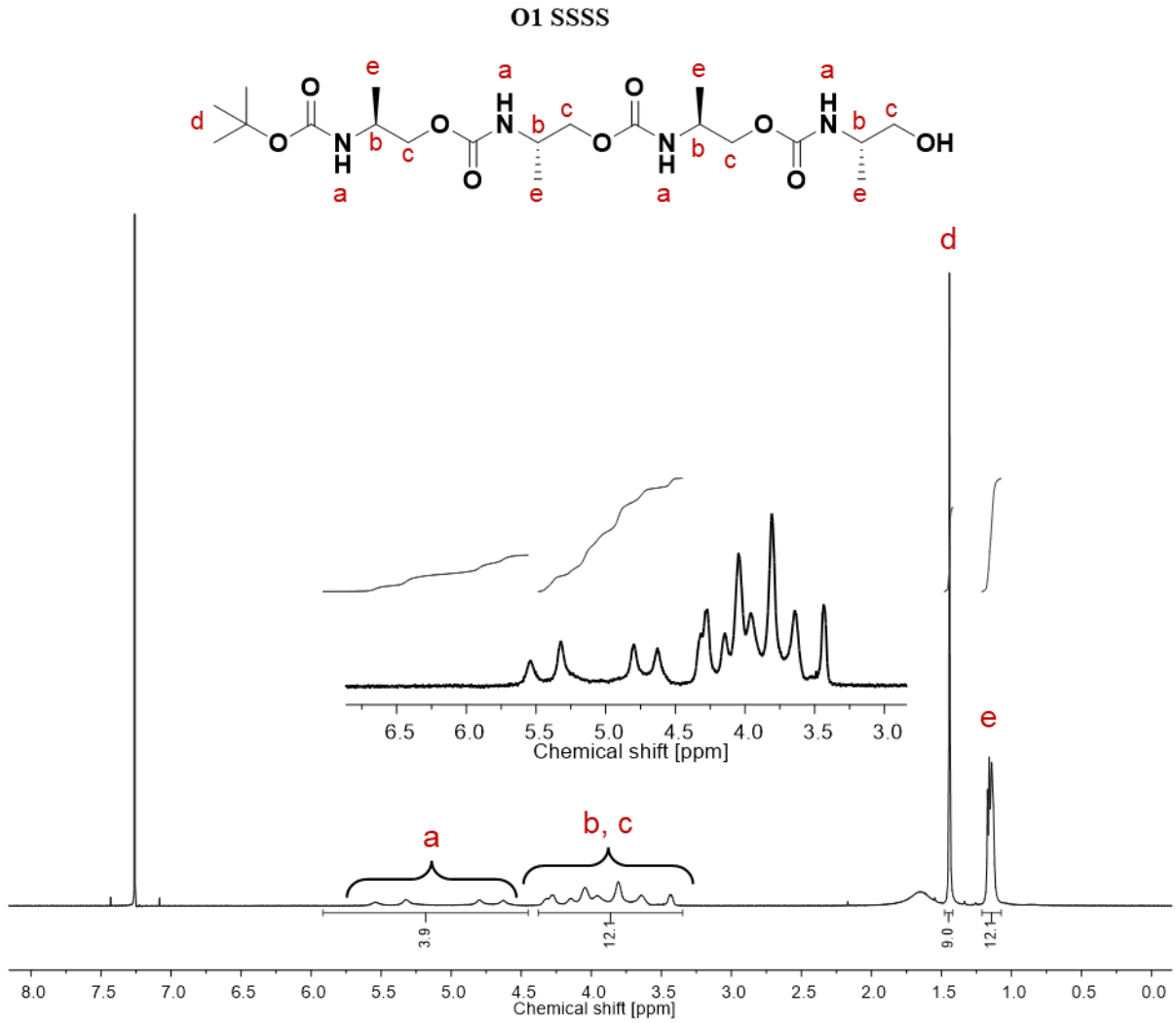

Figure S17. ^{1}H NMR spectrum of **O1 SSSS** recorded at RT, 5 mM concentration in $CDCl_3$.

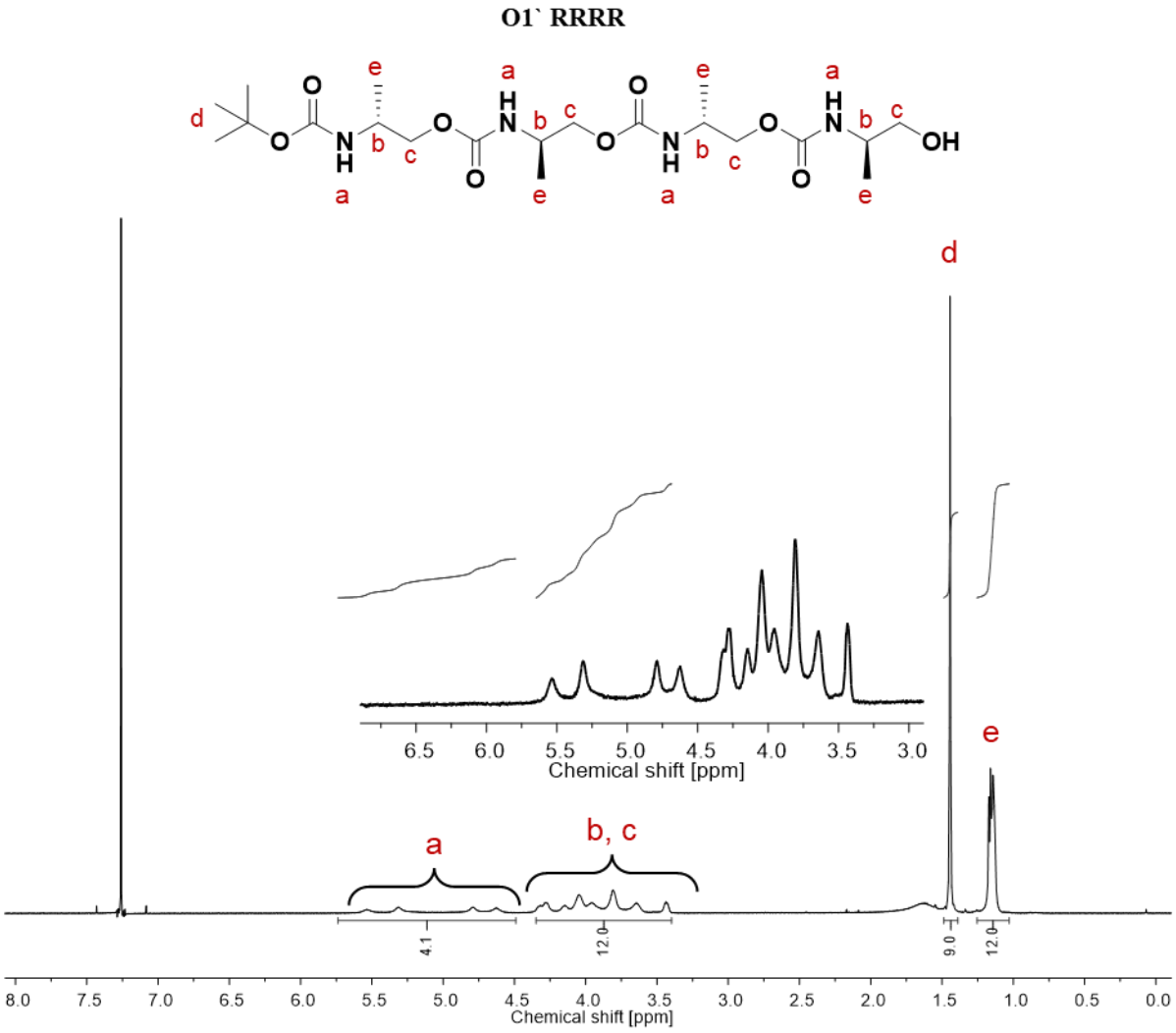

Figure S18. ^{1}H NMR spectrum of **O1` RRRR** recorded at RT, 5 mM concentration in $CDCl_3$.

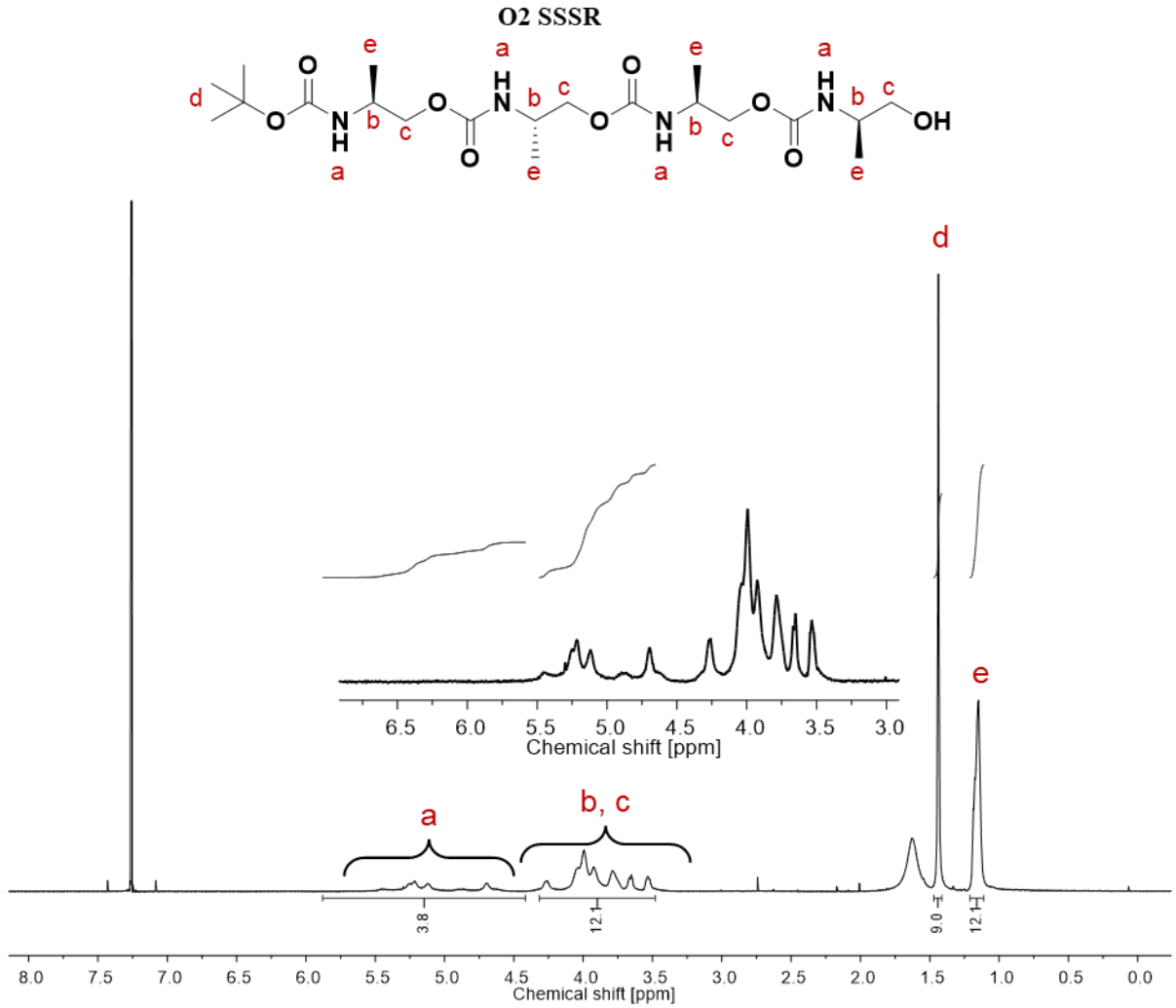

Figure S19. ^{1}H NMR spectrum of **O2 SSSR** recorded at RT, 5 mM concentration in $CDCl_3$.

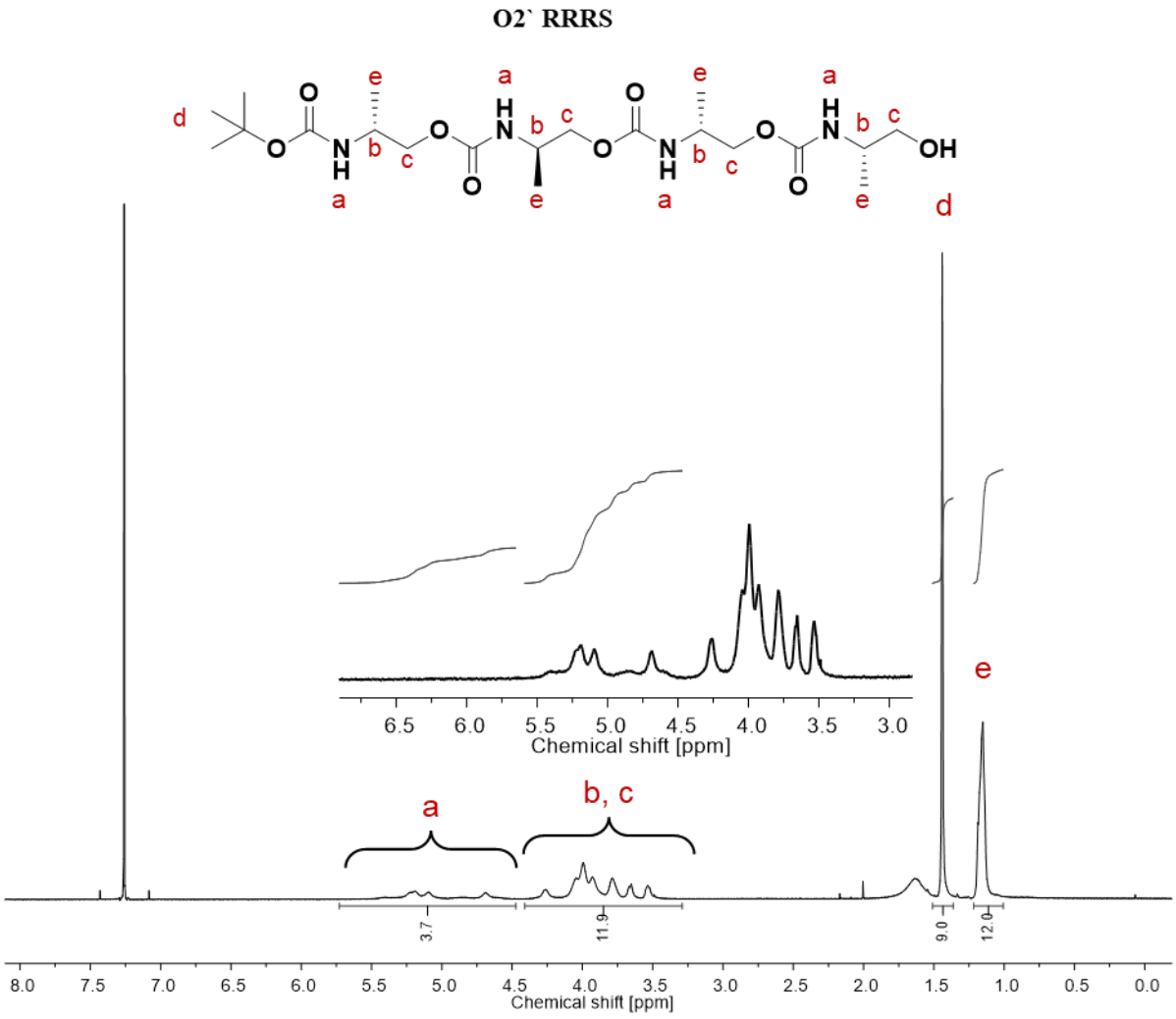

Figure S20. ^{1}H NMR spectrum of **O2` RRRS** recorded at RT, 5 mM concentration in $CDCl_3$.

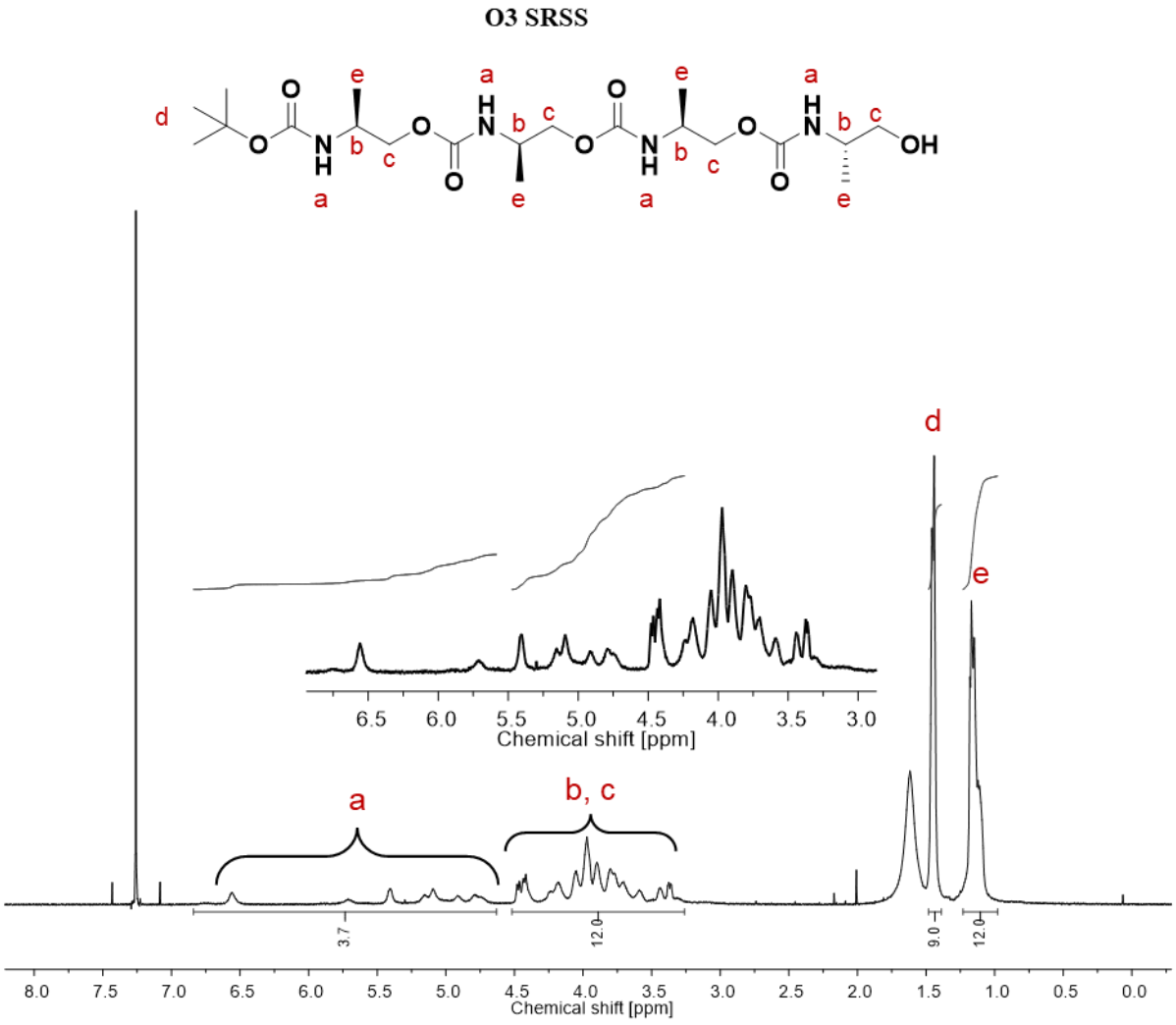

Figure S21. ^{1}H NMR spectrum of **O3 SRSS** recorded at RT, 5 mM concentration in $CDCl_3$.

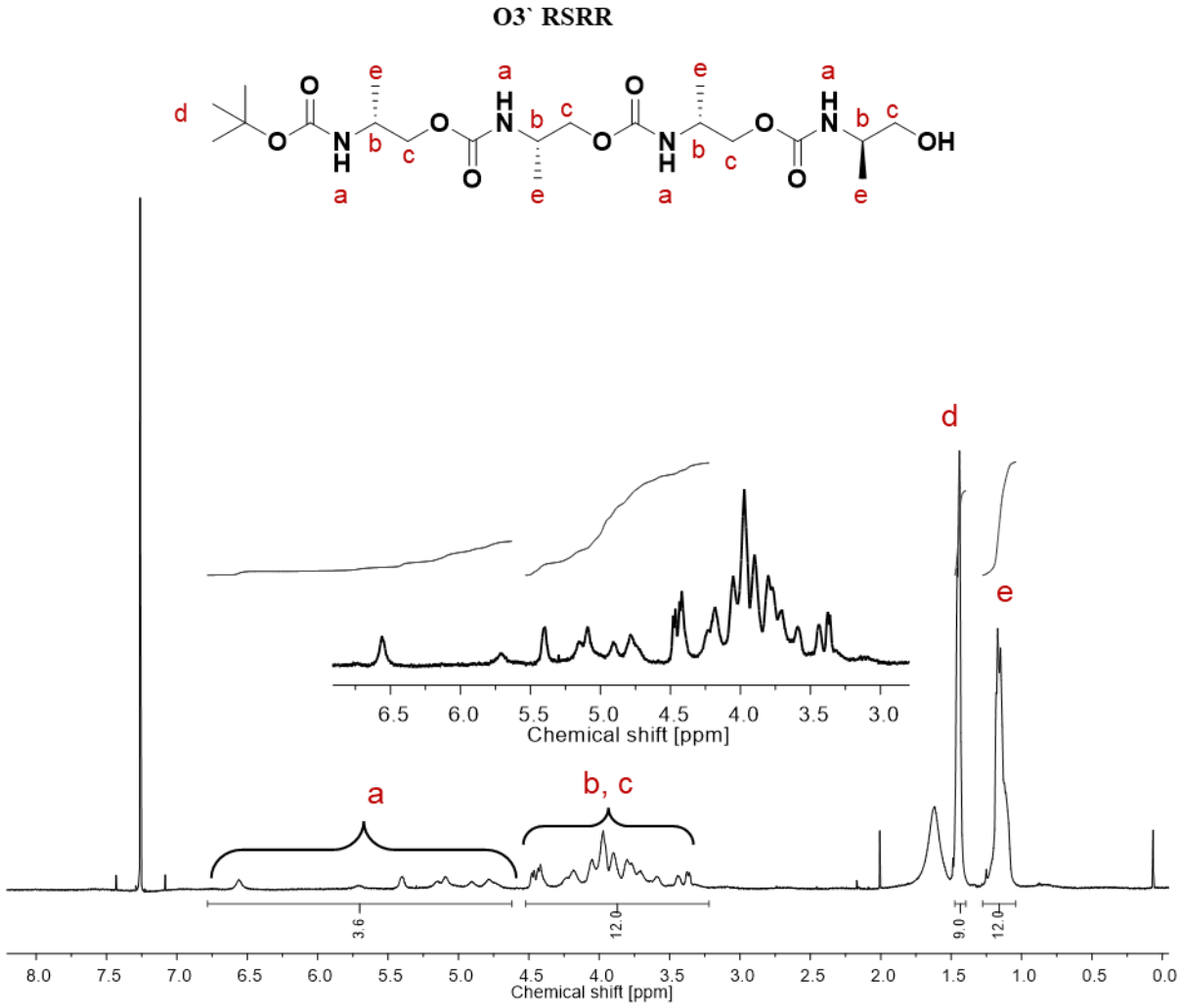

Figure S22. ^{1}H NMR spectrum of **O3` RSRR** recorded at RT, 5 mM concentration in $CDCl_3$.

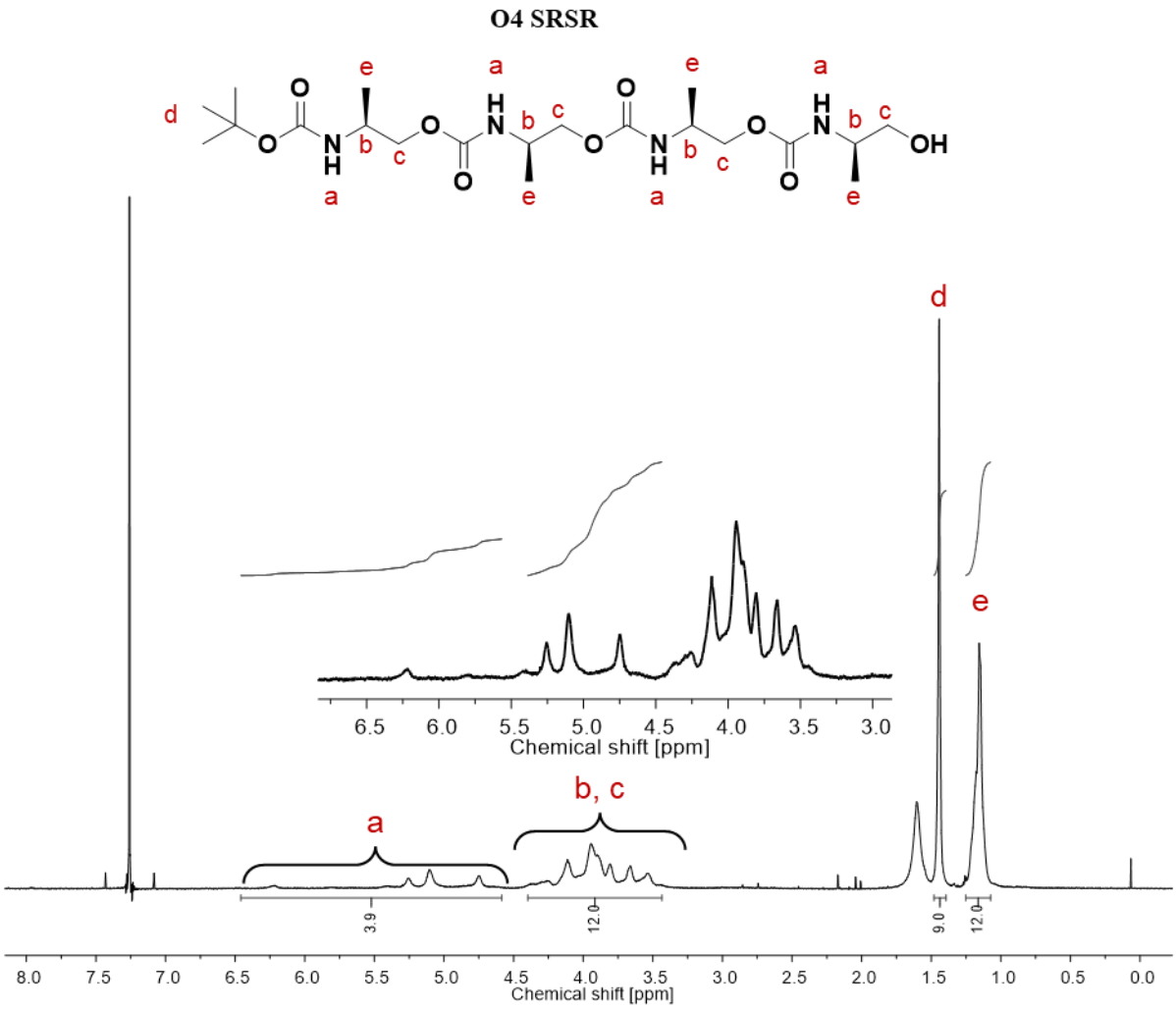

Figure S23. ^{1}H NMR spectrum of **O4 SRSR** recorded at RT, 5 mM concentration in $CDCl_3$.

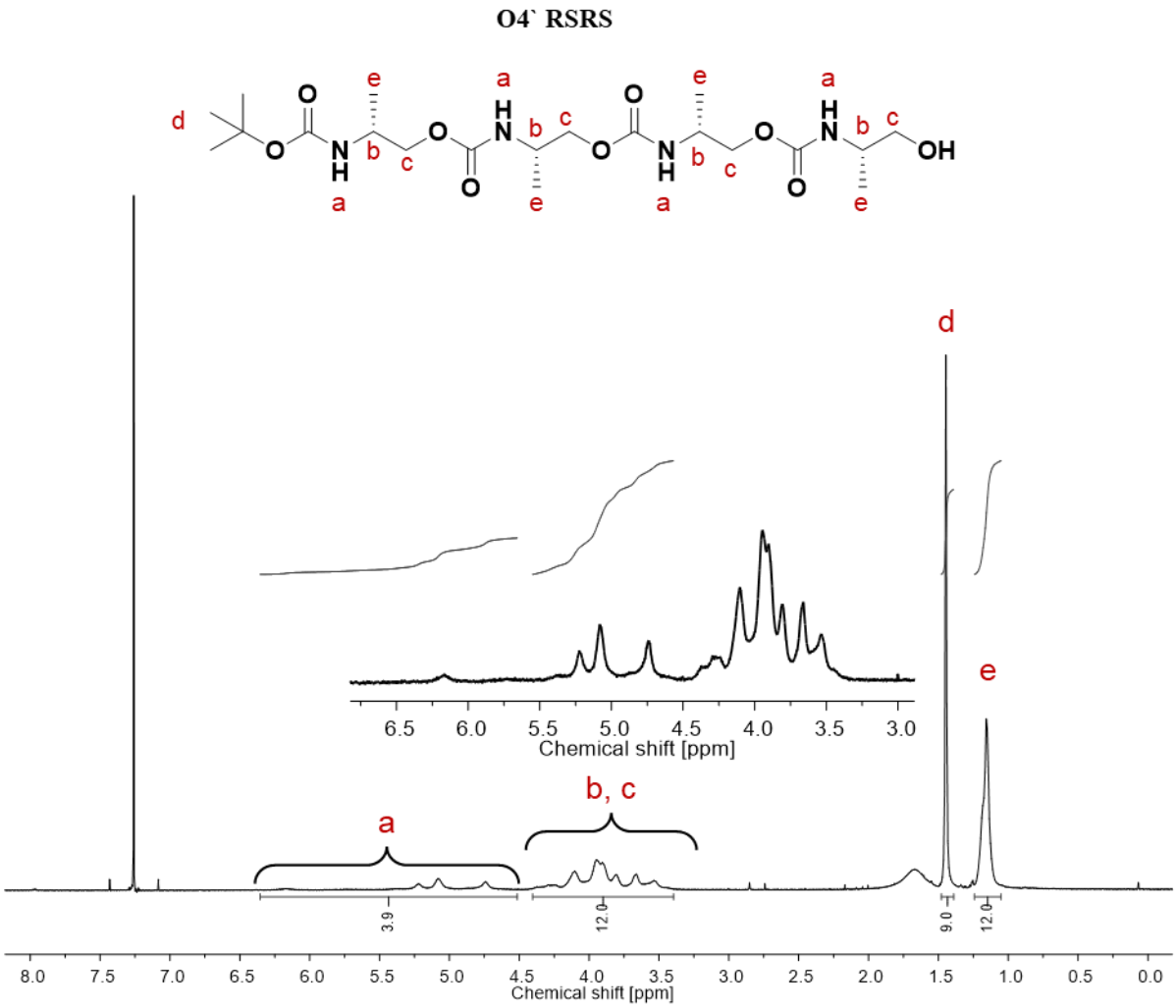

Figure S24. ^{1}H NMR spectrum of **O4` RSRS** recorded at RT, 5 mM concentration in $CDCl_3$.

3.5. ^{13}C Nuclear magnetic resonance spectroscopy

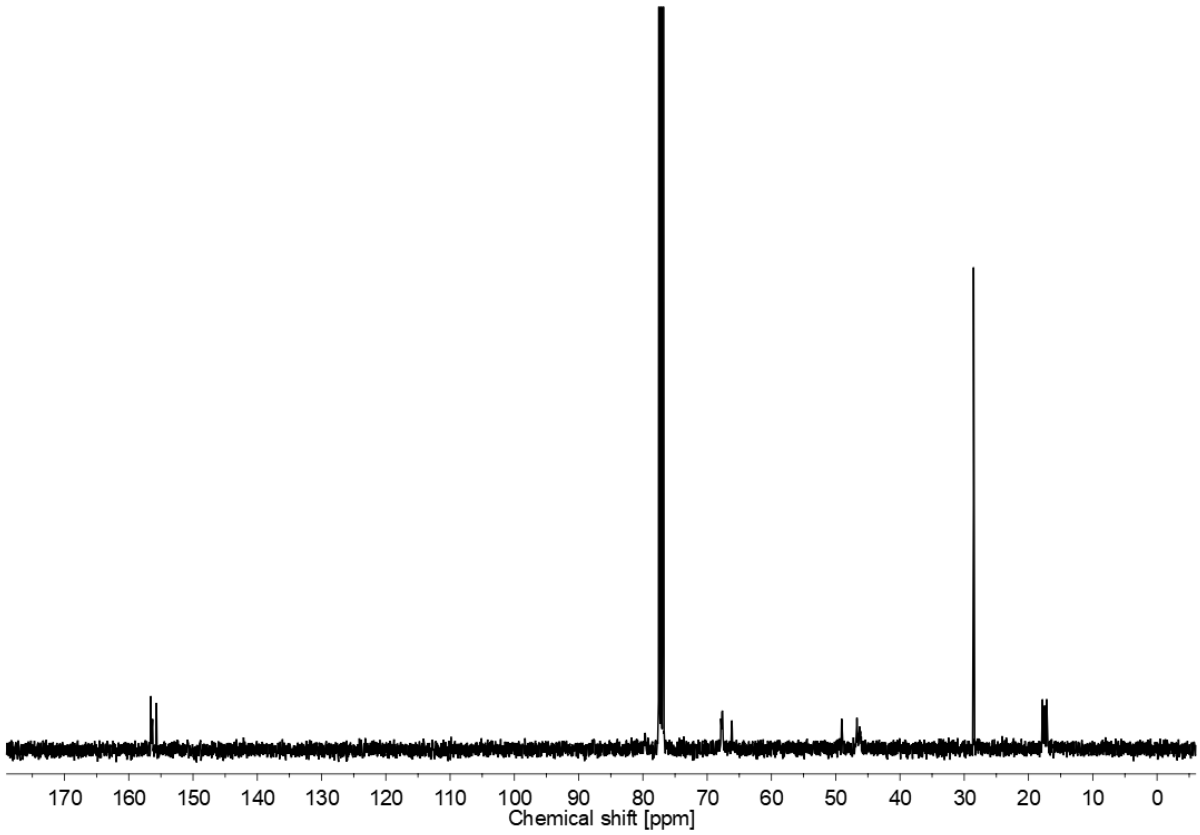

Figure S25. ^{13}C NMR spectrum of **O1 SSSS** recorded at RT (1024 scans), 30 mM concentration in $CDCl_3$.

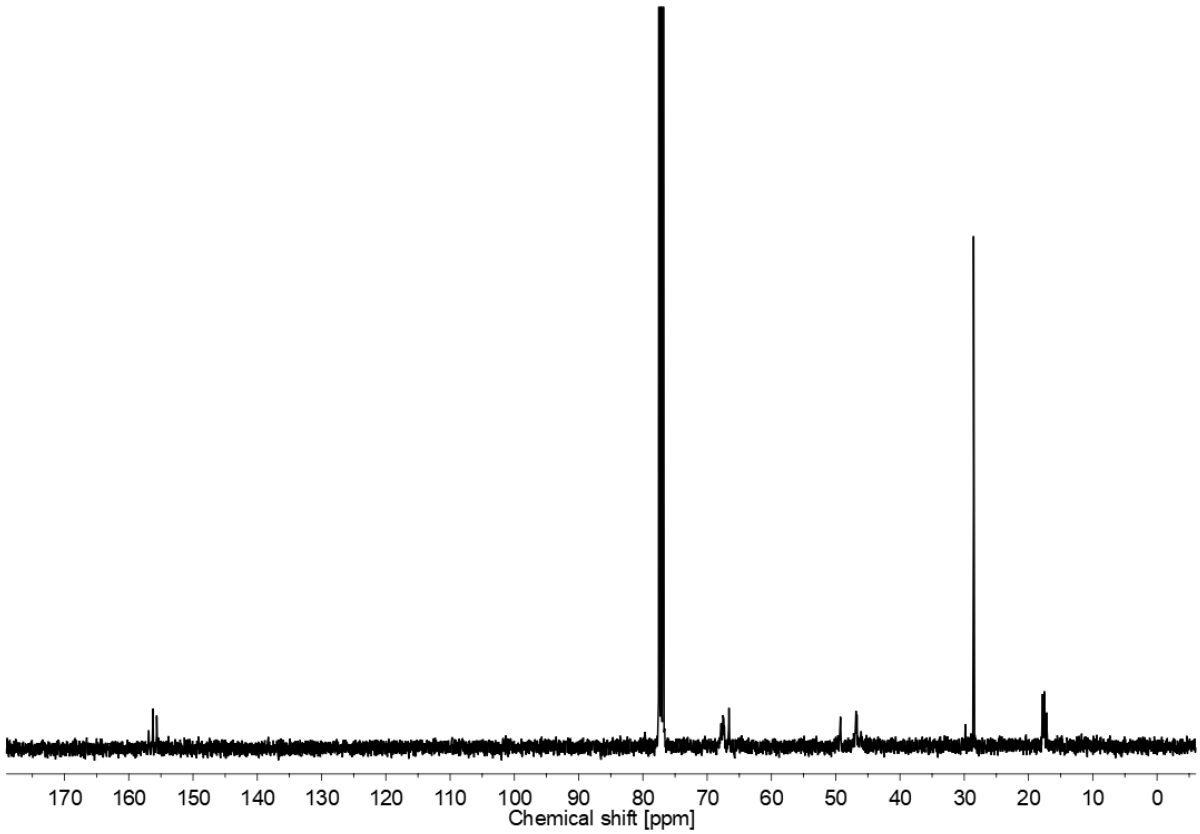

Figure S26. ^{13}C NMR spectrum of **O2 SSSR** recorded RT (1024 scans), 30 mM concentration in $CDCl_3$.

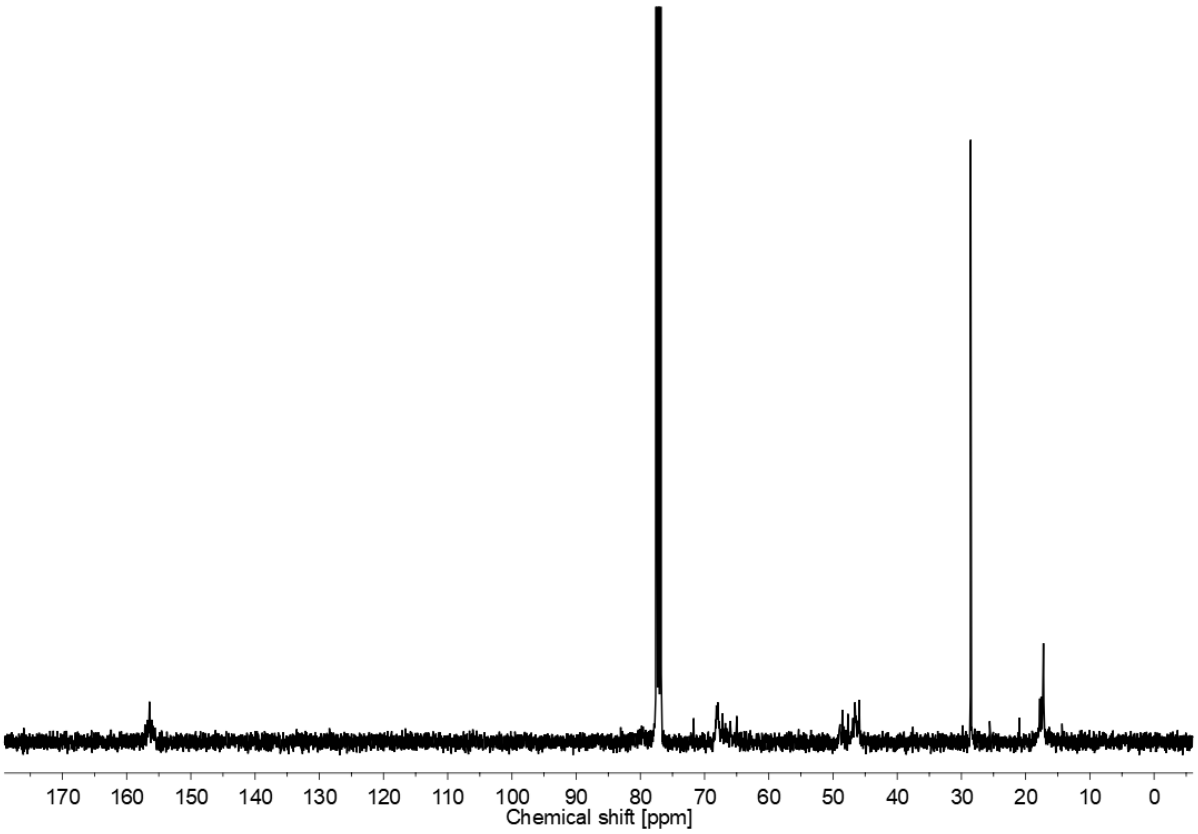

Figure S27. ^{13}C NMR spectrum of **O3 SRSS** recorded RT (4096 scans), 30 mM concentration in $CDCl_3$.

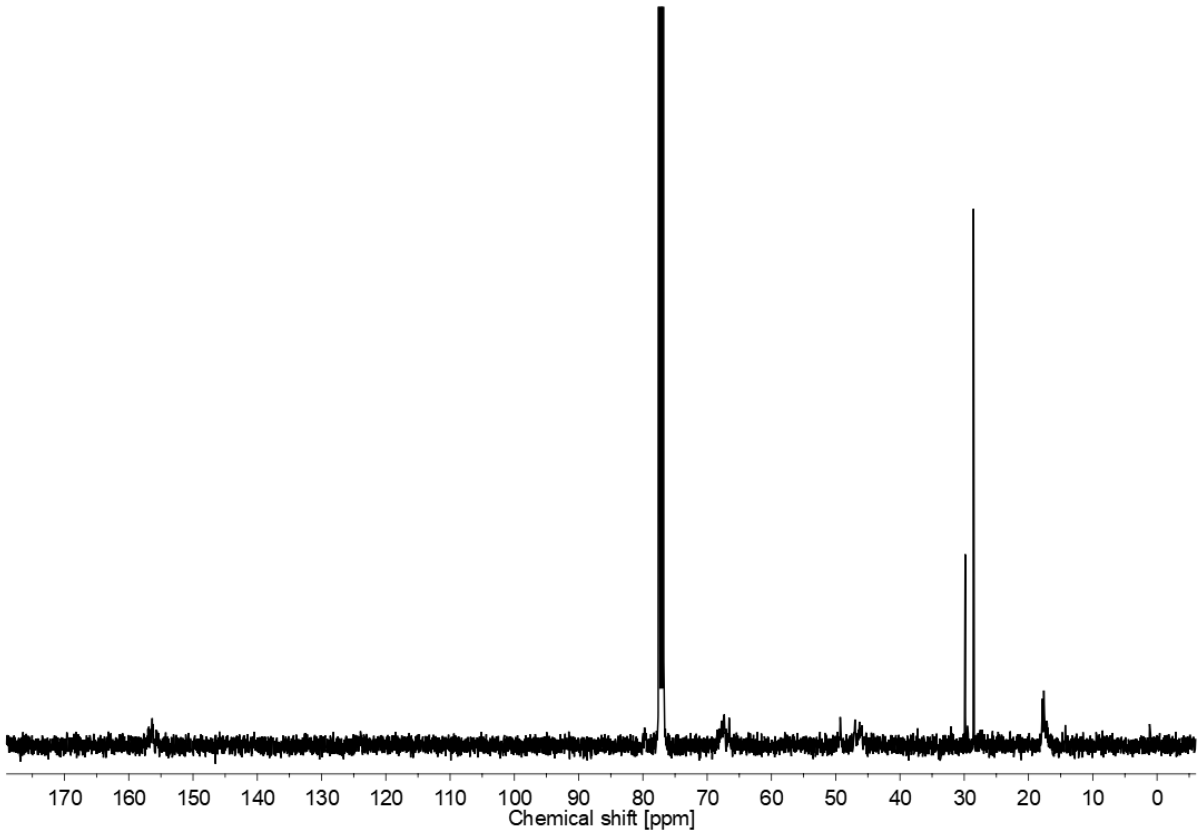

Figure S28. ^{13}C NMR spectrum of **O4 SRSR** recorded RT (4096 scans), 30 mM concentration in $CDCl_3$.

3.6. Differential scanning calorimetry (DSC)

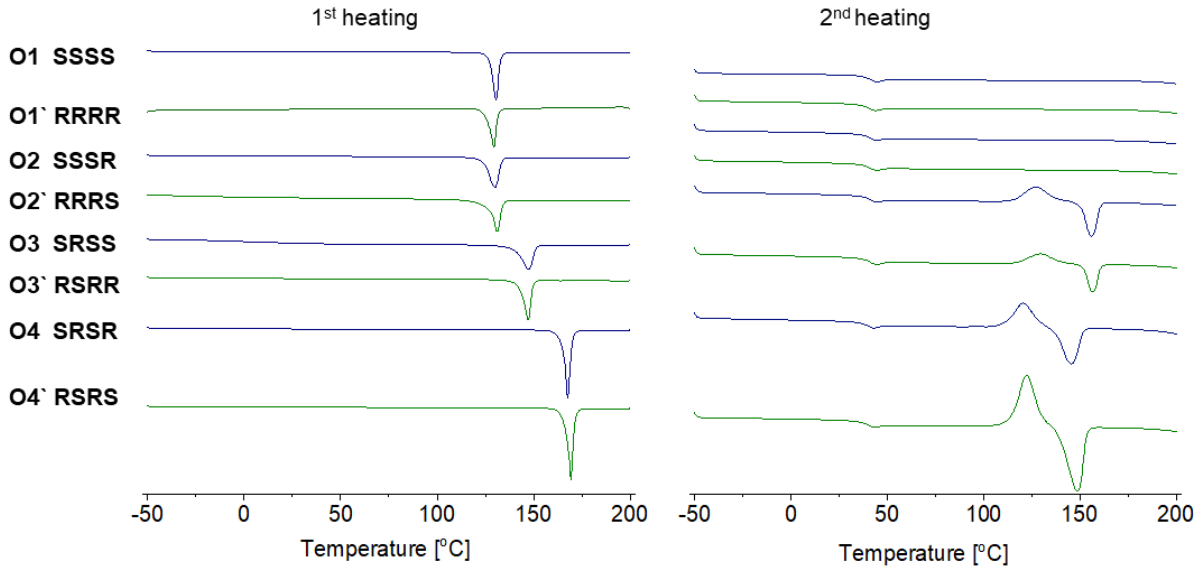

Figure S29. DSC thermograms for oligourethanes O1-O4 and their enantiomers O1`-O4`.

3.7. Crystallography data

3.7.1. Crystal structure of oligomer O3 SRSS

Crystallographic details and refinement parameters can be found in Table S4 below.

Table S4. Crystallographic details and refinement parameters

Sample	**O3 SRSS**
Chemical formula	$C_{20}H_{31}N_4O_9$
Molecular weight (g/mol)	471.49
Crystal system, space group	Triclinic, *P*1
a, b, c (Å)	5.8915(13), 11.084(9), 19.509(1)
α, β, γ (°)	81.81(4), 86.91(4), 89.58(3)
V (Å^3)	1259(3)
Z	2
Temperature (K)	250
Radiation type	CuKα
Diffractometer	Rigaku *XtaLAB Synergy DW*
μ (mm^{-1})	0.83
Crystal size (mm)	0.03 x 0.05 x 0.34
Absorption correction	empirical (multi-scan) CrysAlis PRO 1.171.42.94a (Rigaku Oxford Diffraction, 2023) Empirical absorption correction using spherical harmonics, implemented in SCALE3 ABSPACK scaling algorithm.
T_{min}, T_{max}	0.754, 1.000
No. of measured, independent, and observed [$I > 2\sigma(I)$] reflections	14329, 6454, 4987
R_{int}	0.041
R_1, wR_2, GooF	0.071, 0.203,1.00
No. of parameters	647
No. of restraints	78
$\Delta\rho_{max}$, $\Delta\rho_{min}$ (e Å^{-3})	0.55, -0.36
Flack parameter	-0.1(3)

Refinement

The model was first refined isotropically, then anisotropically. Crystal twinning was observed, and the model was refined as a 2-component twin with the following twin law: -1 0 0 | 0 1 0 | 0 0.5 -1. The placement of hydrogen atoms was performed based on geometry. The disorder was observed in the terminal amino alcohol monomer of both molecules in the asymmetric unit. Particularly, the methyl and hydroxyl groups have been split into two positions, with a partial occupancy of ≈55% and ≈45%. The occupancy of the disordered groups in both molecules was related to each other and refined using the same free variable. The size of the ellipsoids of some of the atoms in the terminal amino alcohols suggests further disorder, but these were not modeled as split. Restraints on C-O and C-C bond lengths between some atoms in the terminal amino alcohols were required and they were set at 1.410(2) Å, and 1.540(2) Å, respectively. RIGU constraints were also applied for the terminal groups of both molecules, and ISOR restraints were additionally applied to -OH oxygen atoms and methyl carbon atom of molecule B. SADI restraint was also applied to -OH oxygen atoms of molecule B.

checkCIF/PLATON report

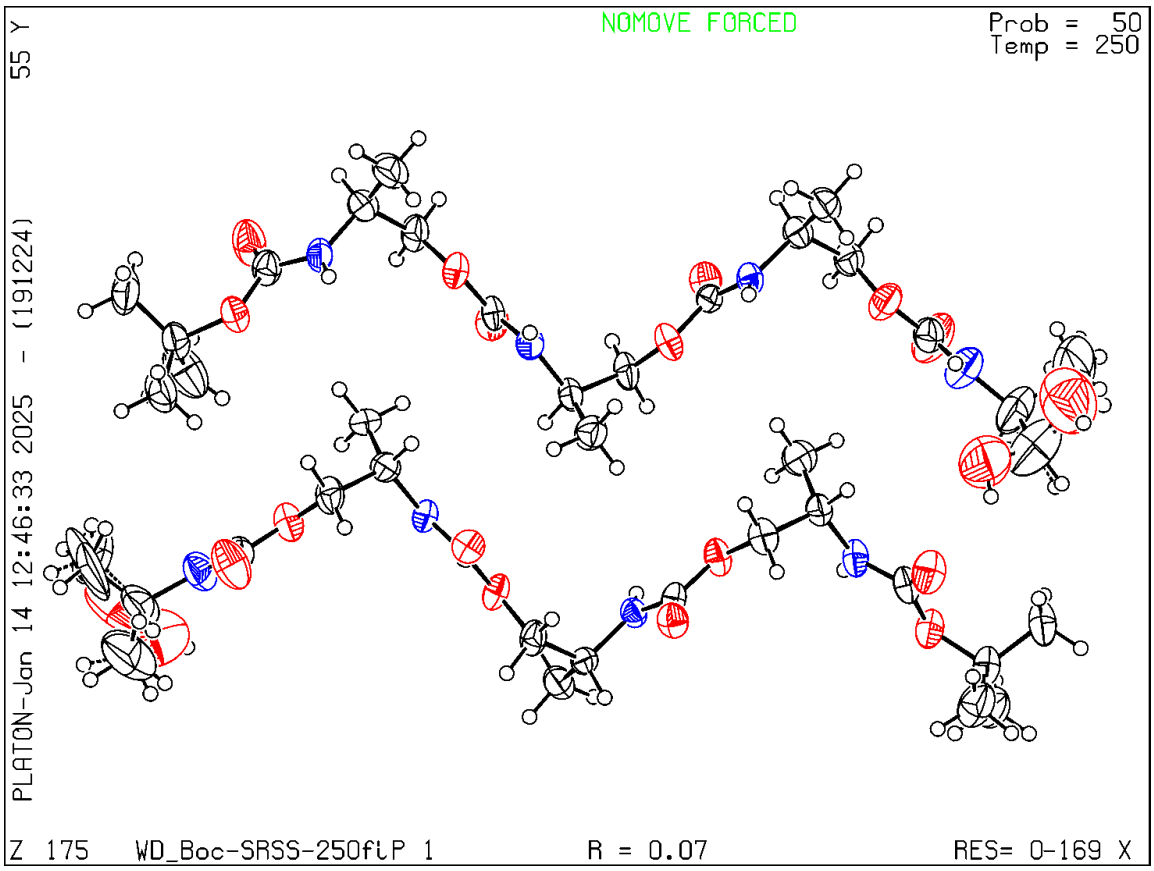

Figure S30. Crystal structure of O3 oligomer SRSS.

Bond precision:	C-C = 0.0118 Å	Wavelength=1.54184	
Cell:	a=5.8915(13)	b=11.084(9)	c=19.509(1)
	alpha=81.81(4)	beta=86.81(4)	gamma=89.58(3)
Temperature:	250 K		

	Calculated	Reported
Volume	1259.0(11)	1259(3)
Space group	P 1	P 1
Hall group	P 1	P 1
Moiety formula	C20 H38 N4 O9	C20 H31 N4 O9
Sum formula	C20 H38 N4 O9	C20 H31 N4 O9

Mr	478.54	478.54
Dx, g cm-3	1.262	1.244
Z	2	2
Mu (mm-1)	0.834	0.833
F000	516.0	502.0
F000’	517.77	
h,k,lmax	7,13,23	7,13,23
Nref	9156[4578]	6454
Tmin,Tmax	0.951, 0.975	0.754, 1.000
Tmin’	0.753	

Correction method= # Reported T Limits: Tmin=0.754 Tmax=1.000

AbsCorr = MULTI-SCAN

Data completeness= 1.41/0.70 Theta(max)= 67.989

R(reflections)= 0.0705(4987) wR2(reflections)= 0.2026(6454)

S = 0.998 Npar= 647

The CheckCIF report revealed no level A alerts but identified five level B alerts in the structure, primarily associated with the disordered terminal amino alcohol units. These B alerts reflect the quality of the crystal received. Despite numerous attempts, the crystallization process consistently produced either poor-quality crystals or none at all. Consequently, obtaining higher-quality data than what is presented here was not feasible.

3.7.2. Crystal structure of oligomer O4 SRSR

Data were collected on a Tecnai G2 sphera equipped with a cheetah D detector. The crystal was cooled at liquid nitrogen temperature during the measurement, to decrease radiation damage. As shown in Fig. S31, the weak data could be indexed and integrated in DIALS using a primitive orthorhombic unit cell.

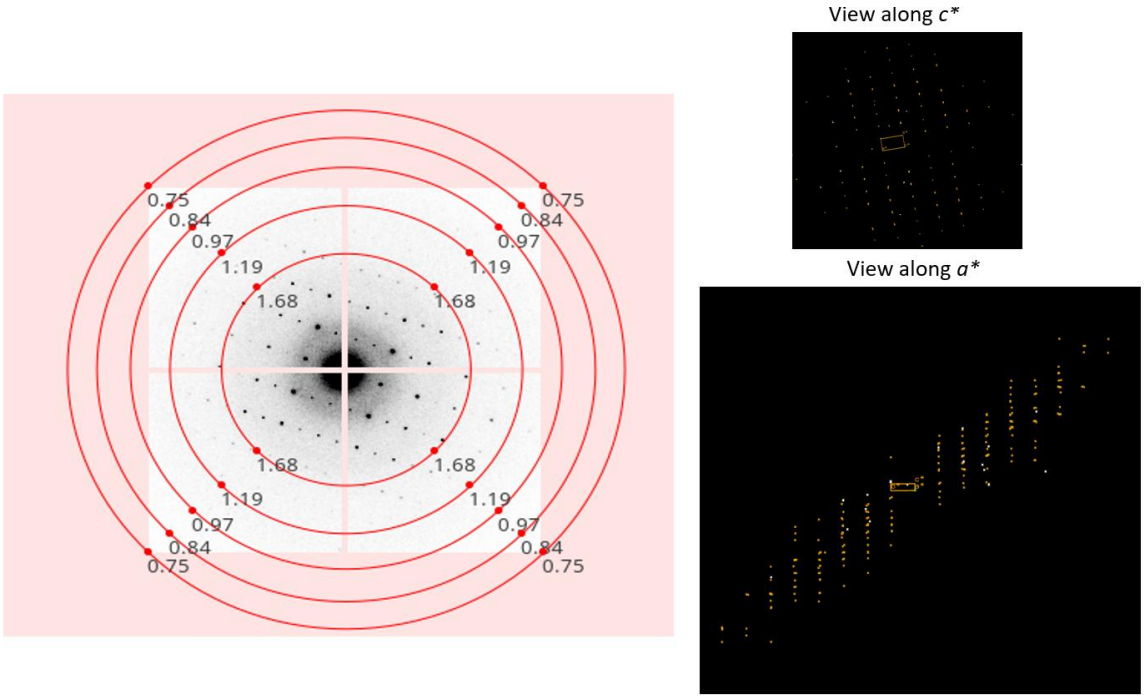

Figure S31. View of a typical image, showing the limited resolution (resolution rings depicted in red). On the right, a view of the reciprocal space (based on the peaks caught by the peak hunting algorithm) is shown along two directions. The reciprocal unit cell is highlighted.

On the total of 26 diffraction datasets that looked reasonable when collecting the data, only 7 were usable for data integration. Each one spanned a limited range due to radiation damage and so the completeness of the dataset is not optimal. Moreover, the data were cut at 1 Å resolution, as very few spots were visible on the images beyond this resolution. However, a plot of I/σ against the resolution indicates that the resolution of the data is closer to 1.6 Å.

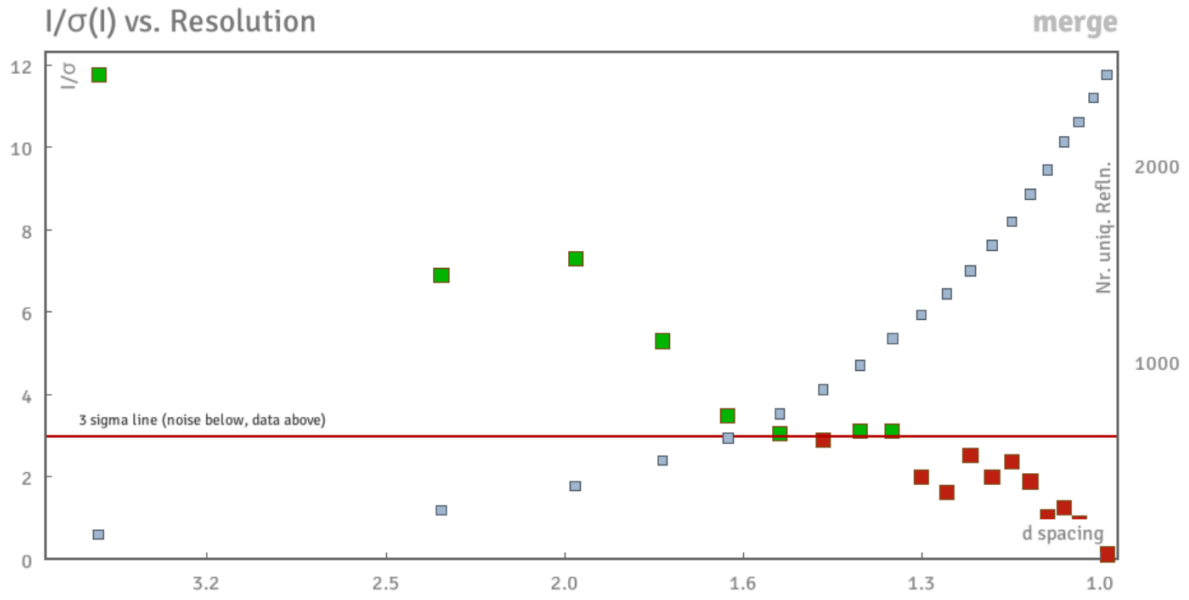

Figure S32. Plot of I/σ against resolution (large square) for the merged data. The small squares indicate the number of unique reflections.

Data were integrated in the DIALS software and were merged using dials.cosym. The data could be solved in SHELXD in a straightforward way. The structure was refined in SHELXL.

The displacement parameters were heavily restrained (rigu on all parameters and eadp on some atoms with the same environment):

RIGU O1 > C34

EADP N5 N12 N19 N27

EADP C25 C10 C3 C17

EADP C11 C18 C26 C4

EADP O8 O15 O22 O30

EADP C20 C13 C6 C28

Some bond restraints were used to regularize really distorted geometry.

DFIX 1.42 O1 C2

DFIX 1.54 C4 C3

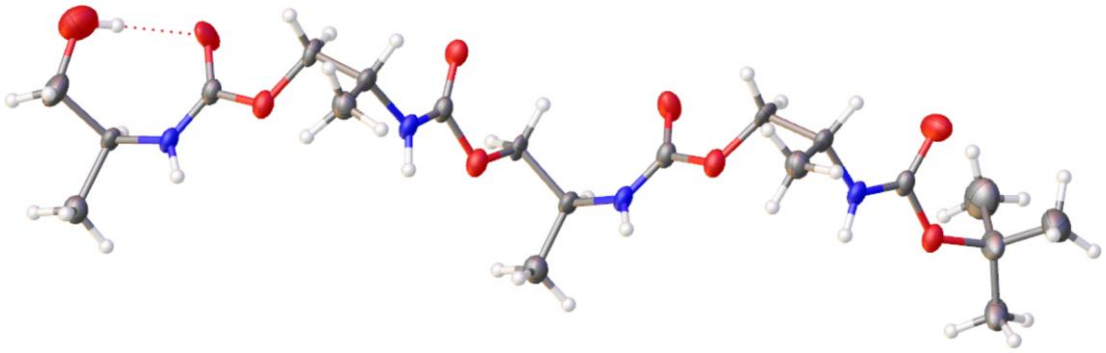

Figure S33. View of the asymmetric unit

Table S5. Crystallographic details and refinement parameters

Space group	$P2_12_12_1$
a/Å	5.759
b/Å	10.709
c/Å	38.068
α/°	90
β/°	90
γ/°	90
Volume/Å^3	2347.6
Z	4
ρ_{calc}g/cm^3	1.354
μ/mm^{-1}	0.000
F(000)	388.0
Radiation	electron (λ = 0.0285)
2Θ range for data collection/°	0.158 to 1.66
Index ranges	$-5 \leq h \leq 5$, $-10 \leq k \leq 10$, $-32 \leq l \leq 32$
Reflections collected	8442
Independent reflections	2001 [R_{int} = 0.1786, R_{sigma} = 0.4050]
Data/restraints/parameters	2001/224/216
Goodness-of-fit on F^2	1.017
Final R indexes [I>=2σ (I)]	R_1 = 0.1245, wR_2 = 0.2771
Final R indexes [all data]	R_1 = 0.1917, wR_2 = 0.2955
Largest diff. peak/hole / e Å^{-3}	0.12/-0.12

3.8. Gibbs free energy (ΔG) analysis

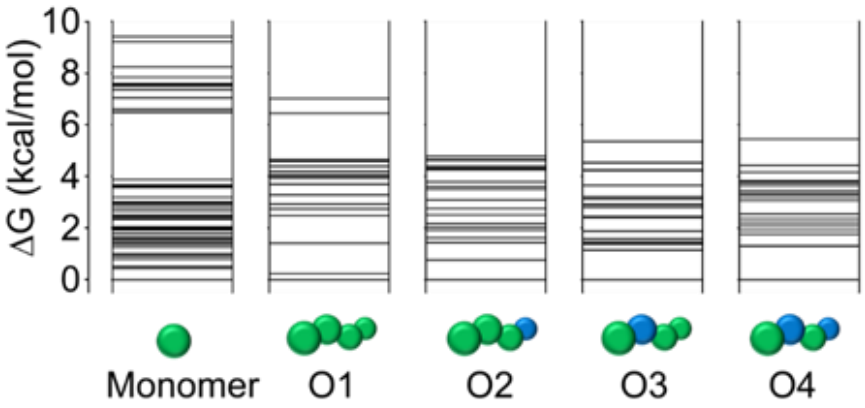

Figure S34. Relative Gibbs free-energy landscapes for the monomer and O1–O4 (HLT). Each horizontal line denotes one conformer. Energies are ΔG relative to the global minimum at 298.15 K and 1 atm, plotted in ascending order.

3.9. Non-covalent interaction analyses (NCI)

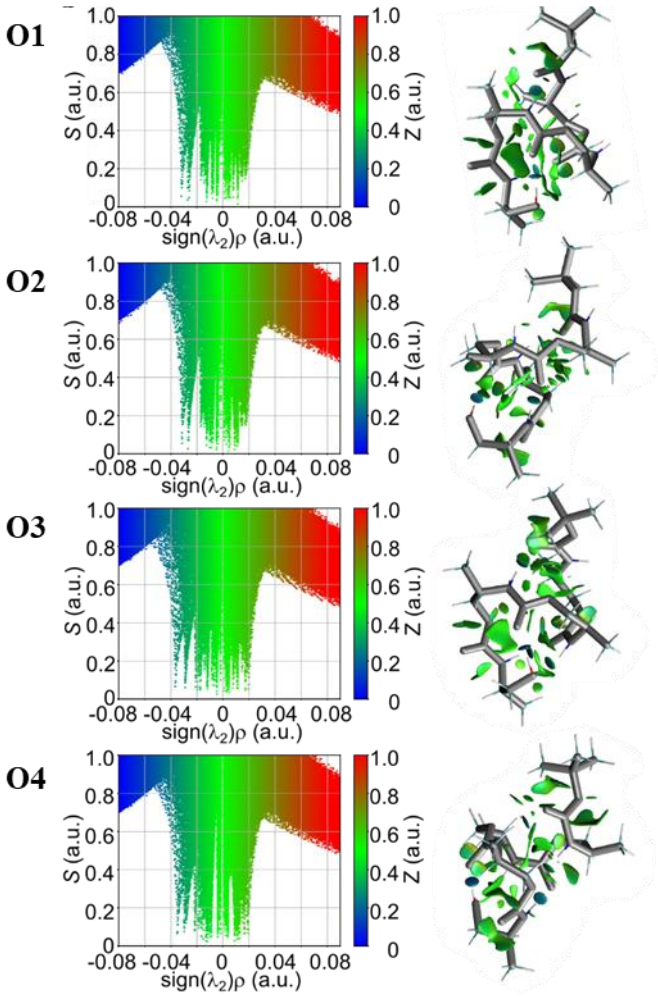

Figure S35. Non-covalent interaction analyses for the lowest energy conformer of each oligourethane O1-O4.

3.10. Torsional angles analyses

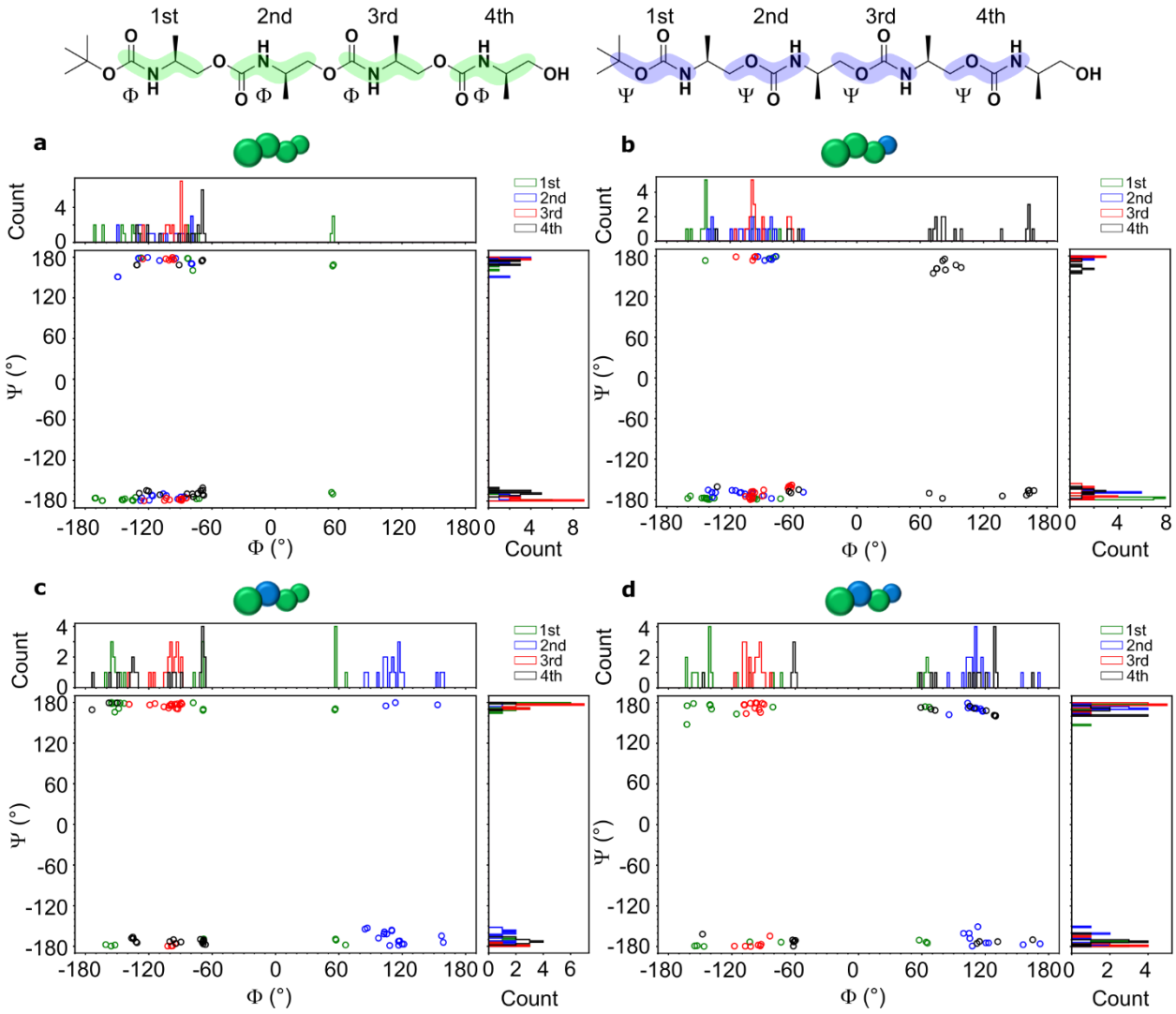

Figure S36. Ramachandran plot of dihedral angles Φ and Ψ for oligourethanes O1-O4 (a-d) representing different shapes. Values of Φ angle flip the sign of their values depending on stereochemistry.

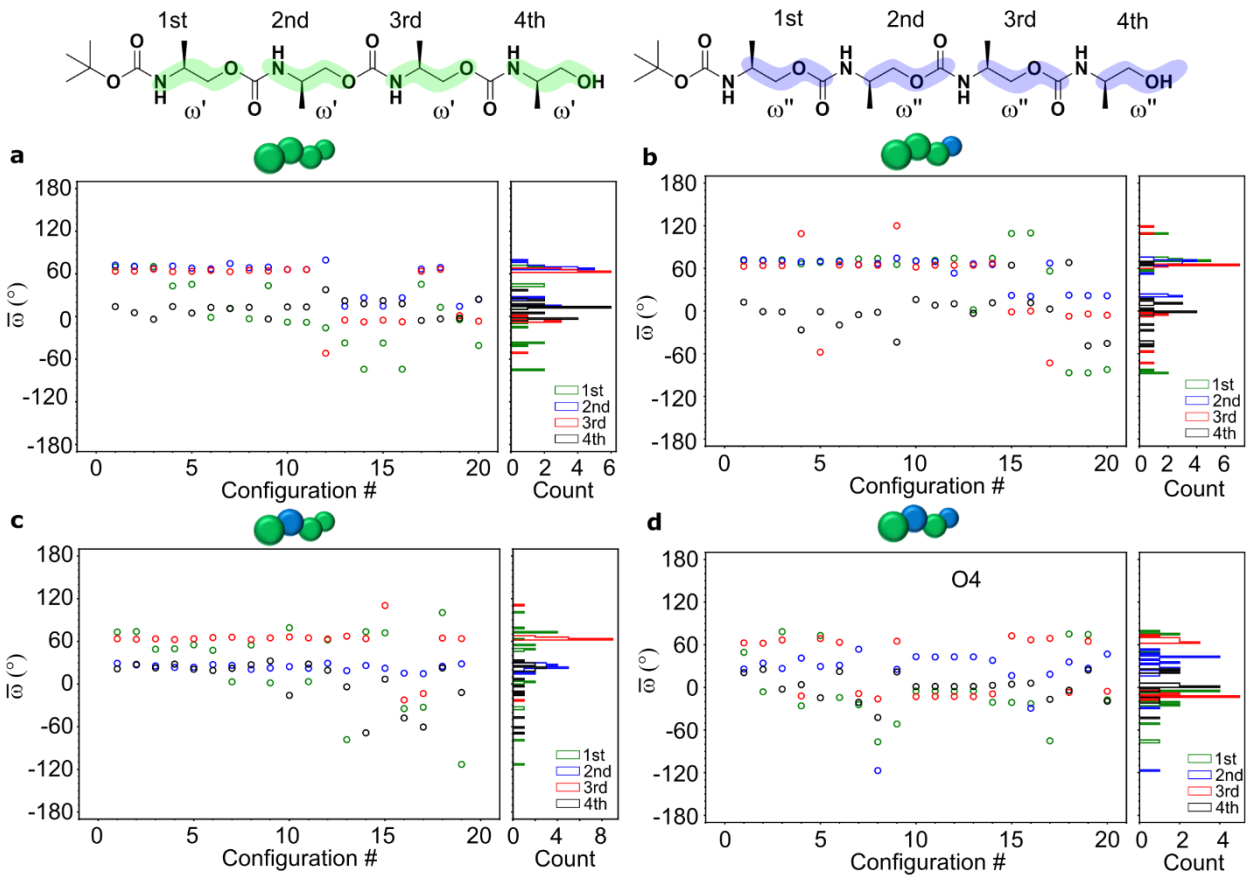

Figure S37. Plot of torsional angles ω of oligourethanes O1-O4 (a-d) representing different shapes.

3.11. ^{1}H Nuclear magnetic resonance spectroscopy (NMR) - variable temperature and variable concentration analyses

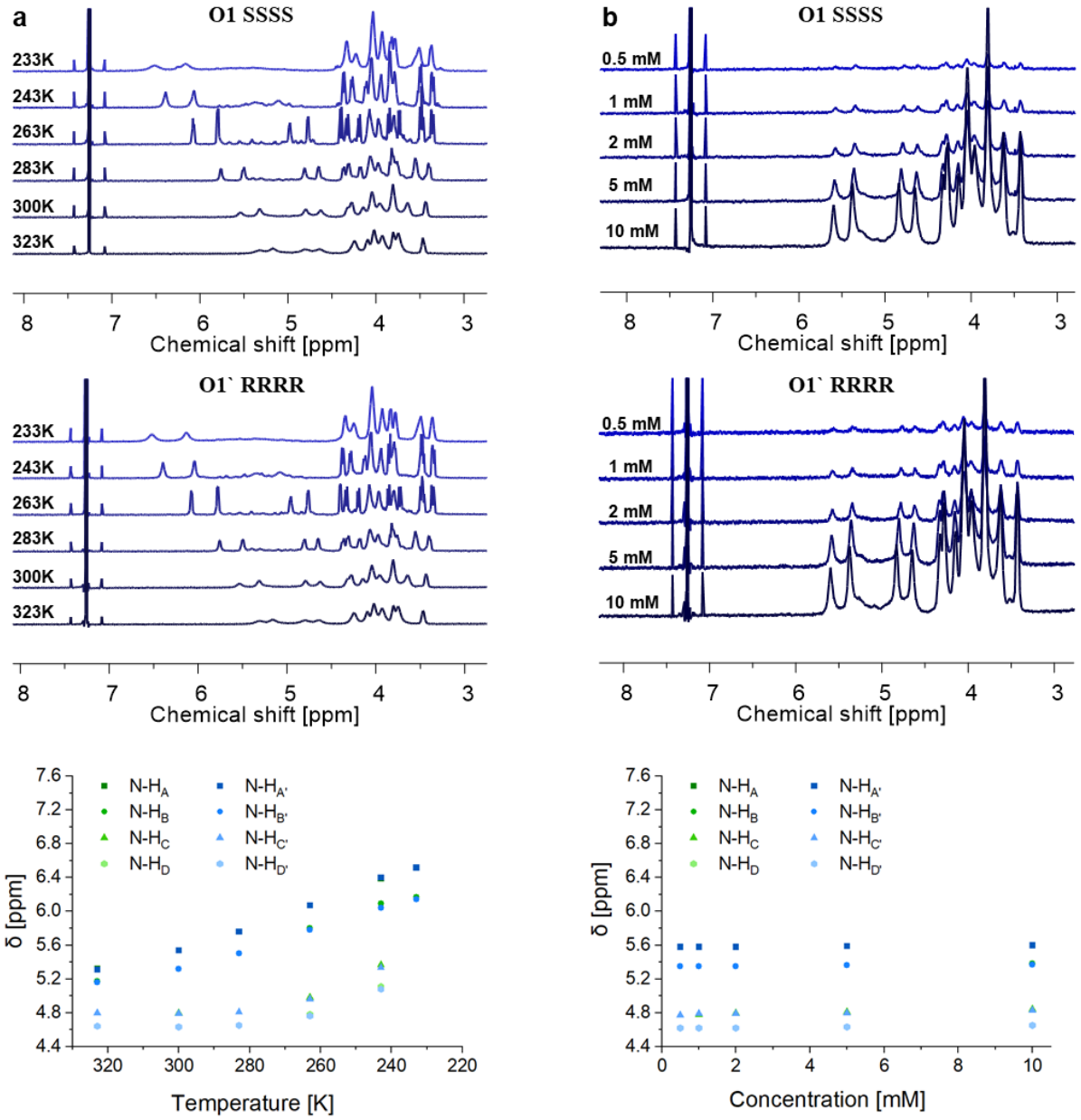

Figure S38. ^{1}H NMR analysis for **O1 SSSS** and **O1` RRRR** in different temperature (a) and concentration (b) ranges in $CDCl_3$. The NH signals occurring in the range 4.4-6.8 ppm shift their position in response to temperature changes and remain in position upon concentration change, as visualized in the plots.

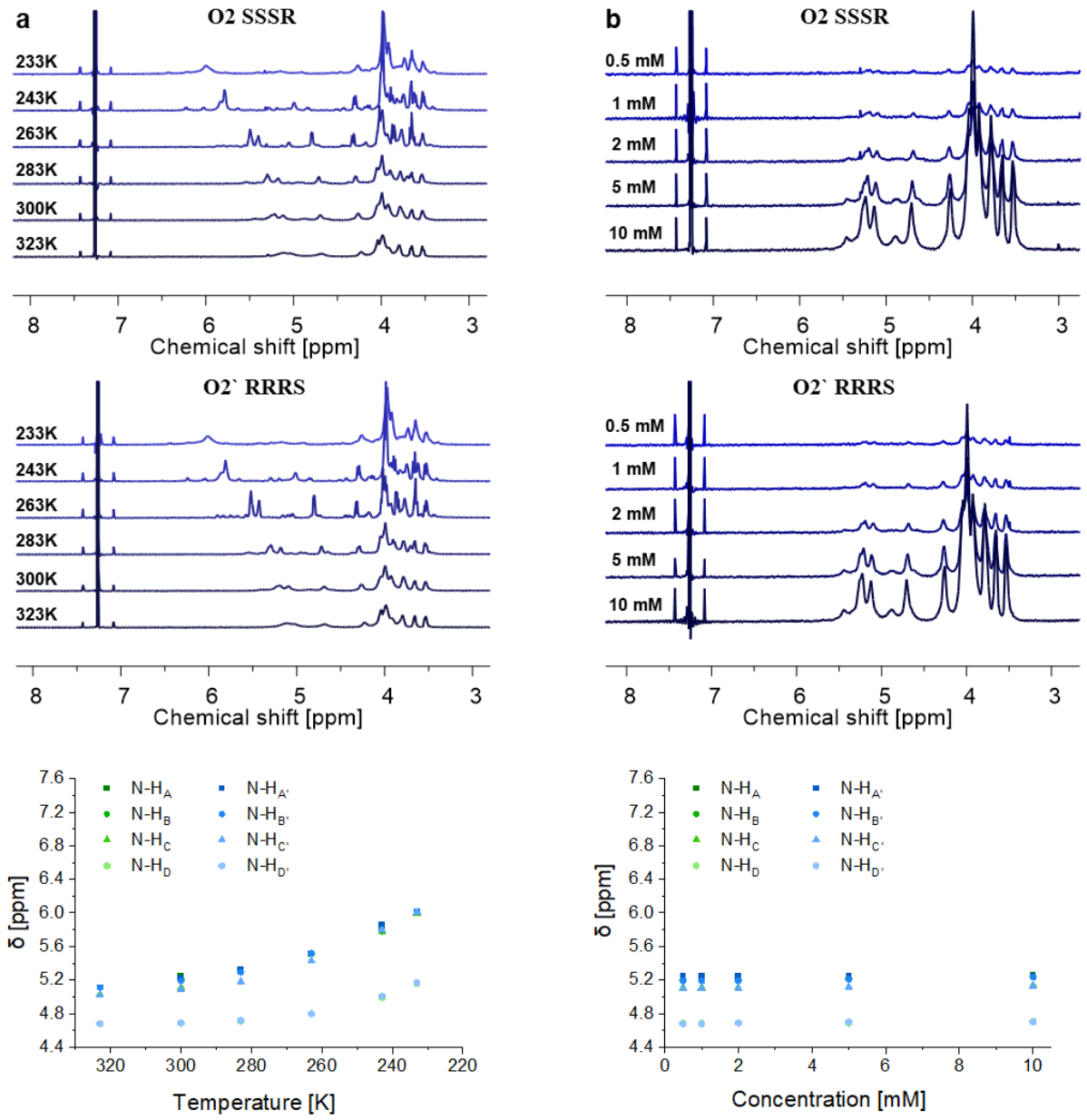

Figure S39. ^{1}H NMR analysis for **O2 SSSR** and **O2` RRRS** in different temperature (a) and concentration (b) ranges in $CDCl_3$. The NH signals occurring in the range 4.4-6.8 ppm shift their position in response to temperature changes and remain in position upon concentration change, as visualized in the plots.

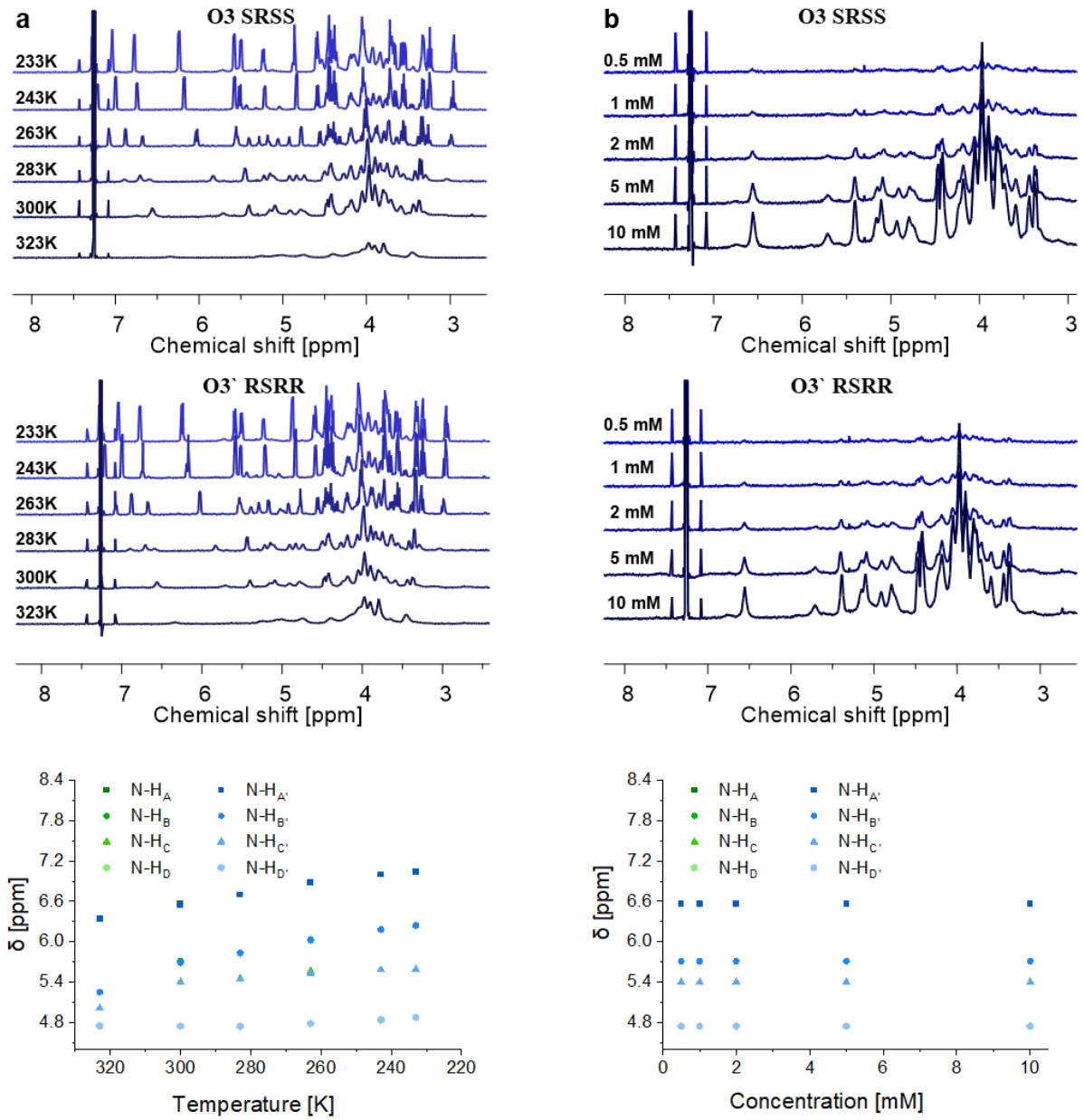

Figure S40. ^{1}H NMR analysis for **O3 SRSS** and **O3` RSRR** in different temperature (a) and concentration (b) ranges in $CDCl_3$. The NH signals occurring in the range 4.4-6.8 ppm shift their position in response to temperature changes and remain in position upon concentration change, as visualized in the plots.

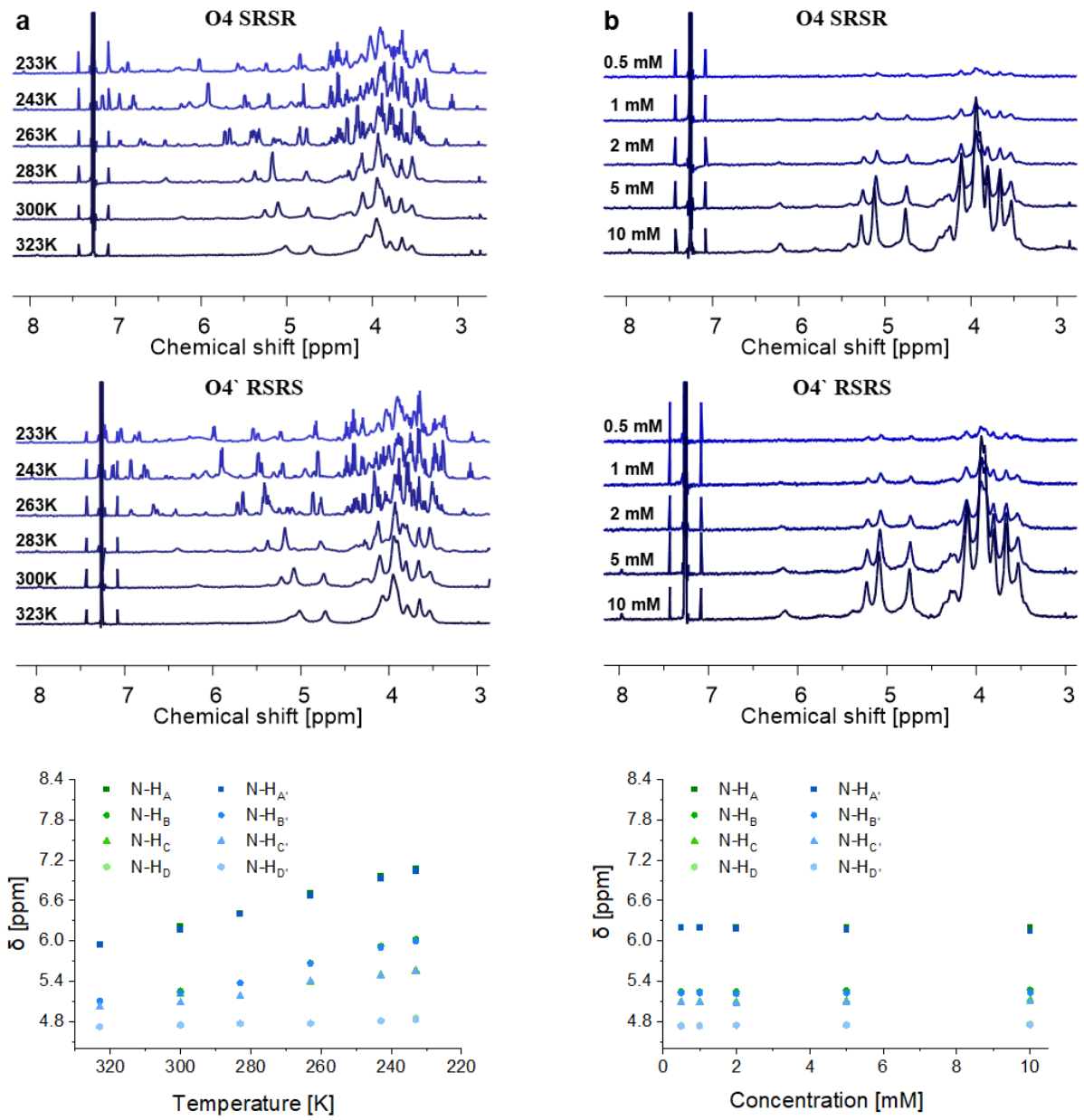

Figure S41. ^{1}H NMR analysis for **O4 SRSR** and **O4` RSRS** in different temperature (a) and concentration (b) ranges in $CDCl_3$. The NH signals occurring in the range 4.4-6.8 ppm shift their position in response to temperature changes and remain in position upon concentration change, as visualized in the plots.

Note: The characteristic downfield shift of δNH proton signals indicates the presence of hydrogen bonds as confirmed by NMR variable temperature experiments. To dispel the uncertainty that the

hydrogen bonds are not a result of intermolecular interactions (i.e. the formation of aggregates), we conducted a variable concentration ^{1}H NMR experiment. As demonstrated in Figures S38-41 irrespective of the oligomer concentration, the δNH values remain practically unchanged, thus excluding the presence of intermolecular interactions. The observations indicate that oligourethane tetramers adopt conformations stabilized by intramolecular hydrogen bonds, and various sequences of chiral units result in different shapes that align with NCI analysis (Fig. S35).

3.12. Infrared spectroscopy (IR)

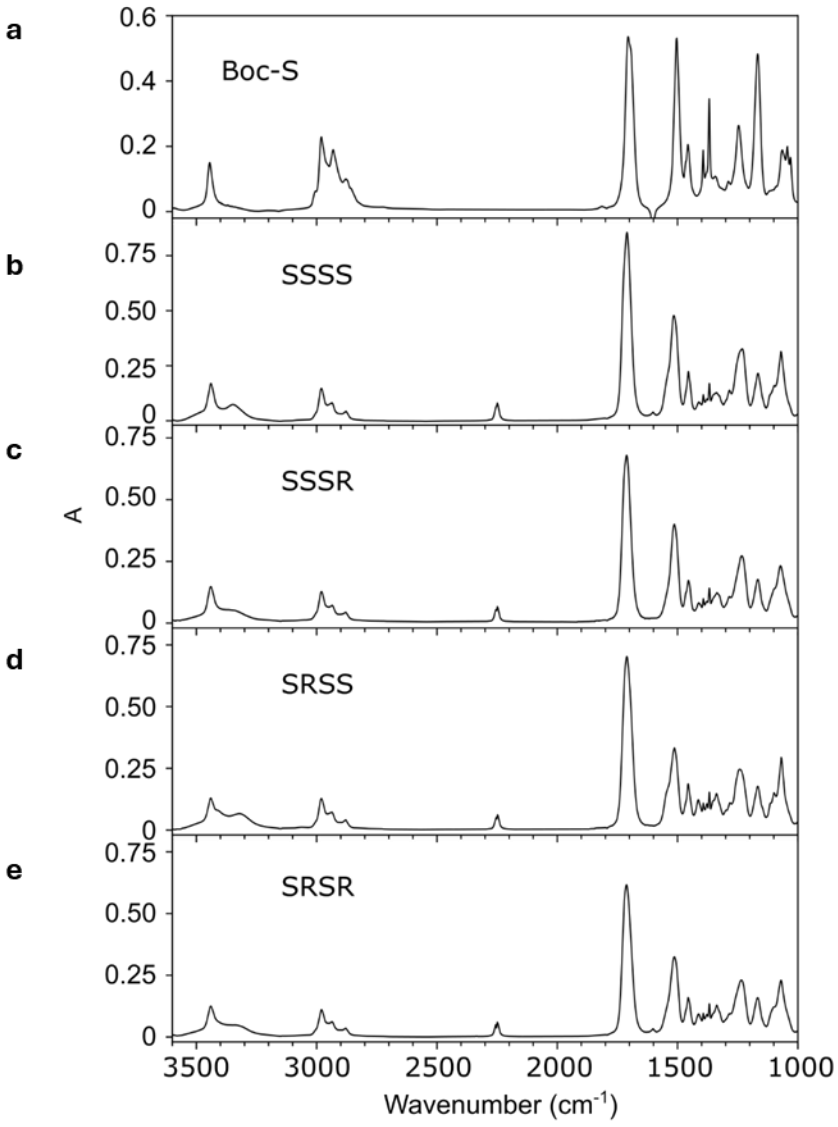

Figure S42. IR spectrum of Boc-protected monomer (a) and oligomers O1-O4 (b-e) from 1000 to 3700 cm^{-1}, RT, monomer: 100 mM, oligomer: 15 mM in $CDCl_3$.

3.13. Vibrational circular dichroism (VCD)

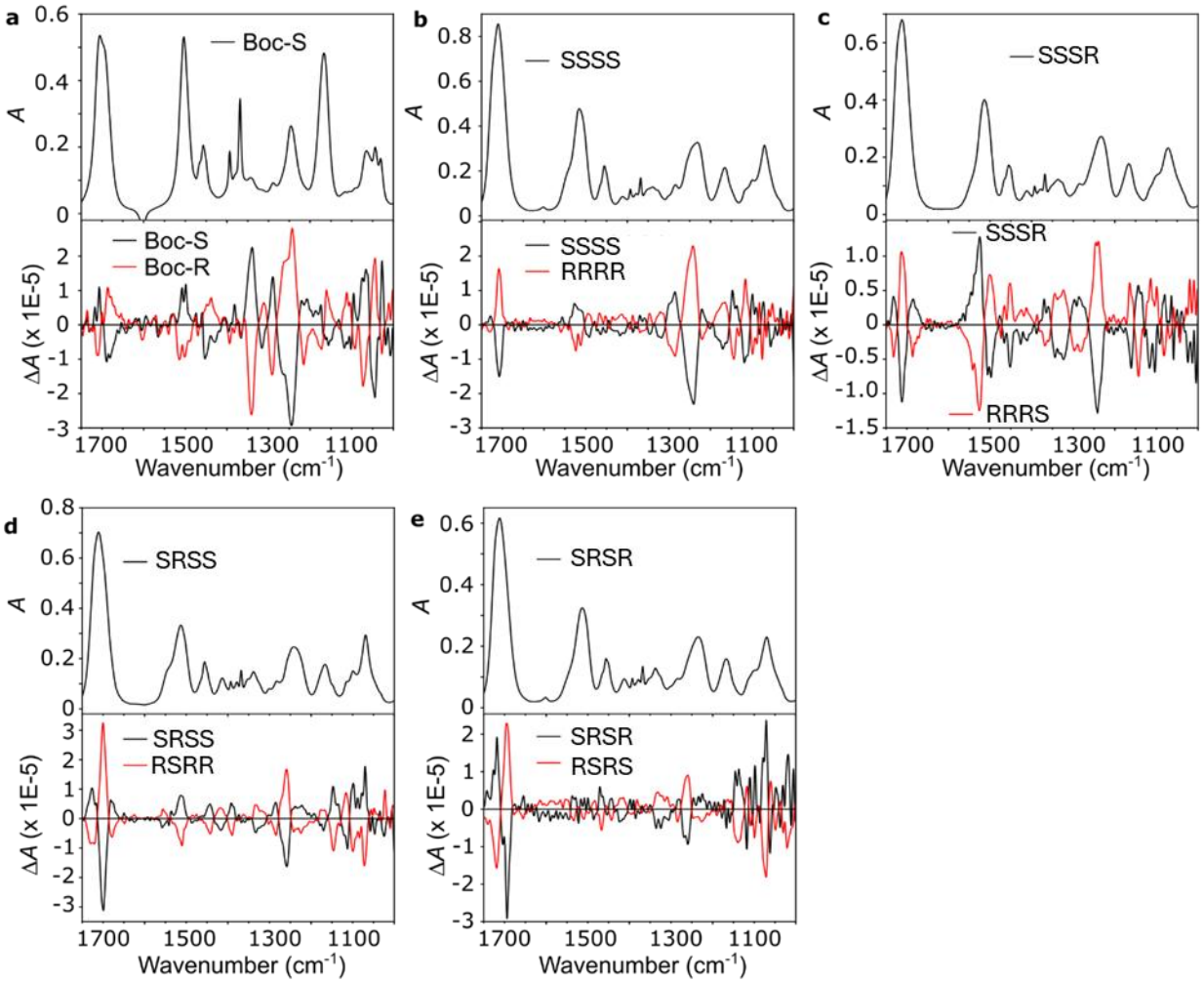

Figure S43. VCD spectra of Boc-protected monomer (a) and O1-O4 oligomers (b-e) along with the IR spectra from 1000 to 1750 cm^{-1}, RT, monomer: 100 mM, oligomer: 15mM in $CDCl_3$.

Table S6. Cosine similarity (Sc) values between the VCD spectrum of each sequence. The cosine similarity is defined as the dot product of the vectors divided by their norms. For example, here VCD spectrum of SSSS and SRSS can be used as vectors to make the normalized dot product (Sc = 0.44). The value Sc of 1 represents the identical spectrum, -1 as opposite spectrum and 0 as orthogonal spectrum.

Sc	**SSSS**	**RRRR**	**SRSS**	**RSRR**	**SSSR**	**RRRS**	**SRSR**	**RSRS**
SSSS	1							
RRRR	-0.97	1						
SRSS	0.44	-0.42	1					
RSRR	-0.43	0.43	-0.98	1				
SSSR	0.68	-0.69	0.19	-0.2	1			
RRRS	-0.7	0.7	-0.19	0.2	-0.95	1		
SRSR	0.19	-0.17	0.62	-0.6	-0.01	0	1	
RSRS	-0.2	0.2	-0.68	0.69	-0.01	0	-0.94	1

3.14. Simulated VCD spectra

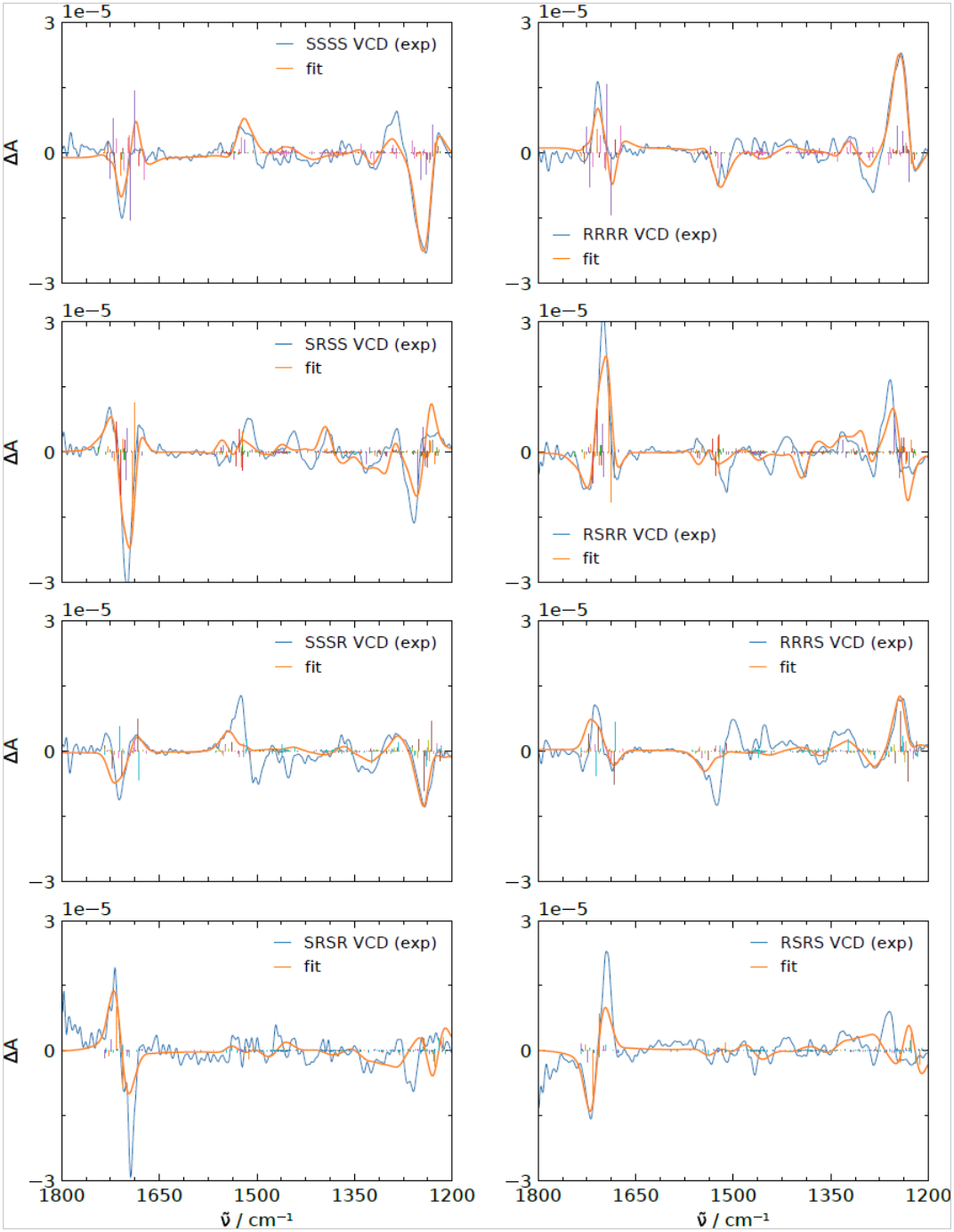

Figure S44. Simulated VCD spectra of O1-O4 oligomers, RT, $CDCl_3$.

Table S7 The weight of conformers from the best fit result of experimental VCD spectrum of O1 (SSSS). Along with the weight, relative energy compared with the lowest energy conformer, dipole moment, and cis/trans geometry of each unit are indicated.

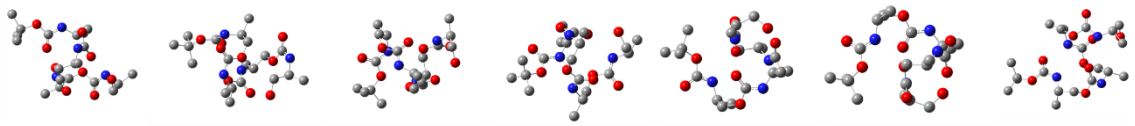

# 1	# 2	# 3	# 4	# 5	# 6	# 7
45%	22%	12%	9%	5%	4%	3%
t-t-t-t	t-c-t-c	t-t-t-t	t-t-t-t	t-t-t-t	t-t-t-t	c-t-t-t

Ranking of conformer	Percentage VCD analysis (%)	Dipole (D)	Cis/Trans	ΔG (kcal/mol)
1	45	10.9	tttt	1.4
2	22	3.0	tctc	4.0
3	12	6.7	tttt	2.7
4	9	6.6	tttt	4.6
5	5	6.8	tttt	3.3
6	4	6.9	tttt	2.9
7	3	10.7	cttt	2.9

Table S8. The weight of conformers from the best fit result of experimental VCD spectrum of O2 (SSSR). Along with the weight, relative energy compared with the lowest energy conformer, dipole moment, and cis/trans geometry of each unit are indicated.

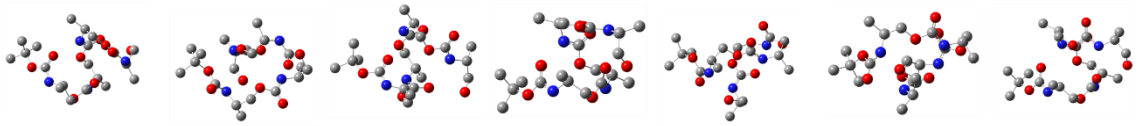

# 1	# 2	# 3	# 4	# 5	# 6	# 7
37%	30%	13%	9%	8%	2%	1%
t-t-t-c	t-t-t-t	t-t-t-t	t-t-t-t	c-t-t-t	c-t-t-t	t-t-t-t

Ranking of conformer	Percentage VCD analysis (%)	Dipole	Cis/Trans	ΔG (kcal/mol)
1	37	9.9	tttc	2.8
2	30	9.4	tttt	4.7
3	13	11.0	tttt	3.8
4	9	7.8	tttt	1.9
5	8	6.3	cttt	4.6
6	2	5.9	cttt	4.3
7	1	11.0	tttt	0.8

Table S9. The weight of conformers from the best fit result of experimental VCD spectrum of O3 (SRSS). Along with the weight, relative energy compared with the lowest energy conformer, dipole moment, and cis/trans geometry of each unit are indicated.

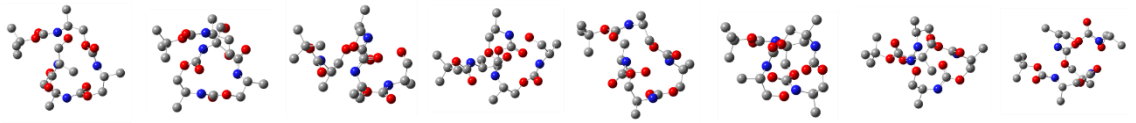

Ranking of conformer	Percentage VCD analysis (%)	Dipole	Cis/Trans	ΔG (kcal/mol)
1	27	2.1	tttt	4.2
2	26	3.1	cttt	4.2
3	16	9.4	tctt	2.8
4	15	9.7	tctt	2.9
5	6	1.7	tttt	4.5
6	5	5.3	tctt	2.9
7	4	6.0	tttt	3.1
8	1	7.1	tctt	1.6

Table S10. The weight of conformers from the best fit result of experimental VCD spectrum of O4 (SRSR). Along with the weight, relative energy compared with the lowest energy conformer, dipole moment, and cis/trans geometry of each unit are indicated.

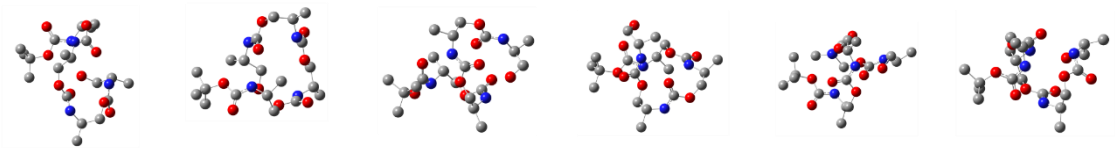

1
42%
t-t-t-t

2
38%
t-t-t-t

3
9%
t-c-t-t

4
4%
t-t-t-t

5
4%
t-t-t-t

6
3%
c-c-t-t

Ranking of conformer	Percentage VCD analysis (%)	Dipole	Cis/Trans	ΔG (kcal/mol)
1	42	5.0	tttt	3.8
2	38	5.1	tttt	2.5
3	9	4.4	tctt	4.2
4	4	7.0	tttt	3.8
5	4	7.7	tttt	5.4
6	3	7.5	cctt	0

3.15. NMR structural analyses

2D NOESY analyses were applied to probe through-space proton interactions, which can indicate whether oligomers adopt linear structures or folded conformations. To perform the structural analysis, it was crucial to accurately assign the signals in the ^{1}H NMR spectrum corresponding to the protons involved in the Nuclear Overhauser Effect (NOE). The assignment was made using 2D Total Correlation Spectroscopy (TOCSY) and Correlation Spectroscopy (COSY) NMR experiments, which enabled the assignment of specific protons in the ^{1}H NMR spectra. The TOCSY spectra provided information enabling the identification of proton groups within individual spin systems, corresponding to monomers in the oligourethane chain. The COSY spectrum delivered insights into direct through-bond couplings between adjacent protons.

Due to the characteristics of the studied oligomers at room temperature, signals in NMR spectra are broadened and overlapped. This is related to hindered free rotation and limited conformational flexibility, which prevents detailed assignments of particular protons. Therefore, to increase the resolution of NMR spectra, we performed analyses at a decreased temperature of 263 K. The decrease in temperature slowed conformational exchange, significantly improving spectral resolution (Fig. S45-60) and allowing better differentiation of signals.

3.15.1. Correlation Spectroscopy (COSY) NMR

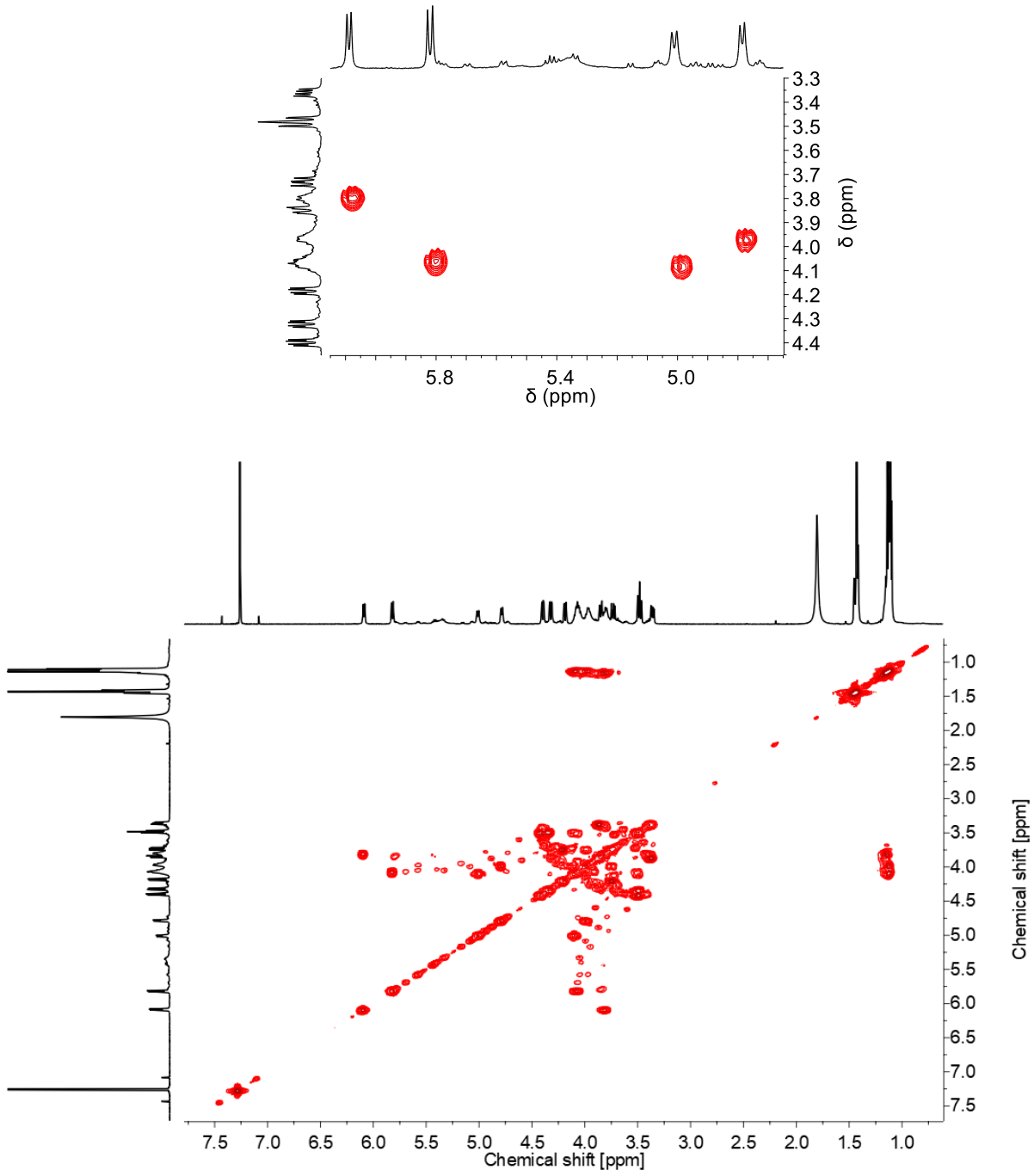

Figure S45. COSY NMR spectrum of **O1 SSSS**, 5 mM in $CDCl_3$, 263K, with zoomed NH proton range (top).

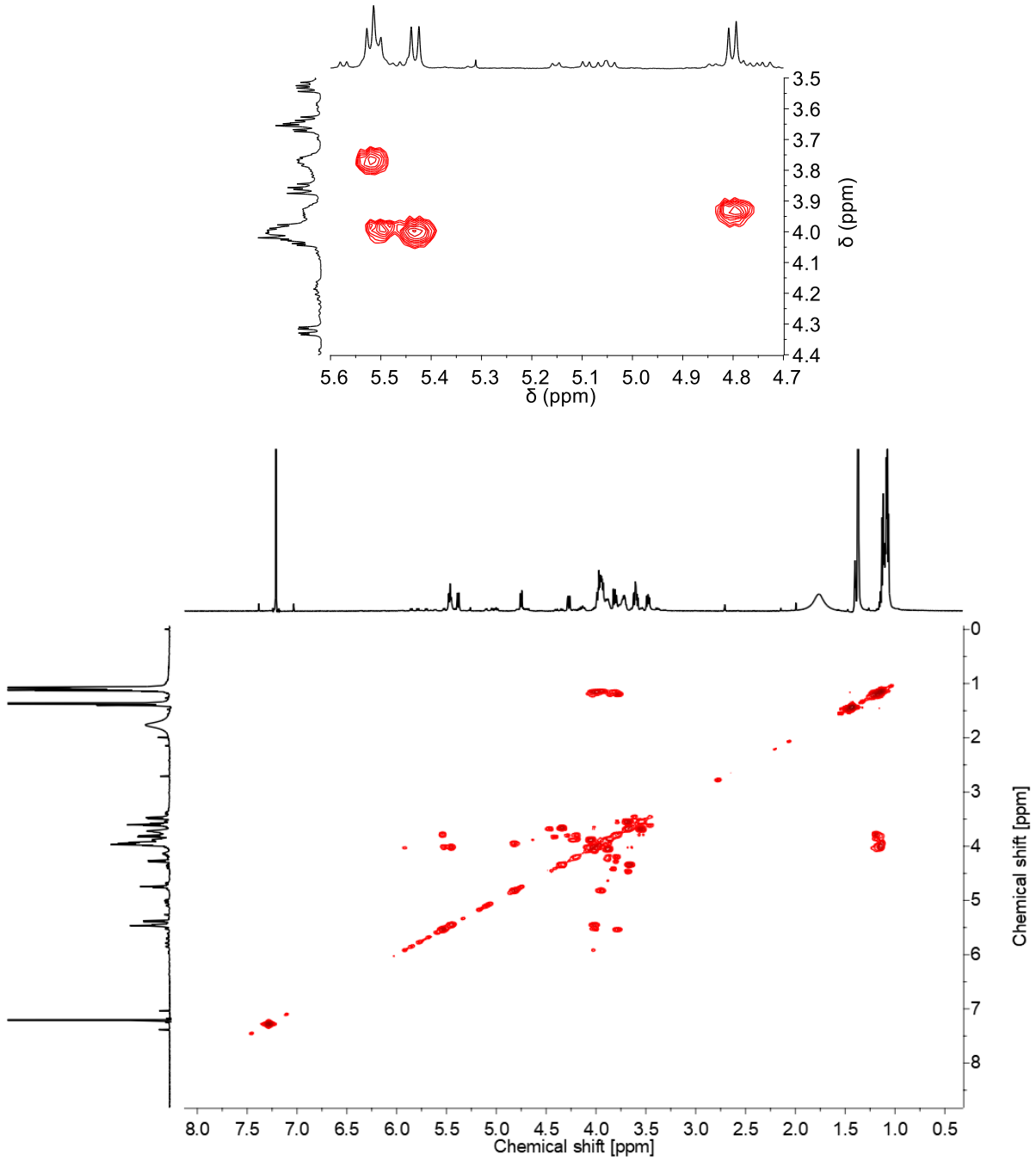

Figure S46. COSY NMR spectrum of **O2 SSSR,** 5 mM in $CDCl_3$, 263K, with zoomed NH proton range (top).

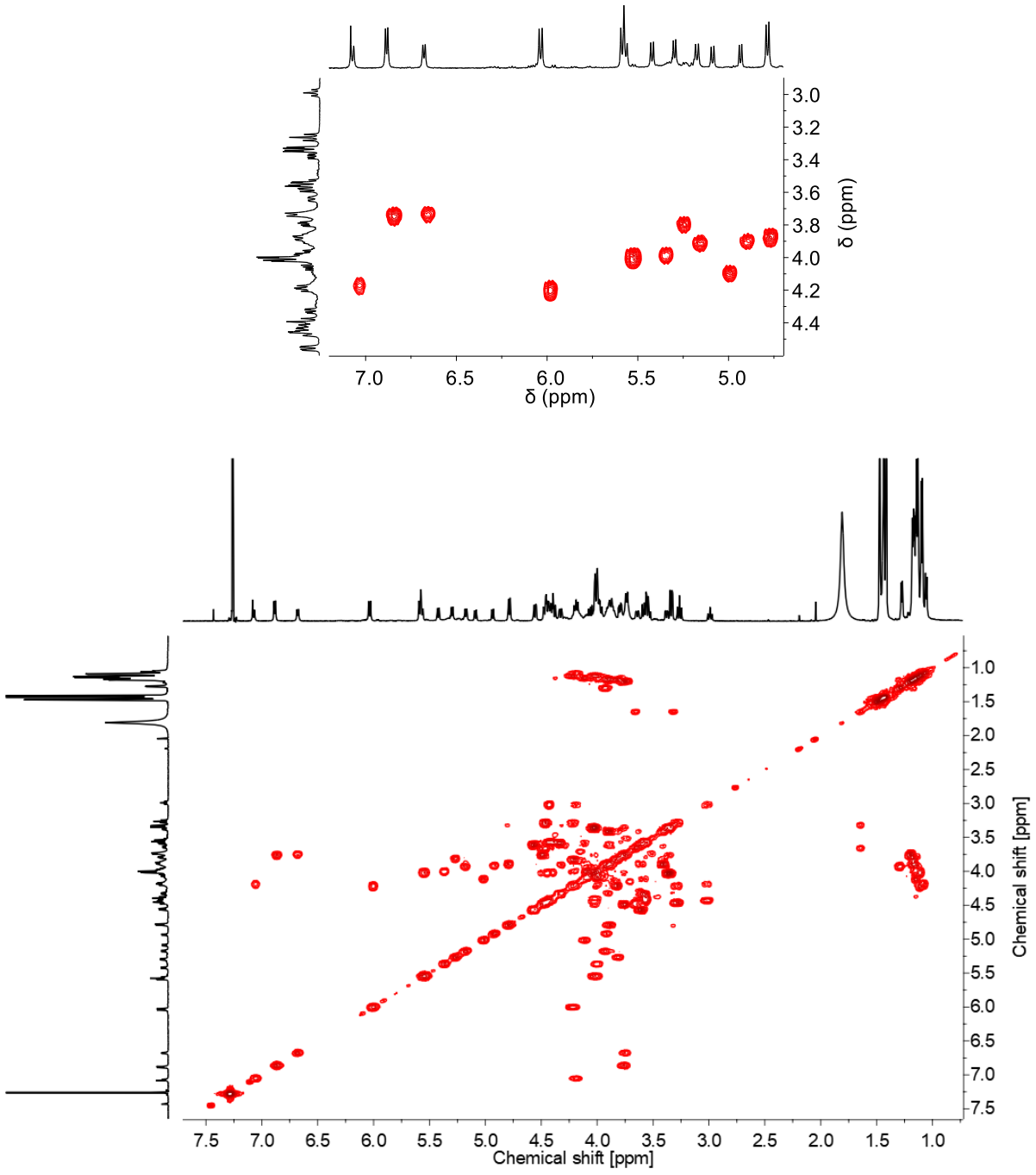

Figure S47. COSY NMR spectrum of **O3 SRSS**, 5 mM in $CDCl_3$, 263K, with zoomed NH proton range (top).

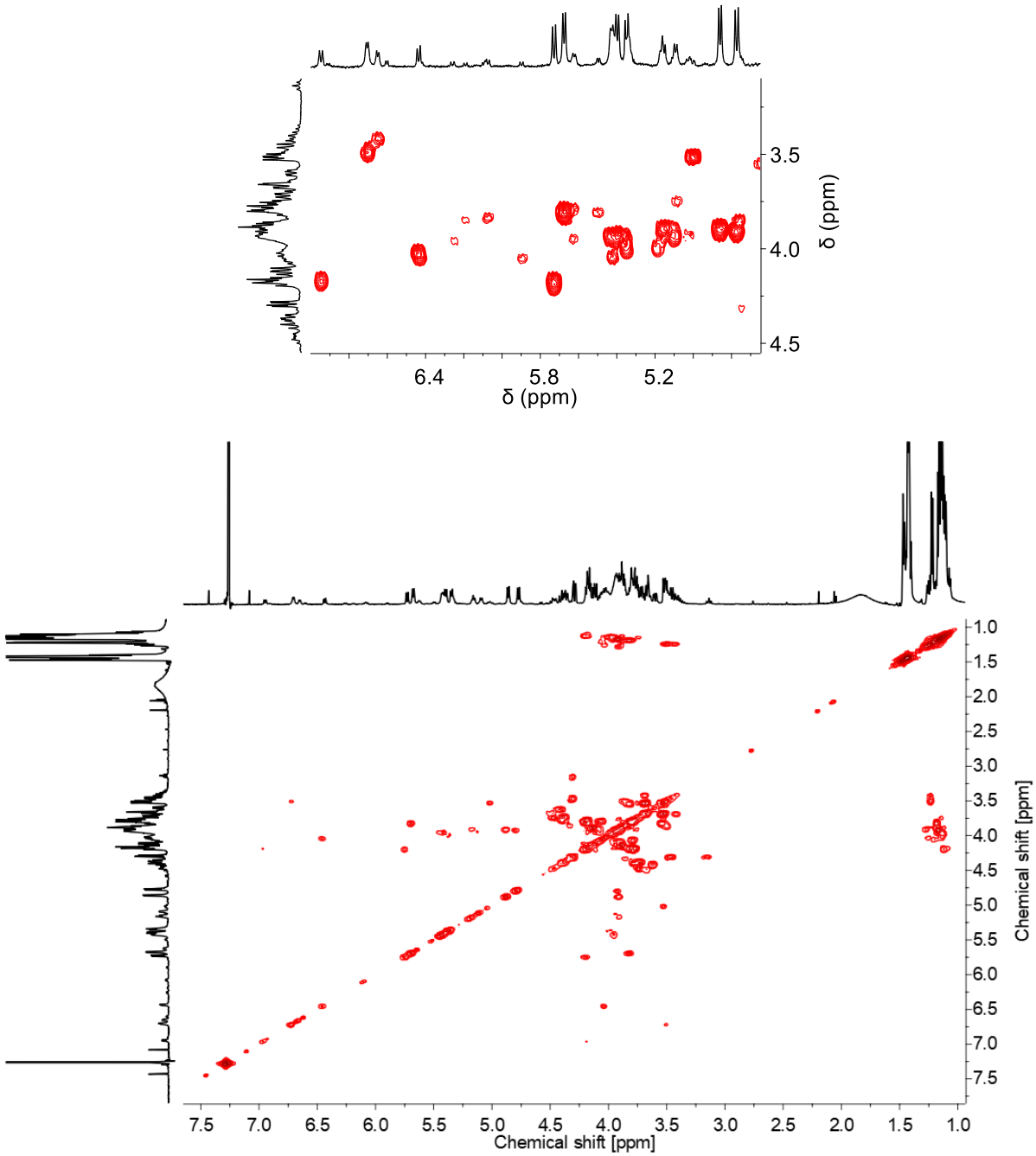

Figure S48. COSY NMR spectrum of **O4 SRSR**, 5 mM in $CDCl_3$, 263K, with zoomed NH proton range (top).

3.15.2. Total Correlation Spectroscopy (TOCSY) NMR

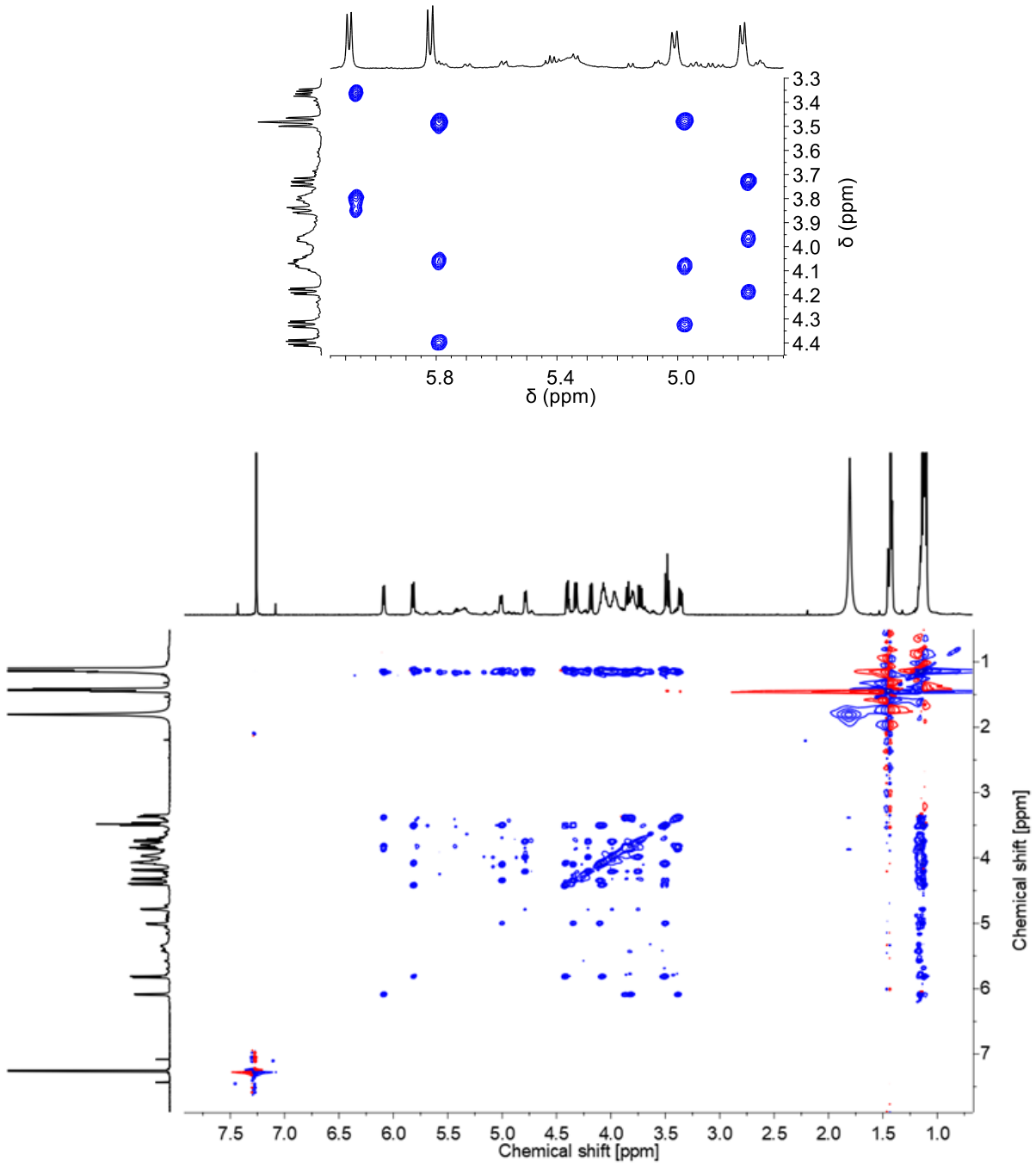

Figure S49. TOCSY NMR spectrum of **O1 SSSS**, 5 mM in $CDCl_3$, 263K, with zoomed NH proton range (top).

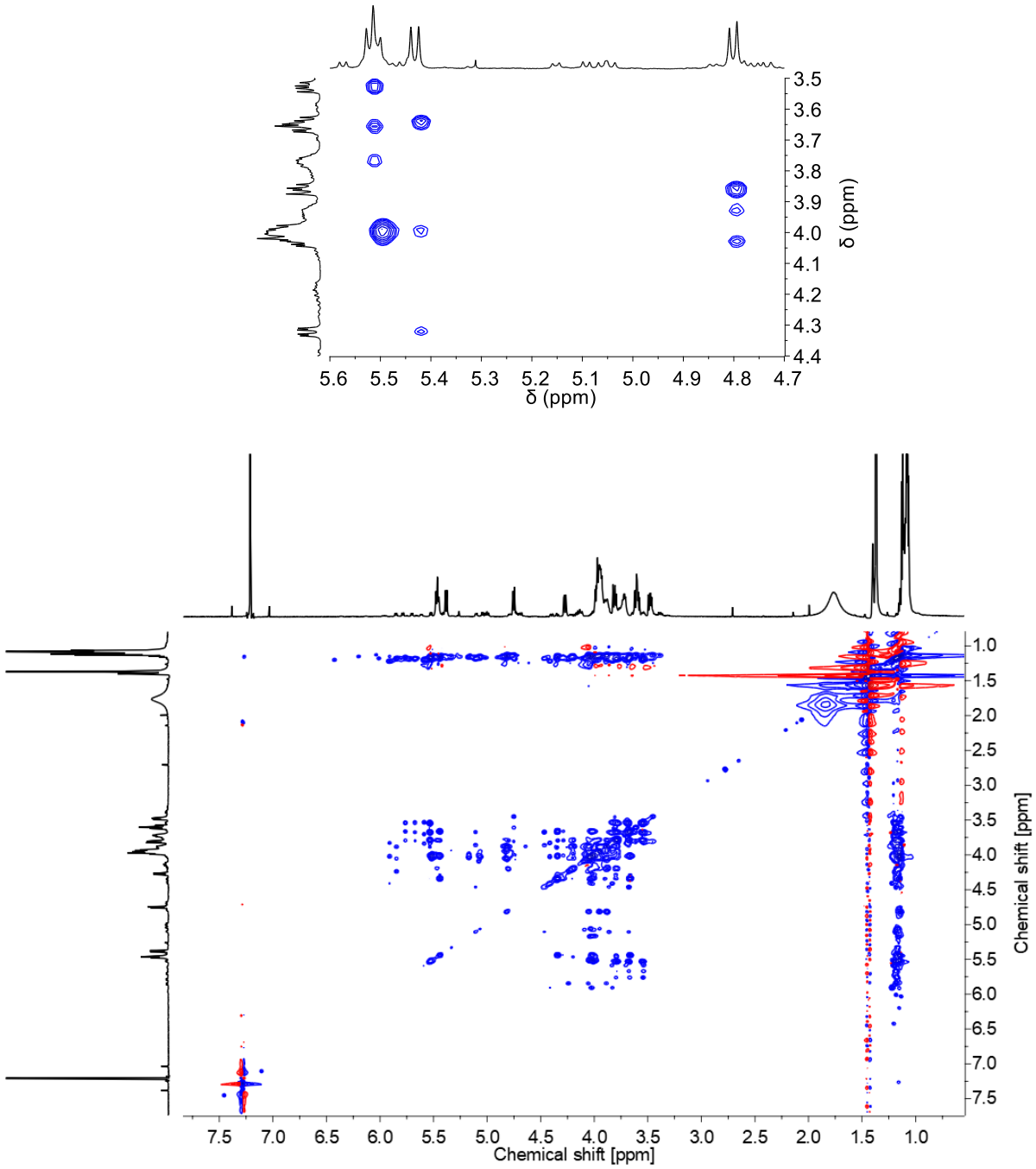

Figure S50. TOCSY NMR spectrum of **O2 SSSR**, 5 mM in $CDCl_3$, 263K, with zoomed NH proton range (top).

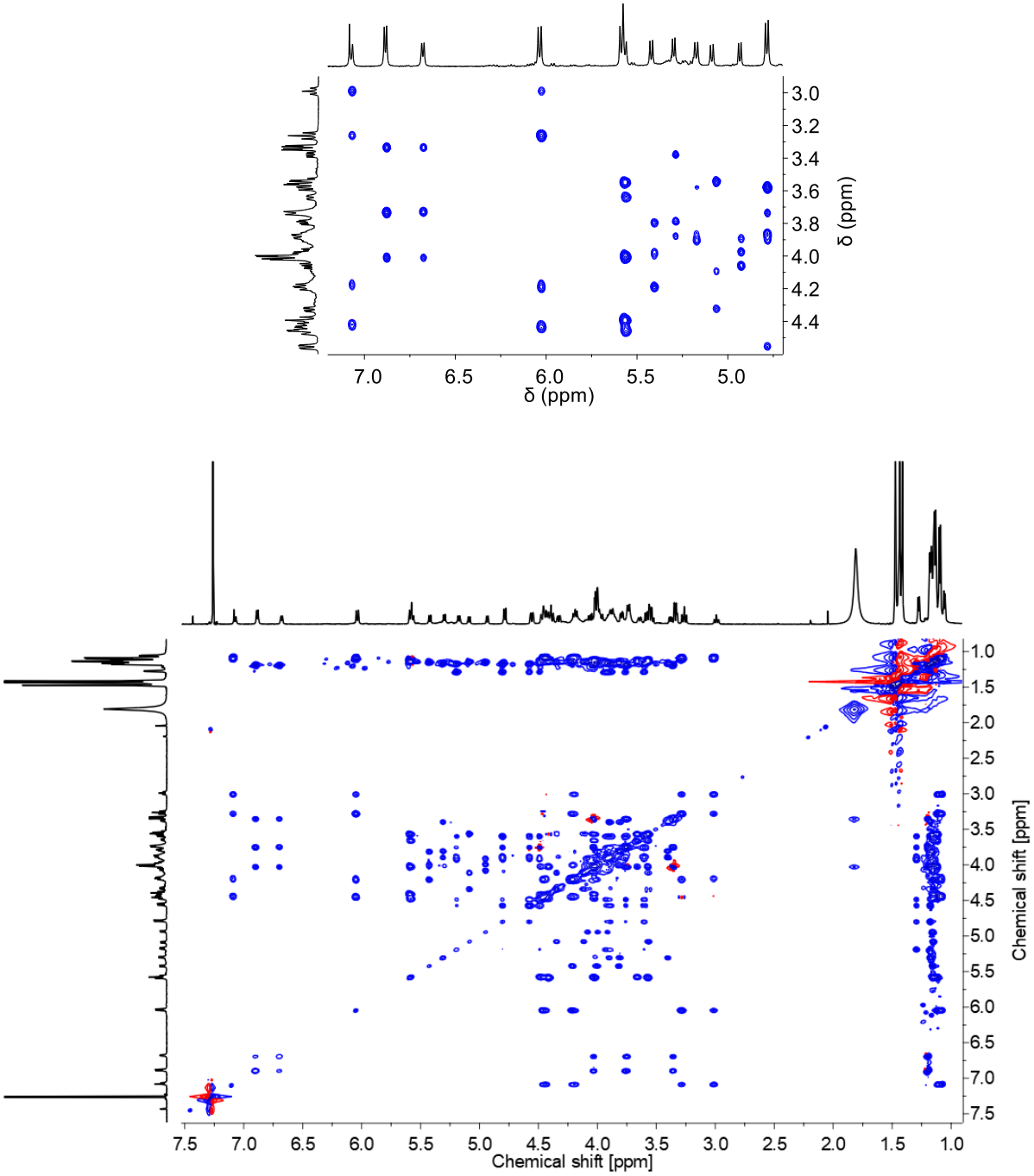

Figure S51. TOCSY NMR spectrum of **O3 SRSS,** 5 mM in $CDCl_3$, 263K, with zoomed NH proton range (top).

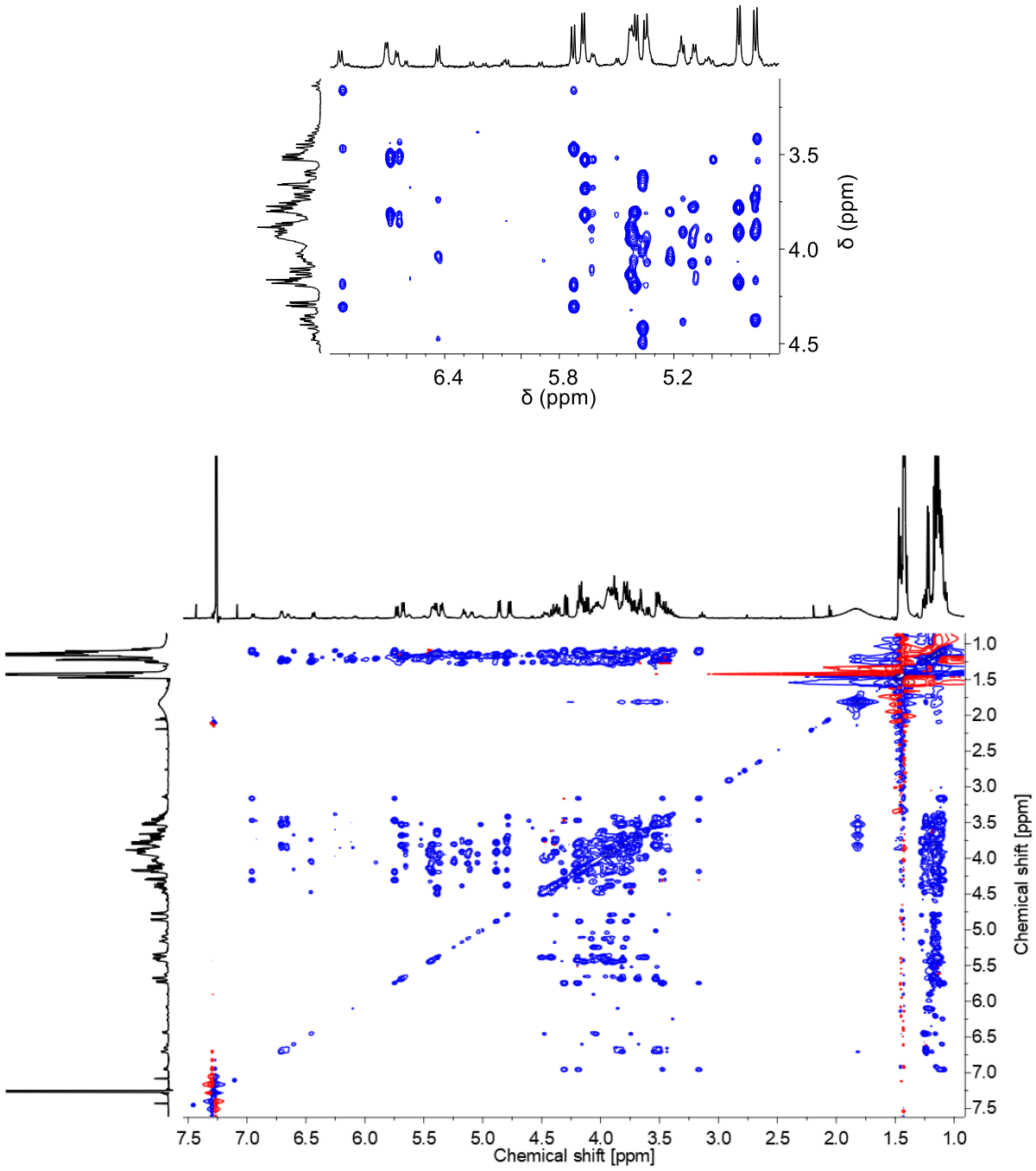

Figure S52. TOCSY NMR spectrum of **O4 SRSR**, 5 mM in $CDCl_3$, 263K, with zoomed NH proton range (top).

3.15.3. Signal assignment in ^{1}H NMR spectra

Signals in ^{1}H NMR spectra of the oligourethanes O1-O4 correspond to different elements of the chain: 1.0-1.2 ppm for CH_3 side-chains, 1.4-1.5 ppm for Boc CH3, 3.1-4.6 ppm for CH and CH_2 and 4.3-6.8 ppm for NH. Signal assignment to individual protons was performed based on TOCSY spectra, which enabled grouping of signals into spin systems corresponding to individual monomer units in the chain. The analysis was supported by COSY spectra, which was used to distinguish between CH and CH_2 protons in the backbone.

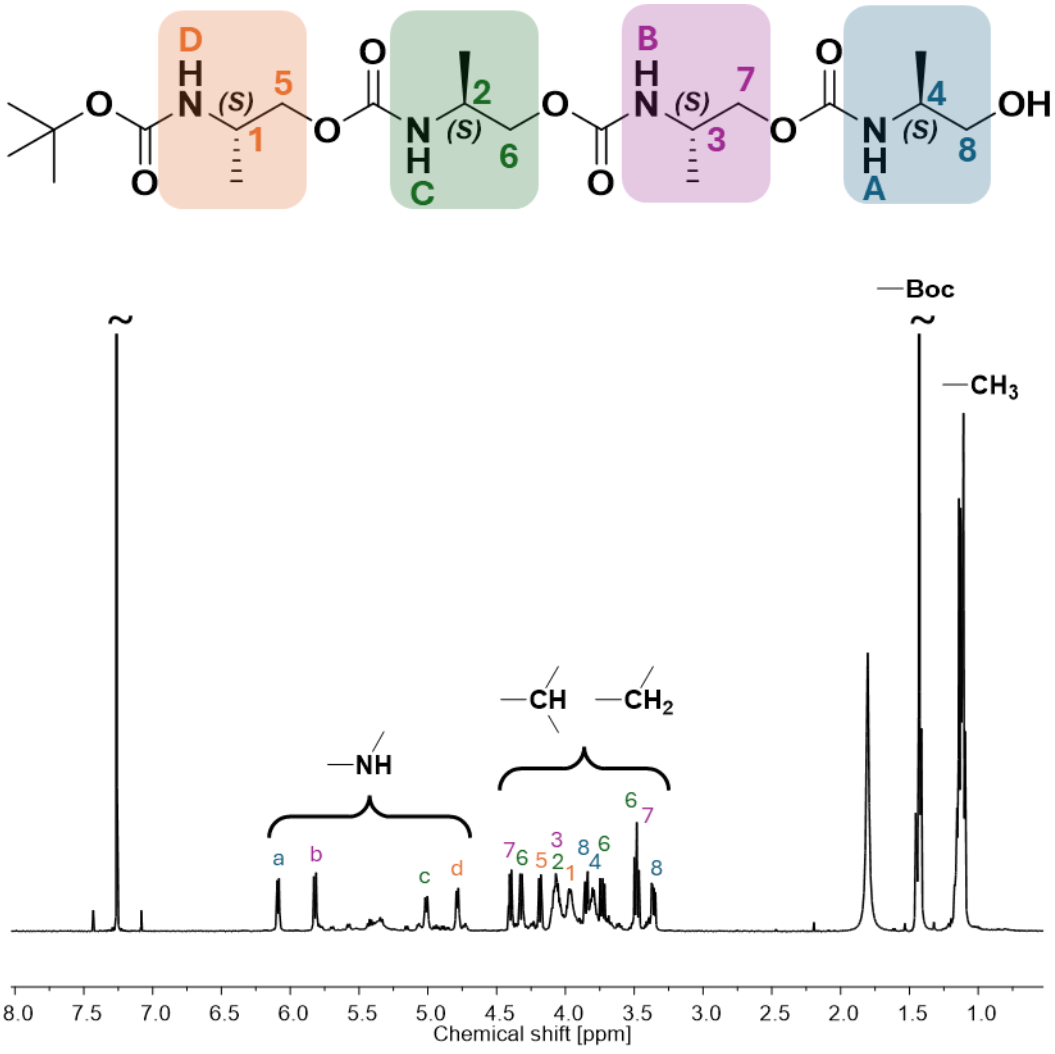

Figure S53. ^{1}H NMR spectra of **O1 SSSS** at 263K with signal assignment, 5 mM in $CDCl_3$. For O1 SSSS signals coming from amine protons (a, b, c, d) are clearly distinguished and well-separated, which enables further structural analysis based on NOESY. In the spectra, we observe one dominant conformation, and signals from other conformers are visible in the baseline as low-intensity features.

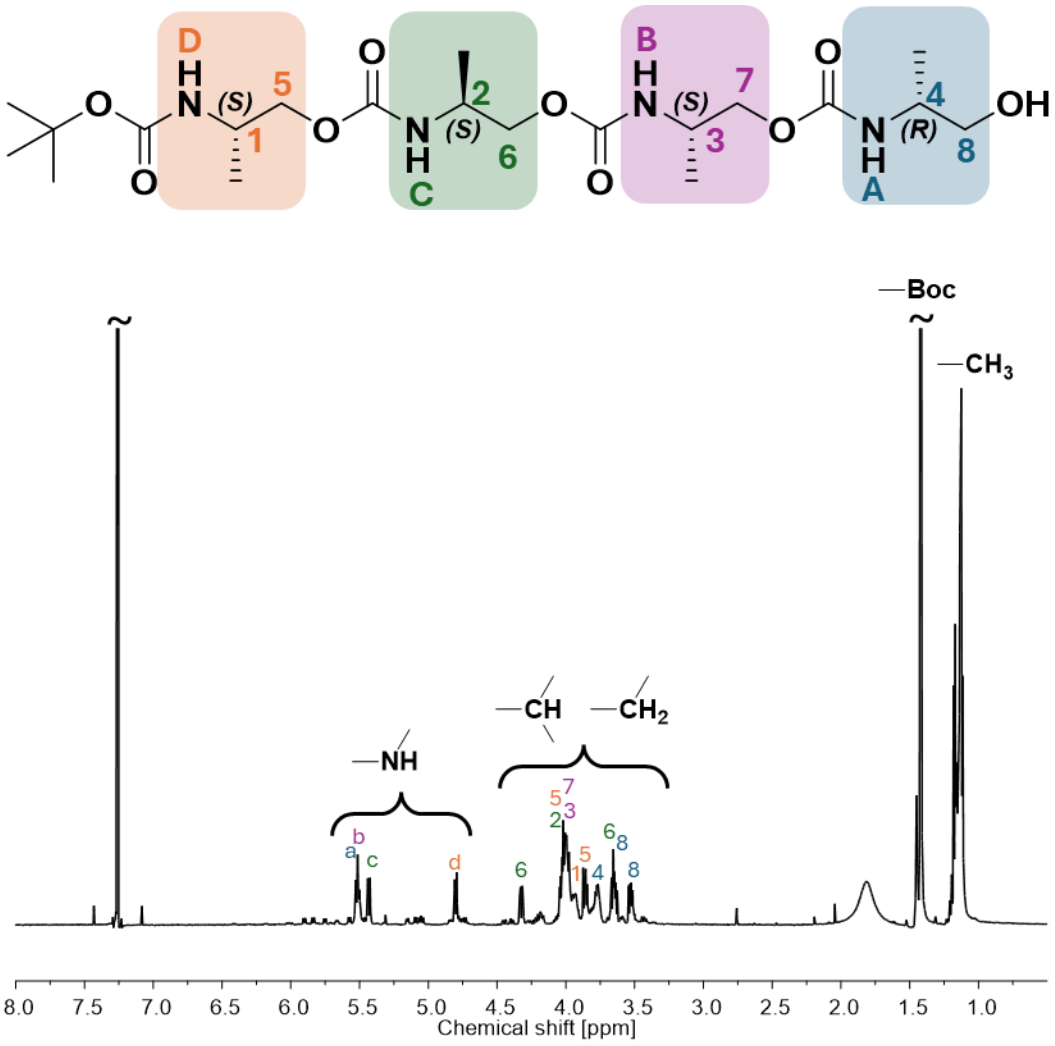

Figure S54. ^{1}H NMR spectra of **O1 SSSR** at 263K with signal assignment, 5 mM in $CDCl_3$. For O2 SSSR signals coming from amine protons (a, b, c, d), the signals are clearly visible; however, signals a and b overlap, so structural analysis based on NOESY does not provide reliable information about the oligomer conformation. In the spectra, we observe one dominant conformation, and signals from other conformers are visible in the baseline as low-intensity features, similar to the case of O1 SSSS.

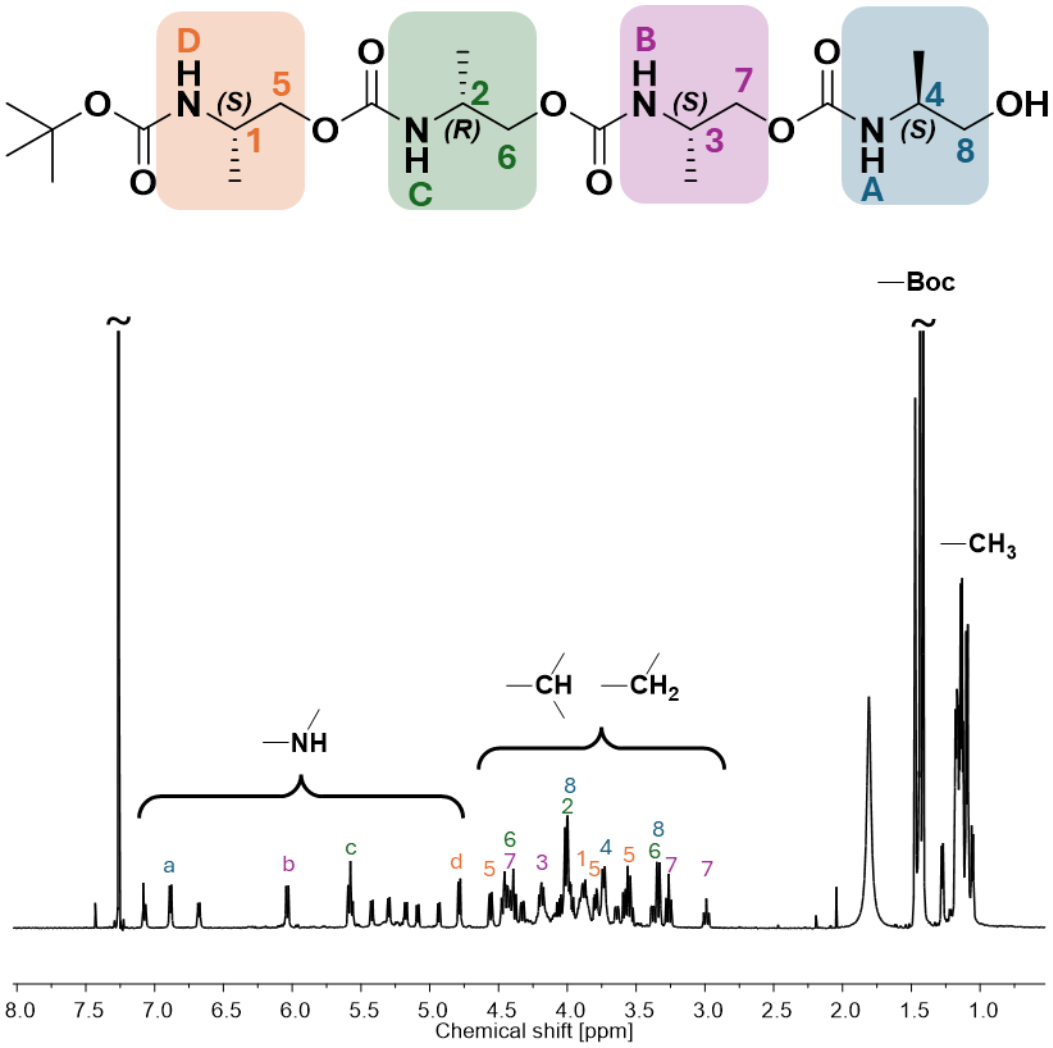

Figure S55. ^{1}H NMR spectra of **O3 SRSS** at 263K with signal assignment, 5 mM in $CDCl_3$. For O3 SRSS, in the spectra, we observe multiple conformers that are clearly visible in the NH range (>4 signals). Based on the integration of NH signals, we selected four HN signals of the highest intensity as representatives for the major conformer (a, b, c, d). Although amine signals are well-separated, we cannot perform structural analysis based on NOESY because signals in the aliphatic backbone proton range significantly overlap, making it impossible to distinguish exact signals coming from the major conformer and perform reliable structural analysis.

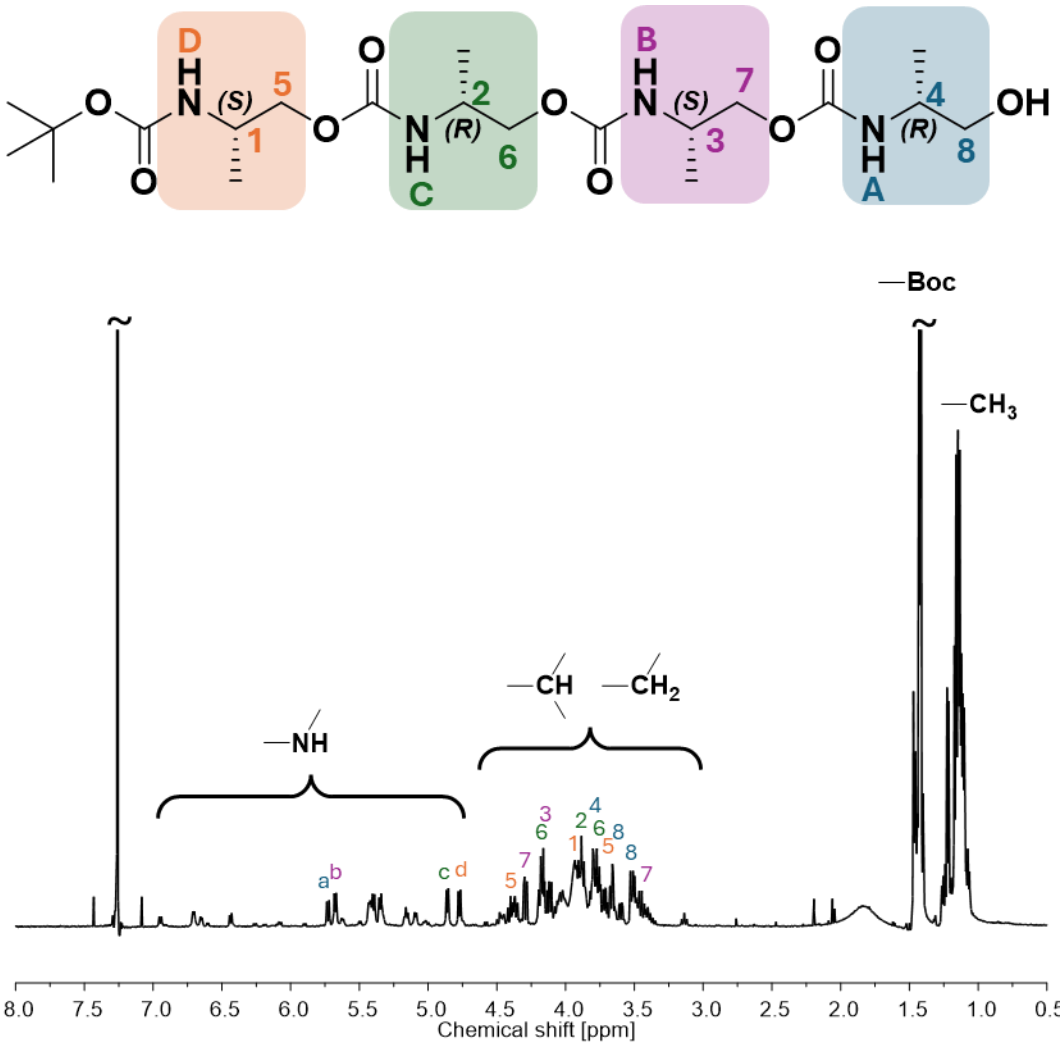

Figure S56. ^{1}H NMR spectra of **O4 SRSR** at 263K with signal assignment, 5 mM in $CDCl_3$. For O4 SRSR, in the spectra, we observe multiple conformers that are clearly visible in the NH range, as in the case of O3. Based on the integration of NH signals, we selected four NH signals of the highest intensity as representatives for the major conformer (a, b, c, d). Nevertheless, neither amine signals nor the aliphatic range are clear; signals significantly overlap, making it impossible to distinguish them and perform a reliable structural analysis.

3.15.4. Nuclear Overhauser Effect Spectroscopy (NOESY)

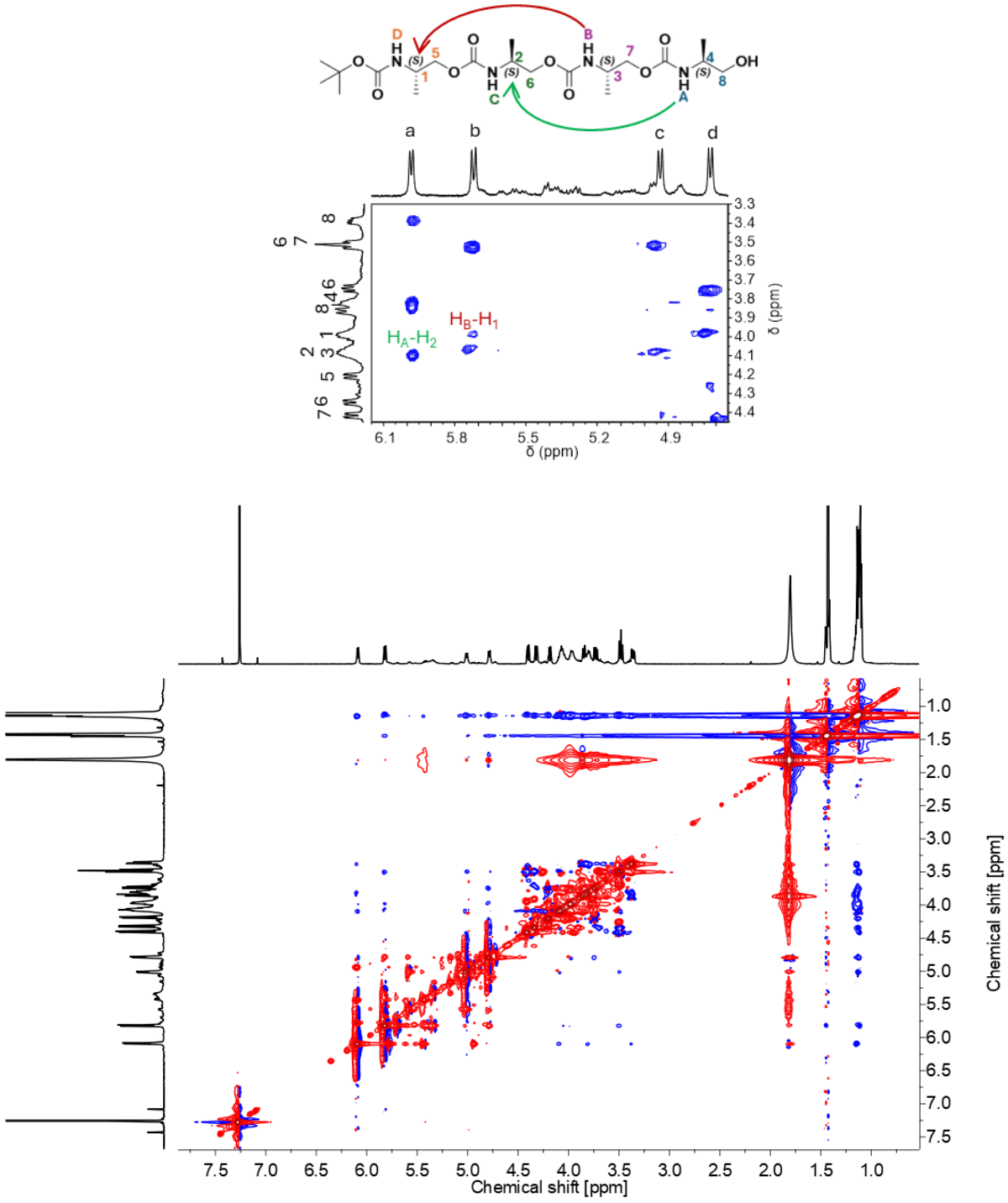

Figure S57. NOESY NMR spectrum of **O1 SSSS**, 5 mM in $CDCl_3$, 263K and zoom of amine region with signal assignments (top). The NOESY signals are marked in the spectra; other signals correspond to TOCSY artefacts.

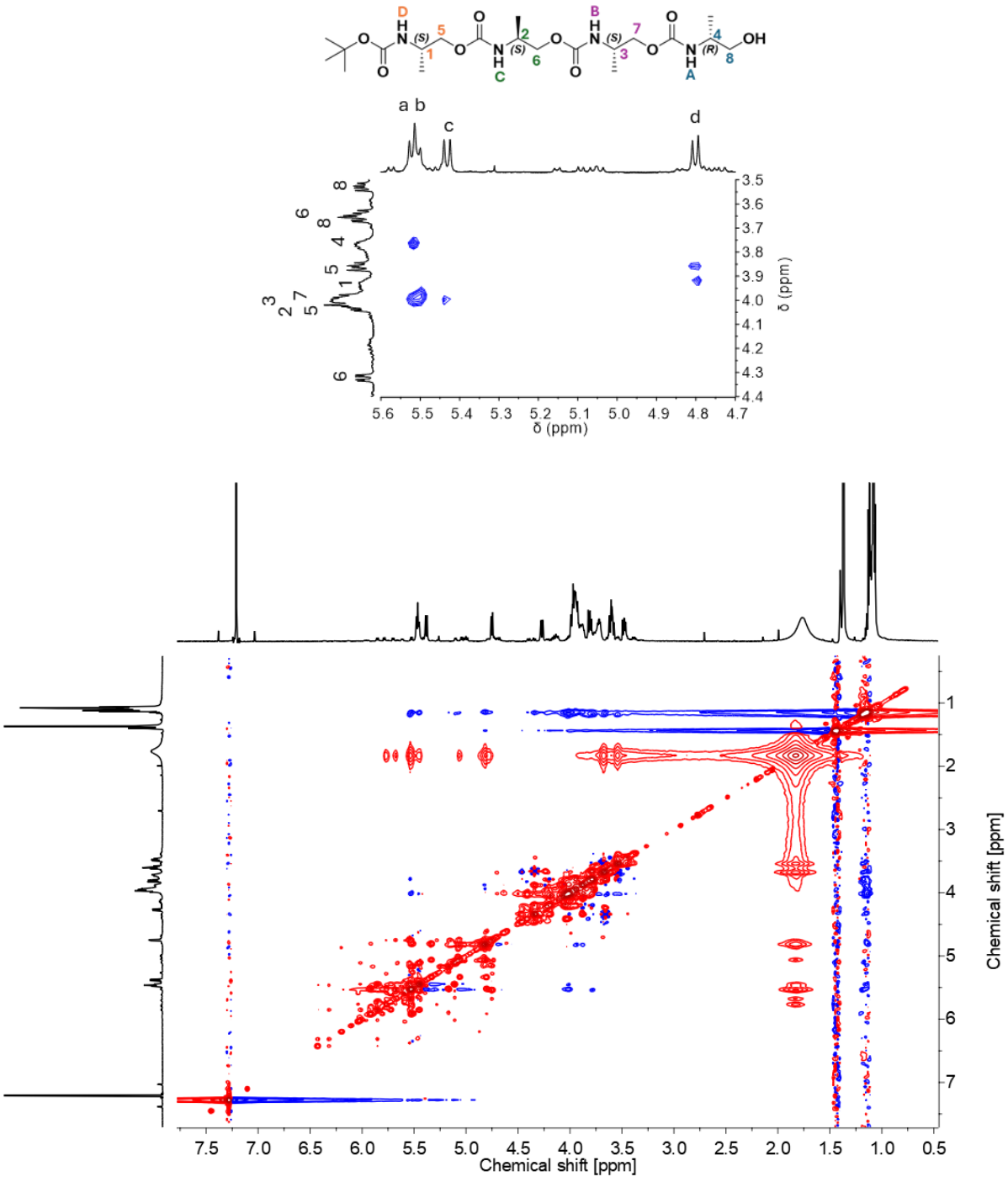

Figure S58. NOESY NMR spectrum of **O2 SSSR**, 5 mM in $CDCl_3$, 263K and zoom of amine region with signal assignments (top).

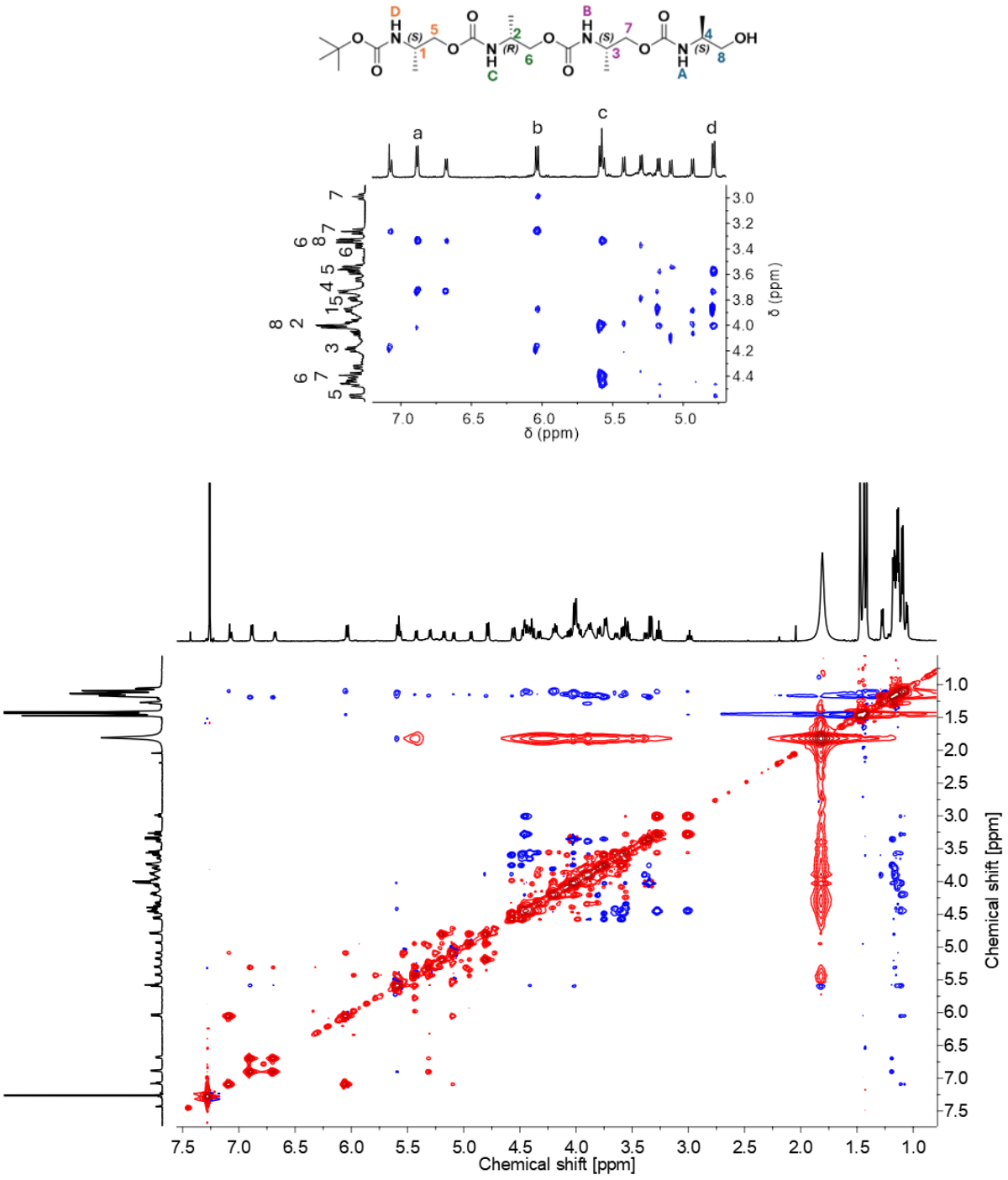

Figure S59. NOESY NMR spectrum of **O3 SRSS**, 5 mM in $CDCl_3$, 263K and zoom of amine region with signal assignments (top).

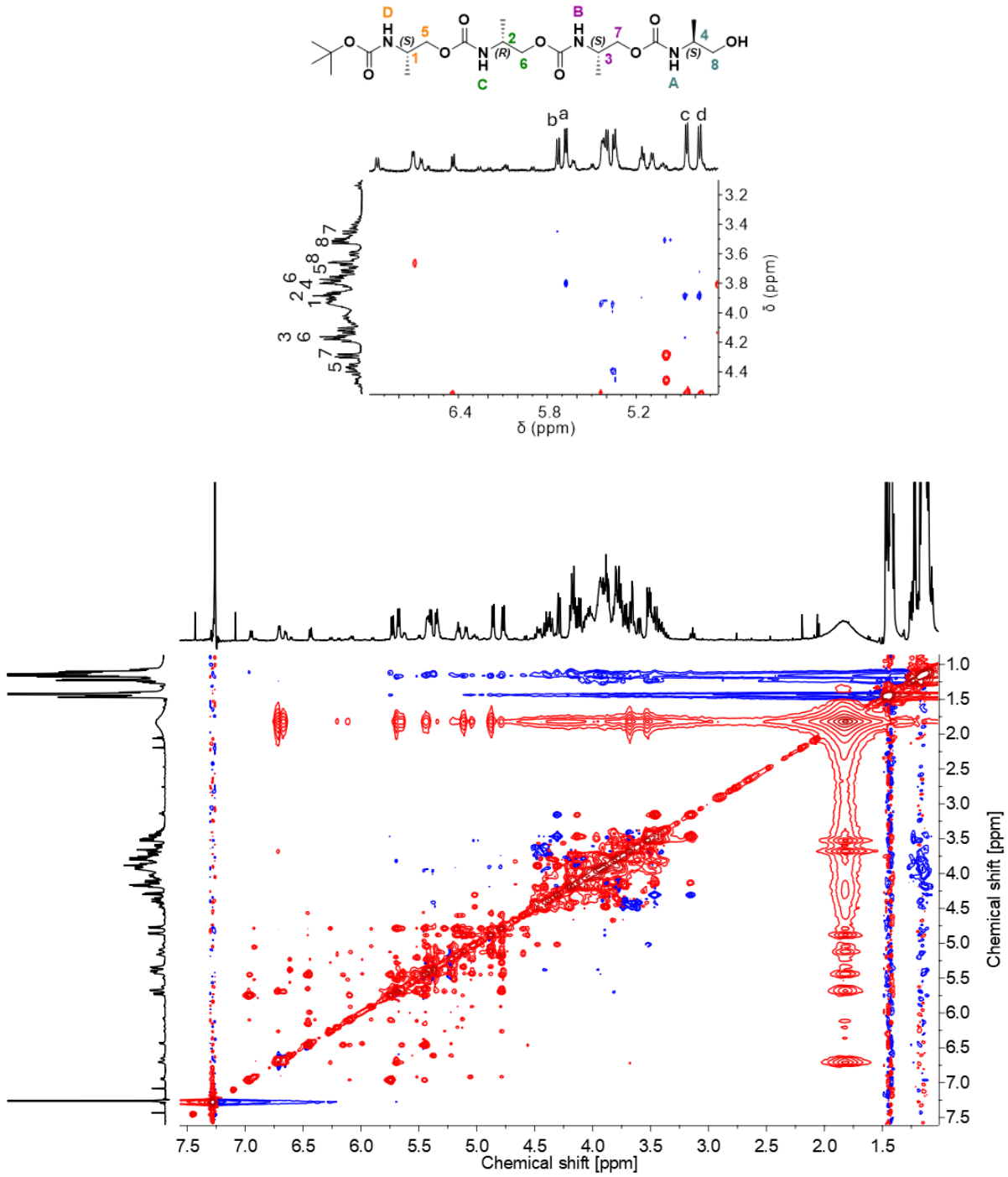

Figure S60. NOESY NMR spectrum of **O4 SRSR**, 5 mM in $CDCl_3$, 263K and zoom of amine region with signal assignments (top).

.

4. BIBLIOGRAPHY

1 W. Forysiak, S. Kozub, Ł. John and R. Szweda, *Polym. Chem.*, 2022, **13**, 2980–2987.
2 S. V. Chankeshwara and A. K. Chakraborti, *Org. Lett.*, 2006, **8**, 3259–3262.
3 W. Forysiak, A. Lizak and R. Szweda, *ChemPhysChem*, 2024, **25**, e202400366.
4 M. Szatko, W. Forysiak, S. Kozub, T. Andruniów and R. Szweda, *ACS Biomater. Sci. Eng.*, 2024, **10**, 3727–3738.
5 P. Cwynar, P. Pasikowski and R. Szweda, *Eur. Polym. J.*, 2023, **182**, 111706.
6 A. F. Perez Mellor, J. Brazard, S. Kozub, T. Bürgi, R. Szweda and T. B. M. Adachi, *J. Phys. Chem. A*, 2023, **127**, 7309–7322.
7 MacroModel Version 9.8 Schroedinger, LLC, New York, NY 2010.
8 E. Harder, W. Damm, J. Maple, C. Wu, M. Reboul, J. Y. Xiang, L. Wang, D. Lupyan, M. K. Dahlgren, J. L. Knight, J. W. Kaus, D. S. Cerutti, G. Krilov, W. L. Jorgensen, R. Abel and R. A. Friesner, *J. Chem. Theory Comput.*, 2016, **12**, 281–296.
9 S. K. Mishra, S. K. Chakraborty, M. E. Samei and B. Ram, *J Inequal Appl*, 2021, **2021**, 25.
10 G. M. Sheldrick, *Acta Crystallogr C Struct Chem*, 2015, **71**, 3–8.
11 A. L. Spek, *Acta Crystallogr D Biol Crystallogr*, 2009, **65**, 148–155.